Cooling, Trapping & Guiding Neutral Atoms with Laser Light

Mark Clifford

Thesis for the degree of

Master of Philosophy

School of Physics and Astronomy,

University of St. Andrews,

St. Andrews, Fife,

Scotland

January 6, 2004

Abstract

In this thesis I investigate systems of diode lasers for trapping and cooling neutral atoms. Light beams for use in atom guiding are also presented. Finally, development of a mirror magneto-optical trap is discussed.

A review of the theory and practice of atom cooling and trapping since it was first proposed is given, together with a discussion of two recent experiments with cold atoms. The work-horse of atom trapping, the magneto-optical trap (MOT), is described. The review continues with the theory of optical guiding of atoms, using both hollow-core fibres and hollow light beams, and a comparison with magnetic guiding.

The criteria needed for a laser to trap cold atoms are presented, followed by an introduction to diode lasers and their characterisation. The creation of an extended-cavity diode laser (ECDL) is described with methods for stabilisation and improvement. The ECDL was experimentally seen to be easily tuneable, stable and with a narrow bandwidth, making it eminently suitable for use as a compact source in various cold atom situations.

A method of stabilising and locking an ECDL using the Zeeman effect is given, together with a comparison with other locking schemes. The locked ECDL was tuned using an optical offset and the frequency shifts recorded. Using very simple equipment, this dichroic atom-vapour laser lock (DAVLL) is shown to lock an ECDL to a caesium absorption feature with very little drift over a long time.

The use of hollow light beams in both trapping and guiding cold atoms is presented. Of the various hollow beams possible, Laguerre-Gaussian (LG) beams are seen to be very suitable, since they can have a dark central region that stays hollow apart from radial scaling with focusing. Their generation, using computer-generated holograms or mode-conversion of Hermite-Gaussian modes, is presented. A comparison with other hollow beams is given, and also a comparison of LG guiding with fibre guiding. Using our ECDL and various holograms, a range of LG modes were experimentally produced with 40% efficiency. The 'hole-size' of the beams varied with azimuthal phase, which was also seen by using a mode-analyser. Such a beam would be useful for guiding atoms from a MOT to be magnetically cooled into a Bose-Einstein condensate.

Finally, the mirror-MOT is introduced as a method for trapping atoms with fewer laser beams than a standard MOT. Normally six beams are needed, but this system only requires four beams. Since the atoms are trapped in close proximity to a (mirrored) surface, this leads to good prospects for transferring atoms from the MOT to a microtrap within the surface. Using this system, there were measured to be about 10^8 atoms trapped, with a trap lifetime of about 0.2 seconds.

Publications

1. M.A.Clifford, J.Arlt, J.Courtial, and K.Dholakia, "High-order Laguerre-Gaussian laser modes for studies of cold atoms," Opt.Comm. **156**, 300-306 (1998)

2. G.P.T.Lancaster, R.S.Conroy, M.A.Clifford, J.Arlt, and K.Dholakia, "A polarisation spectroscopy locked diode laser for trapping cold atoms," Opt.Comm. **170**, 79-84 (1999)

3. M.A.Clifford, G.P.T.Lancaster, R.S.Conroy, and K.Dholakia, "Stabilization of an 852nm extended cavity diode laser using the Zeeman effect," J.Mod.Opt. **47**, 1933-1940 (2000)

4. G.P.T.Lancaster, R.S.Conroy, M.A.Clifford, J.Arlt, K.Dholakia, "Channeling of cold atoms along a Laguerre-Gaussian light beam" Conference paper presented at *Quantum Electronics and Laser Science*, San Francisco, 2000

5. M.A.Clifford, G.P.T.Lancaster, R.H.Mitchell, F.Akerboom, and K.Dholakia, "Realization of a mirror magneto-optical trap," J.Mod.Opt. **48**, 1123-1128 (2001)

Declarations

I, Mark Alastair Clifford, hereby certify that this thesis , which is approximately 100,000 words in length, has been written by me, that it is the record of the work carried out by me, and that it has not been submitted in any previous application for a higher degree.

Date .. January 5, 2004 Signature of candidate

I was admitted as a research student in November 1997 . The higher study of which this is a record was carried out in the University of St.Andrews between 1997 and 2000.

Date .. January 5, 2004 Signature of candidate

I hereby certify that the candidate has fulfilled the conditions of the Resolution and Regulations appropriate for the degree of M.Phil. in the University of St.Andrews and that the candidate is qualified to submit this thesis in application for that degree.

Date .. January 5, 2004 Signature of supervisor

In submitting this thesis to the University of St.Andrews I understand that I am giving permission for it to be made available for use in accordance with the regulations of the University Library for the time being in force, subject to any copyright vested in the work not being affected thereby. I also understand that the title and abstract will be published, and that a copy of the work may be made and supplied to any *bona fide* library or research worker.

Date .. January 5, 2004 Signature of candidate ..

Acknowledgements

I would like to thank my supervisor, Prof. Kishan Dholakia, for giving me the chance to work with him, and for the help he has given throughout my time in St.Andrews, especially in view of my continuing ill health.

Additionally, I want to thank my colleagues, both those with whom I have worked, and those who have just lifted the spirits around the lab.: Gavin, Jochen, Richard, Jacqui, Alisdair, William, Orik, John and Daniel, amongst others.

Furthermore, I want to acknowledge the Engineering and Physical Sciences Research Council (EPSRC) for funding my work through an embedded studentship with Kishan Dholakia.

Last but not least, I want to thank my mother, family and friends for all their love and support, and especially Helen for keeping me sane through all this.

Y gwir yn erbyn y byd

Contents

Introduction

Cooling and trapping of neutral atoms by using laser beams is an area of research which has seen a lot of interest in the last decade, resulting in a fast expansion and some dramatic developments. These include the ability to cool atoms down to unprecedented kinetic temperatures (as low as 20nK when combined with evaporative cooling) and then hold the cloud of atoms isolated in the middle of a vacuum system for many seconds. This source of atoms may then be used as a reservoir to supply other experiments, which may require guiding the atoms to a geographically separate area where they can be affected by other environments.

This thesis covers my studies of laser light as used in the cooling, trapping and guiding of neutral rubidium and caesium atoms. Firstly, I will give a background to the various areas being researched in laser trapping, cooling and guiding of atoms. Some of the theory of atom cooling and trapping is presented, including sub-Doppler cooling and the Sisyphus effect, proceeding into a look at the magneto-optical trap (MOT) which is the most used tool for capturing atoms. Recent experiments with cold atoms are summarized, such as the atomic fountain and an atom interferometer for the measurement of gravity. The ideas and theory behind laser guiding of atoms are presented, giving reasons why one might want to, and outlining some experiments with guided atoms. Optical guiding using hollow-core fibres and annular cross-sectioned light beams are discussed, as

well as the use of magnetic fields in guiding, together with a comparison of these methods.

A study of diode lasers and their use in spectroscopy and atom trapping follows, giving a comparison with other sources and the criteria needed to trap cold atoms. After describing how a diode laser works and how it can be used with feedback to create a highly tunable laser source, the characterisation of the lasers built by me is given. The method for recording the saturated absorption spectra of rubidium and caesium is presented. The next chapter continues on from the previous chapter and presents a method for stabilising and locking the extended-cavity diode laser (ECDL)already built using the Zeeman effect produced by annular permanent magnets. Experimentation with this dichroic atomic-vapour laser lock (DAVLL) system using caesium atomic vapour showed that the locked laser frequency drifted approximately 5MHz/hour.

Having studied the source of laser light itself, this work will look at the production and use of hollow-core light beams, specifically Laguerre-Gaussian (LG) modes. Certain LG modes have a 'non-diffracting' dark hole in a bright ring or annulus. These can be used for repumping in a MOT, resulting in a reduction in light-induced loss. Also, these beams are useful for guiding atoms without the need for hollow-core fibres and the inherent problem with Van der Waals forces. Various methods for producing LG beams are mentioned, but specifically the use of holograms with Gaussian beams, and mode-conversion of Hermite-Gaussian beams. A comparison with other hollow beams, such as Bessel beams, is made, and also with fibre guiding. Experimental results show the different size holes that can be produced from holograms, together with the differing azimuthal phase of the light beam. Some studies of hollow fibres for use in atom guiding are also studied, and the two methods of using light to prevent sticking are discussed. Some recent experiments of fibre guiding in other laboratories are given.

Various MOTs have been used for cooling and trapping atoms in St.Andrews. Once such, the mirror-MOT is discussed in detail. Using the apparatus described in this work, it is possible to reduce the number of trapping beams required from six to four. Atoms are trapped in close proximity to a (mirrored) surface, which would be useful elsewhere for loading cold atoms into microfabricated magnetic traps within the surface. By drilling a hole in the mirror, it also makes for a suitable source for guiding atoms optically. The number of atoms and the trap lifetime were experimentally found. It was also possible to move the captured atom cloud by imbalancing the currents in the magnetic coils of the trap.

Chapter 1

Cooling, Trapping and Guiding atoms with laser light

1.1 Introduction

The idea of cooling atoms down to near absolute zero has been around since at least 1950. It was suggested by Kastler that 'optical pumping' could be used to cool or heat the atom. This would be achieved by using the resonant exchange of angular momentum between atoms and polarized photons to align the spins of atoms, or put them out of equilibrium. Later, Hänsch and Schawlow [1] suggested laser cooling of neutral atoms, using resonant exchange of linear momentum between photons and atoms to reduce their kinetic energy. Wineland, who had suggested similar cooling of ions, gave potential applications of cold atoms in fields such as ultrahigh resolution spectroscopy, atomic clocks, collisions, surface physics and collective quantum effects [2]. At the time, atoms had only been cooled to a few hundred microkelvin. However, within three years of that article, temperatures were down to only a few microKelvin, and later improvements

allowed unprecedented kinetic temperatures (as low as 20nK). The Nobel Prize in Physics for 1997 was awarded for 'developments of methods to cool and trap atoms with laser light' to S.Chu, C.N.Cohen-Tannoudji and W.D.Phillips.

Cooling of neutral atoms is one thing, and can be performed on moving atoms. However, in order to allow certain experiments, trapping of the cooled atoms is necessary. Cooling will have stopped the atoms from moving about quite so fast, but they are still able to drift about, so various methods of containing them have been developed. Magnetic fields can be used on their own or in conjunction with optical beams to form a magneto-optical trap. It is also possible to contain the cold atoms by utilising the dipole force. These will be discussed later.

Once the atom sample has been cooled and trapped, it can become a source for various experiments. However, it will probably be necessary to transport the atoms to another piece of apparatus in order to carry out those experiments. Guiding of cold neutral atoms can be done in two ways - using a hollow core fibre or a 'hollow' laser beam. As such, these 'tubes' can be thought of as 'atom hosepipes' [3]. Light is used in both these cases. For the hollow fibre, it prevents the atoms sticking to the walls of the tube, using the dipole force and evanescent waves. The dipole force can be used to dispense with the fibre altogether and guide atoms down the 'dark' region in an annular cross-section laser beam. Fibres could be used to extract atoms from a low-quality supply chamber to an ultra-high vacuum analysis chamber. Isotopes could also be separated since they can be frequency selected. The losses from transverse momentum diffusion in evanescent mirror cavities can be eliminated by the transverse confines of a fibre guide. Atoms can be manipulated and probed optically through fibre walls without the constraints of a cumbersome vacuum enclosure. Another prospect is brought about by the guiding of cold atoms in fibres, because at low temperatures the atomic de Broglie wavelength becomes comparable to the transverse dimensions of

the hollow core. The atoms thereby propagate in modes much like optical modes in conventional fibres. This gives the possibility of fibre-atomic interferometry in analogy with its fibre-optic counterpart. References [4–10] give a lot of the theory and early experiments in cooling and trapping.

1.2 Theory

1.2.1 Why cool and trap?

It would be much easier to analyse atoms if they were not speeding around a large volume. Cooling and trapping can allow this to be done. Atoms are confined in a relatively perturbation free environment, Doppler shifts can be considered insignificant, and long interaction times are possible. This makes them suitable for taking precision measurements of, for example, gravity [11], time [15], and the recoil of an atom after absorbing a single photon [16]. It is also a suitable source or reservoir of cold atoms, which can be 'tapped off' to be guided in a beam, as will be discussed later in this chapter. These atomic beams are perfect for atom optics [17], atom interferometry [11, 16], and atom lithography [18]. Examples of experiments with cold atoms are given in section 1.3.2 below.

1.2.2 Trappable atoms (Na, Rb, Cs, etc.)

Theoretically it should be possible to laser cool any atom. However, in practice it is difficult to produce the laser power needed to cool some atoms through non-linear processes. This is particularly true for those atoms whose cooling transitions are in the ultraviolet region. In addition, many thousands of photons

need to be scattered on the cooling transition, so all spontaneous emission from the excited state should be into the ground or metastable state, rather than one of the vast number of other metastable states. Primarily, if an atom has no cycling absorption/emission transitions, then cooling cannot take place using the following method. For these reasons the following atoms [19] have so far been the primary candidates: Hydrogen (^1H) and Chromium (^{52}Cr) have also been

metastable noble gas atoms	$^4He^*$	$^{20}Ne^*$	$^{40}Ar^*$	$^{84}Kr^*$	$^{132}Xe^*$
alkali-metal atoms	^7Li	^{23}Na	^{39}K	^{85}Rb	^{133}Cs
alkaline-earth atoms		^{24}Mg	^{40}Ca	^{88}Sr	^{138}Ba

laser cooled. In fact, the evaporative cooling process developed for hydrogen was refined and first used to super cool other atoms.

To begin with, laser cooling and trapping was accomplished with sodium, because it is easy to produce a thermal beam. The cooling transition can be driven by a continuous wave dye laser, operated by one of the most efficient and reliable dyes, Rhodamine 6G. With the advent of other tuneable sources, such as laser diodes and Ti:sapphire lasers, research has turned towards the heavier alkaline metals, rubidium (Rb) and caesium (Cs). These have a similar level structure, but their resonance lines are in the near infrared.

1.2.3 Laser cooling (including the Doppler effect)

In order to cool and trap atoms with laser light, the momentum transfer from photons scattering off an atom causing recoil is utilised. This could be thought of as a free-wheeling car being bombarded by a stream of tennis balls. A single ball would have imperceptible effect on the car, but many (millions) would

certainly slow it somewhat. The momentum given to the atom by each photon is minute, typically changing its velocity by about one cm/s. However, if the strong atomic transition is excited, it is possible to scatter more than 10^7 photons per second, giving much larger accelerations (10^4.g) and thus more cooling. The atom soon returns to the ground state by spontaneously emitting a photon. By the conservation of momentum, the atom recoils again, in the opposite direction to that of the emitted photon. However, since this is a random process with a symmetric distribution given by the appropriate radiation pattern, it doesn't contribute to the net change in momentum when averaged over many cycles of absorption/spontaneous emission or a large sample of atoms. Figure 1.1a) illustrates how the velocity of an atom, on average, changes by an amount $\hbar k/m$ each time it runs through its cycle. Figure 1.1b) shows the specific case for Rb. Essentially all the trapping and cooling is done by one laser, tuned slightly (1-3 natural linewidths) to the low frequency (red detuning) of the F=2→F' transition of ^{87}Rb. Unfortunately, in about one excitation in 1000, the atom decays to the F=1 state instead of the F=2 state. Since the atom is now out of resonance with the trapping laser, another laser is needed to repump (or excite) the atom back to the 5P F'=1 or 2 state, from where it will decay back to the 5S F=2 state (and back in resonance with the trapping laser). In Figure 1.1b), this repumping laser is called the "hyperfine pumping laser".

The power required for optical pumping is only a few milliWatts for both 'hyperfine' (F=1→F'=1,2) and trapping (F=2→F'=3) transitions. Visible clouds of trapped atoms can be obtained with as little as 1.5mW of trapping laser power. However, the number of atoms trapped is proportional to the laser power, so using at least 5mW of laser power makes setting up the trap much easier. The trapping laser must have an absolute frequency stability of a few megaHertz, which is accomplished by eliminating mechanical vibrations and temperature drifts, as

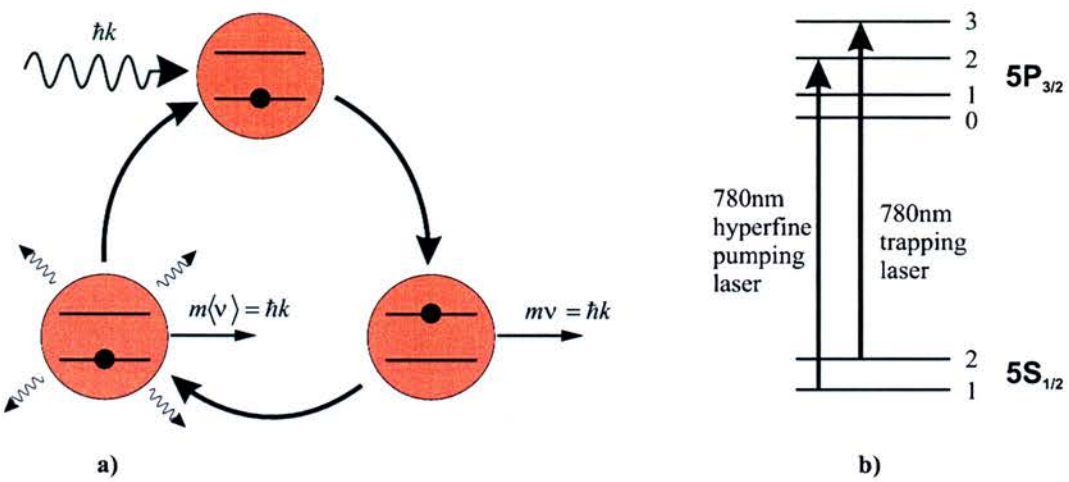

Figure 1.1: *a) The cooling cycle: A two-level atom, initially in its ground state (top), absorbs a photon with momentum ħk. The atom enters its excited state and increases its velocity by ħk/m in the direction of the incoming beam. The internal atomic energy is released by spontaneous emission of a photon, in a direction described by a symmetric probability distribution, so the average velocity change associated with this process is zero. The atom returns to the ground state and is ready to start the cycle again. b)* ^{87}Rb *energy levels*

mentioned in chapter 2. The laser frequency is also locked to the atomic transition frequency by using a feedback loop. This loop incorporates a saturated absorption signal of some sort, as discussed in the next chapter.

Using the Doppler effect [20] makes the photon scattering rate velocity dependent. See figure 1.2 for the basic principle. In the diagram, ν could be written ν_{laser} and $\Delta\nu$ as $\Delta\nu_{Doppler}$. An atom moving towards the laser beam will see the laser frequency ν_{laser} (ν in the diagram) shifted by an amount $(-V/c)\nu_{laser}$, where V is the velocity of the atom in the direction of the laser beam. As a result, if the laser frequency is below the atomic resonance frequency, the atom will scatter photons at a higher rate if it is moving towards the laser beam (V negative) than if it is moving away. The process is normally referred to as Doppler cooling. The time-averaged interaction can be separated into a mean cooling force, and a diffusive term, which accounts for the stochastic nature of the spontaneous emission. With laser beams striking the atom from six orthogonal directions, the only remaining force on it is the velocity-dependent part, opposing the motion of the atom. Thus, the atomic motion is strongly damped and the atomic vapour will be cooled. This arrangement of lasers is known as "optical molasses" and can be seen in figure 1.3, but with the magnetic coils added to make a magneto-optical trap (MOT) as discussed in the next section. In practice, there need only be three beams with retro-reflecting optics (mirror and quarter-wave plate) to provide the remaining three beam directions (figure 1.3).

1.2.4 Trapping atoms

The optical molasses is not itself a trap. This is because it is not possible to have optical potential minimum in a vacuum, as suggested by the equivalent of the

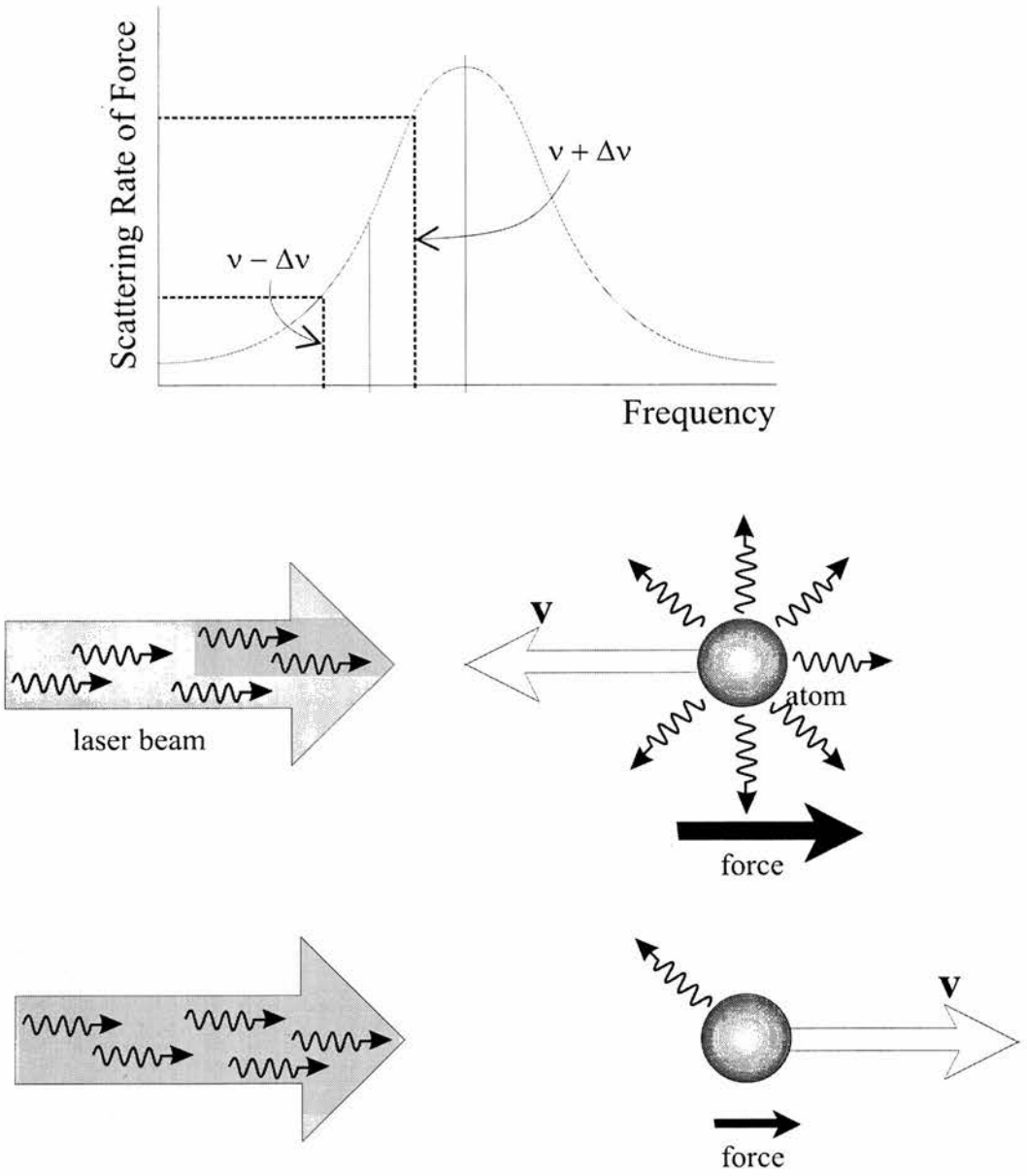

Figure 1.2: *Graph of the atomic scattering rate versus laser frequency. As shown, a laser is tuned to a frequency below the peak of the resonance. Due to the Doppler shift, atoms moving in the direction opposite to the laser beam will scatter photons at a higher rate than those moving in the same direction as the beam. Therefore, there is a larger force on the counter propagating atoms.*

electrostatic Earnshaw theorem[1]. The flow of optical energy cannot be directed inwards everywhere on the surface of the trapping region, implying that the force cannot be directed inwards everywhere either. Although it provides viscous damping, the atoms are free to diffuse around, and can escape the interaction region. It is therefore necessary to produce a potential well of some sort in space in which to keep the trapped atoms. In the magneto-optical trap [21], two anti-Helmholtz magnetic coils apply a spherical quadrupole magnetic field to the trapping region and the optical molasses is provided by circularly polarized light. The laser is tuned below resonance to provide cooling. The energy levels of the atoms are Zeeman shifted by the magnetic field, controlling the rate at which a particular atom scatters photons from the beams, and thus is pushed to one specific point in space. Therefore, not only does this hold the atoms in place, but it also increases their density since they are all being pushed to the same position. Figure 1.3 shows a magneto-optical trap.

Unfortunately, in a MOT, the atom density is limited by light assisted collisions between the atoms and by a radiation pressure exerted by a repumped atom on its neighbours. A way round this problem is to use a dark-spot MOT. This is made by excluding the repumping light from the centre of a magneto-optical trap. Atoms are thus optically pumped into the lower hyperfine state and no longer couple to the cooling light. The result is a dramatic reduction in the light-induced loss, giving trap densities of up to 10^{12} atoms/cm^3. The pumping rate depends on the excited state hyperfine splitting, since optical pumping into the dark ground state relies on off-resonant excitation of the second highest hyperfine level in the excited state. For the heavier alkaline metals (Rb and Cs), the splitting is 20 to 50 linewidths, so the dark-spot MOT requires an extra beam, close to resonance

[1]Earnshaw's theorem prohibits an electrostatic field from trapping a charged particle in a stable manner. The same is true for magnetic fields and monopoles.

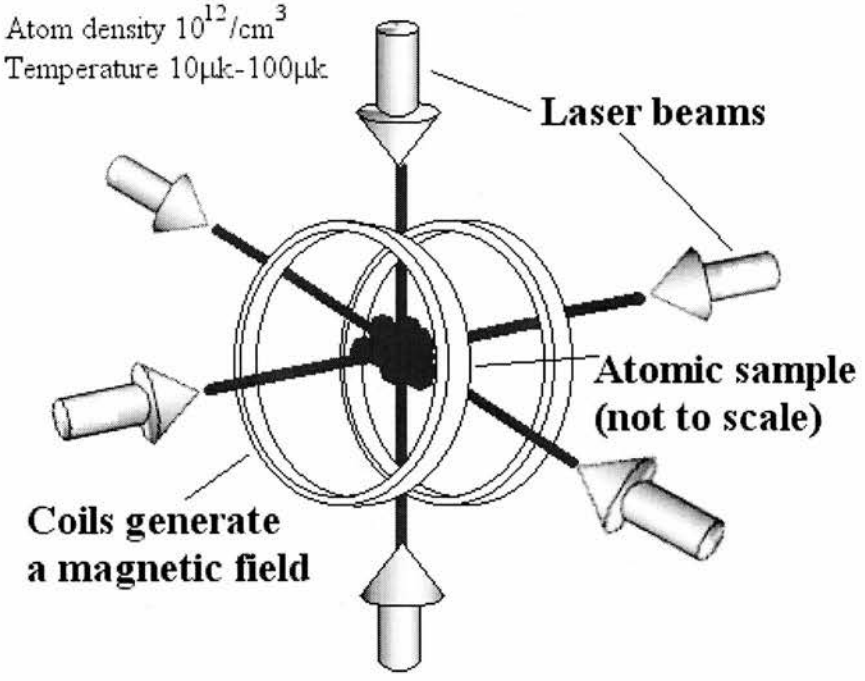

Figure 1.3: *Schematic of the MOT. Two coils with opposite currents produce a magnetic field which is zero in the middle and changes linearly along all three axes.*

with the second highest hyperfine level, to efficiently pump atoms outside the trap centre back into the ground state. A Laguerre-Gaussian beam, which is circularly symmetric and has radial index $p = 0$, consists of a ring in cross-section and would be a suitable source for this sort trap.

1.2.5 Sub-Doppler cooling & the Sisyphus effect

The first demonstration of optical molasses seemed to agree with the Doppler theory (which limits laser cooling to about several hundred μK, as given by $k_B T_D \equiv \frac{\hbar\gamma}{2}$). Later it was seen that the behaviour was not exactly as calculated. Surprisingly, the results were better than expected! It was decided that there must be more to optical molasses than Doppler theory. To understand the process it was necessary to drop the two simplifying assumptions of Doppler theory, the two-level nature of the atom and the pure state of polarisation of the light field. This led to a new sub-Doppler theory. Firstly, alkali atoms have several Zeeman sublevels in the ground state g, which are degenerate in the absence of external fields. They correspond to the possible eigenvalues of the projection of the total angular momentum on a given axis. These sublevels allow the important effect of optical pumping, which results in a particular distribution of populations (and coherences) in steady state among the various sublevels. This distribution depends on the laser polarization.

Another important element of the new cooling mechanisms is the existence of polarization gradients, which are unavoidable in three-dimensional molasses. Due to interference between the laser-beams, this polarization changes very quickly over one wavelength. This means that both the equilibrium population distribution and the light shift of the sublevels depends on the atom's position in the laser wave.

In the example of a one-dimensional molasses where the two counter propagating waves have equal amplitudes and orthogonal linear polarization., there would be strong polarization gradients. This is because the polarization of the total field changes continuously over one eighth of a wavelength, from linear to σ^+ (circularly polarized anticlockwise) to linear in the next $\lambda/8$, to σ^- (clockwise), and so on along the z axis of the stationary wave (Figure 1.4a). In the example of an atomic transition from the ground state with total angular momentum $J_g = 1/2$ to the excited state e with $J_e = 3/2$, there will be two Zeeman sublevels in the atomic ground state g (see Figure 1.4). Considering an atom at rest located at z=$\lambda/8$ with polarization there being σ^- (Figure 1.4), it can absorb a σ^- photon and jump from $g_{+1/2}$ to $e_{-1/2}$. From this state it can decay to $g_{-1/2}$ (or absorb another photon and 'try again' if it decays back to $g_{+1/2}$). However, if it absorbs a σ^- photon from $g_{-1/2}$ it will jump to $e_{-3/2}$, from which it can only decay to $g_{-1/2}$. Therefore, in the steady state, all of the atomic population is optically pumped to $g_{-1/2}$ (assuming that the laser intensity is low enough for the excited state population to be negligible). As shown on the energy level diagram in Figure 1.4, the σ^- transition from $g_{-1/2}$ is three times as intense as that starting from $g_{+1/2}$. The light shift Δ'_- of $g_{-1/2}$ is thus three times larger (in magnitude) than the light shift Δ'_+ of $g_{+1/2}$ (assuming the laser is red detuned to give negative light shifts). If the atom was at $z = 3\lambda/8$, where the polarization is σ^+, the previous conclusions are reversed. The population is all in $g_{+1/2}$ and the light shifts are such that $\Delta'_+ = 3\Delta'_-$. Finally, if the atom is at a point where the polarization is linear (e.g. $z = 0, \lambda/4, \lambda/2, \ldots$), symmetry shows that the two sublevels are equally populated and undergo the same light shift. This is all summarized in Figure 1.4b), which represents the light-shifted energies and the populations of the two ground state sublevels for an atom at rest in z.

The force on an atom at rest spatially obviously averages to zero, since the popu-

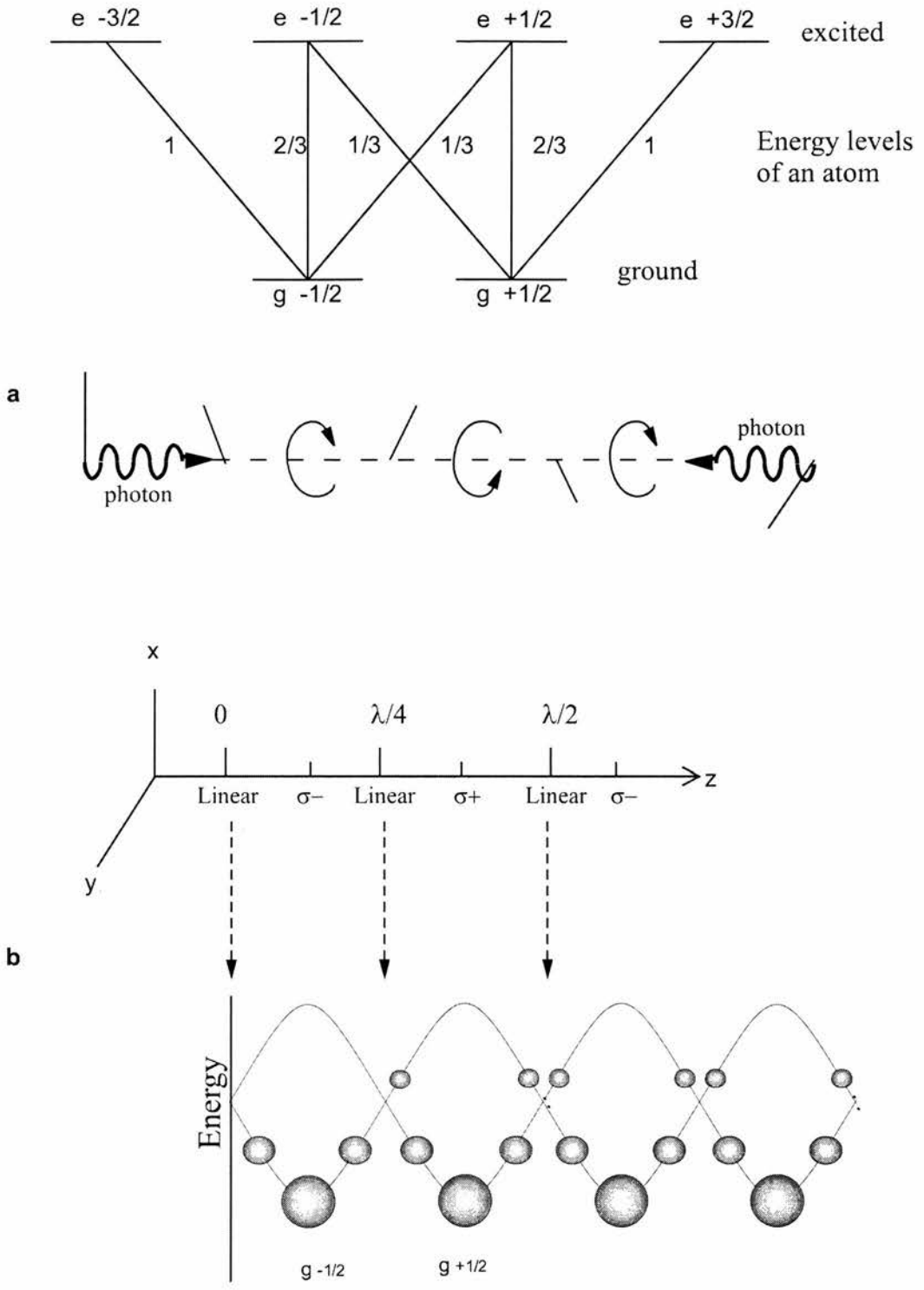

Figure 1.4: *Light shifts in a polarizing gradient. a)counter propagating laser beams with orthogonal linear polarizations; b)light-shifted energies and populations of the two ground-state sublevels of this atom, population is proportional to circle size.*

lation is symmetrically distributed around the 'hills' and 'valleys'. Upon moving, the atom disturbs this symmetry and an average friction force appears. Remembering that optical pumping takes a finite time τ_p to establish the population distribution, consider an atom moving to the right from point $z = \lambda/8$. Here the population is pumped into the bottom of a valley. If the velocity of the atom is such that it travels at least $\lambda/4$ during the time τ_p, then it will usually remain on the same sublevel and climb the potential hill. At the top of the hill, it is highly probable that it will be optically pumped to the bottom of the potential valley (at $g_{+1/2}$ in this case). From there, the same sequence can be repeated, so that like Sisyphus in Greek mythology, the atom always seems to be climbing potential hills, transforming part of its kinetic energy into potential energy. It is the time lag τ_p that is responsible for the new friction mechanism. The effectiveness of the mechanism remains even when the laser intensity is reduced, causing the time lag to grow longer.

1.2.6 Evaporative cooling - Bose-Einstein condensates [22]

To decrease the temperature of the trapped atoms still further, evaporative cooling is used. Originally suggested for cooling magnetically trapped hydrogen, this idea was applied with great success to trapped alkaline metal atoms. The principle is as follows. When two atoms of roughly the same energy collide, the final energies have a range of possible values. If the hotter atom can escape, the net effect after re-thermalisation is to leave the remaining sample cooler. For the evaporative cooling process to be sustained, there must be more than 100 elastic collisions per trap lifetime, otherwise the effect would be only velocity selection. To attain this threshold using laser cooling, the density or the trap lifetime must be increased. Since the density is capped (at $< 10^{12} cm^{-3}$) by the presence of

near-resonant light, the atoms can be transferred to a trap that does not rely on light scattering, i.e. a magnetic trap. Therefore the 'small' anti-Helmholtz coils may be turned off and much larger ones used to create a magnetic trap, with the lasers off. The atoms of a well defined (hot) energy can now be ejected by driving a radio-frequency (rf) transition to the anti-trapped state. In this way, Rb atoms have been cooled to 170nK for studying Bose-Einstein condensation [23]. The condition for this Bose-Einstein condensation (BEC) in a gas can be expressed in terms of the deBroglie wavelength λ_{dB} associated with the thermal motion of the atoms as

$$n\lambda_{dB}^3 \geq 2.612... \tag{1.1}$$

where n is the spatial density of the atoms. In effect, this means that the atomic wave functions are overlapping each other. Thus, what was seen as a cloud of many atoms becomes one 'super atom', a new state of matter unlike anything previously experienced.

1.3 Historical Perspective

1.3.1 Nobel Prize 1997

As mentioned in the introduction of this chapter, the Nobel Prize in Physics for 1997 was awarded for 'developments of methods to cool and trap atoms with laser light' to S.Chu, C.N.Cohen-Tannoudji and W.D.Phillips. This was of course the culmination of many years work for these men.

1.3.2 Experiments with cold atoms

Slow atoms are very useful for precision frequency measurements, following on immediately from the uncertainty principle. However, the experimental implementation of this is less straightforward. Zacharias suggested aiming a thermal beam upwards and detecting only atoms in the slow tail of the distribution (velocities <6m/s) in his 1954 proposal for an improved caesium frequency standard. This fountain geometry would not only allow interrogation times of order 1s, but the atoms would fall back under the influence of gravity and only one field region is needed because then atoms pass through it both on their way up and down. Unfortunately, collisions with the faster atoms effectively removed the slow tail. The first demonstration of an atomic fountain based on laser cooled atoms was performed in 1989 [30]. Figure 1.5 shows the layout of apparatus for this experiment. The system was set up to trap and cool a sample of sodium atoms and subsequently launch them with a velocity of 2-3 m/s. The central component was a magneto-optical trap, formed inside a large vacuum system. A thermal Na beam filled the trap using a chirped slowing technique (a fixed frequency laser with a frequency shift produced by a broad-band electro-optic modulator and repumping added by another modulator). The atoms were launched on ballistic trajectories by applying a short pulse of light, resonant with the $^2S_{1/2}, F = 2 \rightarrow ^2 P_{3/2}, F' = 2$ transition, entering from below. For a 3.6msec launch pulse, the atoms scattered around 80 photons to give an initial velocity of 2.4 m/s and a fountain height of 30cm. The atoms were detected by first pulsing the pump laser (1msec) to excite the atoms to the $^2P_{3/2}$ level, and then ionising them with a 10nsec, 25mJ pulse from another laser at 355nm. These ions were then detected on a microchannel-plate detector. A variable delay allowed the photo-ionising pulses to be fired anywhere within the 500msec free-flight time in the fountain. The groundstate hyperfine transition at 1.772 GHz was excited by the application of two short

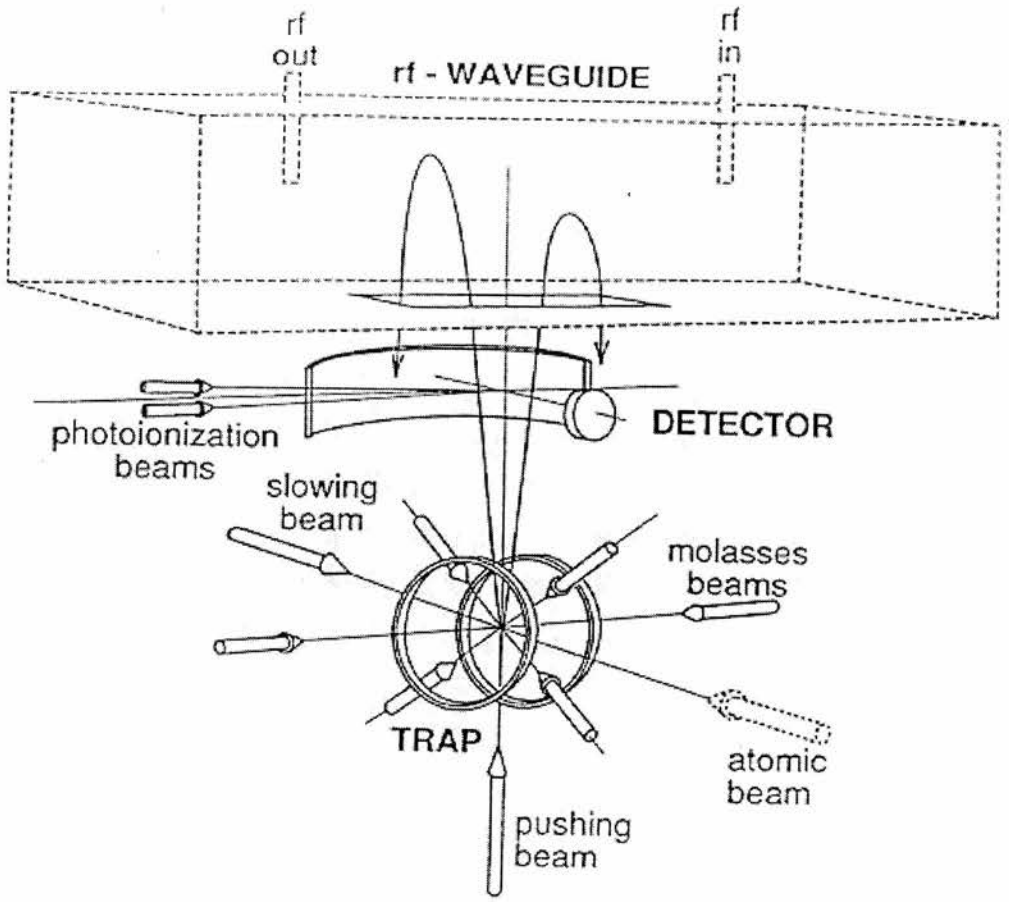

Figure 1.5: *Schematic diagram showing the experimental set-up used to produce a cold-atom fountain. The main components are the magneto-optical trap, the rf waveguide, and the detection region. From reference* [30]

$\pi/2$ rf pulses as the atoms were turning around inside a waveguide. For an integration time (between the two rf pulses) of ΔT=255ms, the expected linewidth, $\Delta\nu = 1/2\Delta T = 2Hz$ was observed.

Atomic interferometers of the Mach-Zehnder type can be made, based on stimulated Raman transitions [11]. This is related to the technique of Raman cooling, where a two-photon transition between two hyperfine levels in the ground state is used to select a narrow velocity class and push it towards zero velocity. Using two lasers separated in frequency by the hyperfine splitting, and tuned well below the excited state, a two-photon Raman transition is induced between the groundstate hyperfine levels, $|1>$ and $|2>$. If an atom initially in state $|1>$ is excited by a $\pi/2$ Raman pulse, the output is a coherent superposition of $|1>$ and $|2>$. If the lasers are counter propagating, the excited hyperfine component receives a momentum kick, $\sim 2\hbar k$. Thus, a $\pi/2$ pulse acts as a 50:50 beamsplitter. For a π pulse, atoms are transferred from $|1>$ to $|2>$ or vice versa, and momentum is transferred, simulating a grazing incidence mirror. A Mach-Zehnder interferometer can therefore be formed by a $\pi/2$ - π - $\pi/2$ pulse sequence. The output (i.e. state $|1>$ or $|2>$)depends on the relative phases of the interfering wavepackets and the $\pi/2$ Raman pulses. By directing the beams vertically, the Mach-Zehnder interferometer can be used to measure the acceleration due to gravity, g. While travelling through the interferometer, one wavepacket is, on average, at a higher gravitational potential than the other is, which appears as a phase shift. A sensitivity of $\Delta g/g = 3 \times 10^{-8}$ with $\sim$30 minutes integration time has been demonstrated by Kasevich *et al* [11].

1.4 Guiding of Cold Atoms

1.4.1 Introduction

Now that there is a ready source of cold trapped atoms, a beam of atoms can be tapped off. This can be done by drilling a hole in one of the reflecting optics of the trap [24]. With no light incident from this direction (in a small area), the atoms can escape out into a diverging beam. See figure 1.6. A 'plug' beam can

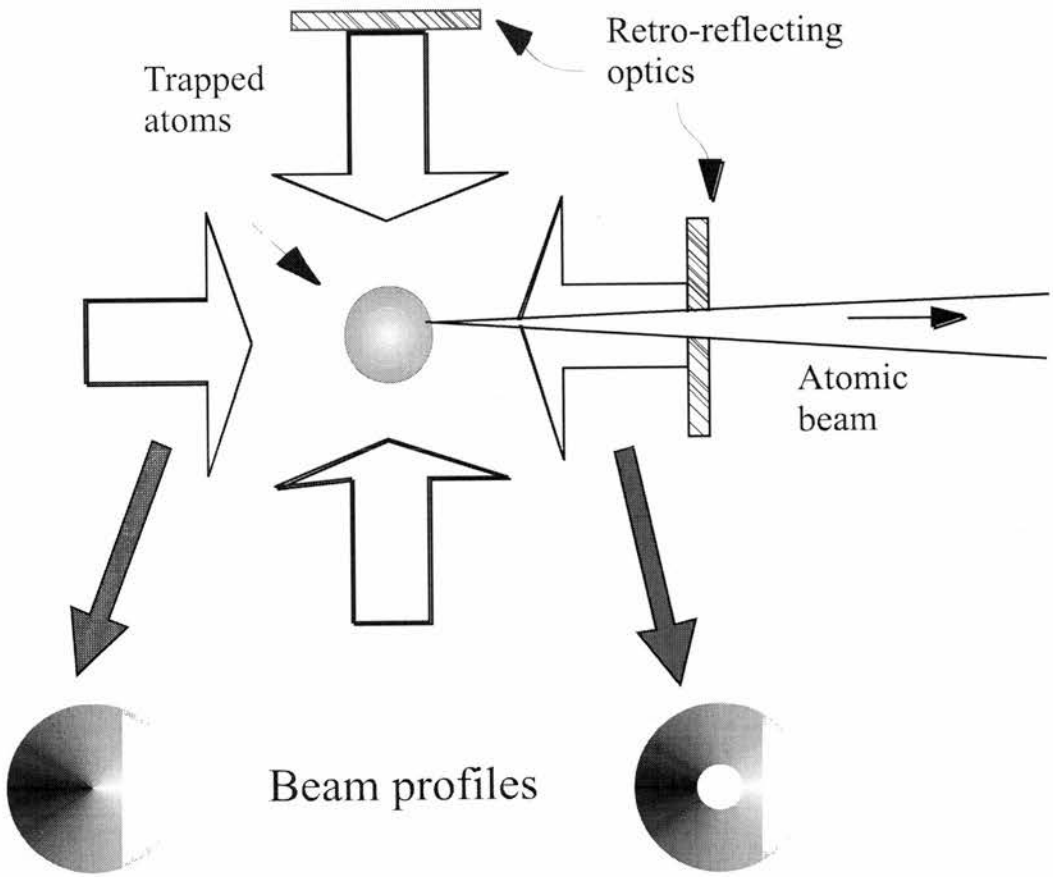

Figure 1.6: *Method for extracting an atomic beam from the atom trap*

be used to stop atoms from escaping until required. This would be a laser beam at the trapping frequency and crossing the atomic beam path within the trap. It directs the atoms from the 'escape path' back into the trapping laser beams and

thus back to the centre of the trap.

1.4.2 Why guide atoms?

Fibre-guided atoms may facilitate many atomic physics experiments. For example, atoms could be extracted from a low-quality supply chamber and transported to an ultra-high vacuum analysis chamber. This can also be used to separate isotopes, since each isotope can be frequency selected. The losses from transverse momentum diffusion in evanescent mirror cavities can be eliminated by the transverse confines of a fibre guide. Also, atoms can be manipulated and probed optically through the fibre walls without the constraints of a cumbersome vacuum enclosure. Another prospect is brought about by the guiding of cold atoms in fibres, since at low temperatures the atomic de Broglie wavelength becomes comparable to the transverse dimensions of the hollow core. The atoms thereby propagate in modes much like the optical modes of conventional fibres, giving the possibility of fibre-atomic interferometry in analogy with fibre-optic interferometry.

1.4.3 Laser Guiding - the dipole force

It is now useful to guide this atomic beam, for example down a hollow core fibre. However, the atoms are likely to stick to the fibre walls, due to the Van der Waals forces between atom and wall. This force increases greatly as an atom approaches the wall. To overcome this problem, the outer annular glass region of the fibre is filled with laser light that repels the atoms from the walls by the dipole or 'gradient' force. This works on the idea that light has linear momentum equal to $p = h/\lambda$, and also exerts a radiation pressure.

Any atom placed in a near-resonant laser field will either be attracted to or repelled from regions of high intensity, depending upon whether the laser is detuned below or above the atomic resonance frequency. This can be used to stop atoms from sticking to the side of a hollow glass fibre, for example. The effect is due to the dipole force. See figure 1.7, which shows a microscopic sphere in a light beam with an intensity profile as depicted. The relative refractive index between the particle and the medium , n, dictates how light is diffracted as it passes through the sphere. If n is greater than 1, the light is refracted towards the centre of the sphere, changing direction and gaining momentum in the +z direction. It didn't have any momentum in this direction initially, so to conserve momentum the sphere moves towards the higher light intensity. The opposite will happen for a sphere of $n < 1$, using a similar argument.

To apply this argument to atoms, the Kramers-Kronig relations can be used to define refractive index around an atom's absorption frequency. Figure 1.8b) shows this, with figure 1.8a) being the feature given when atoms absorb light. It can be seen that depending on whether the laser frequency is above or below the atom's absorption frequency, the atoms will have a refractive index greater or less than one.

The fundamental concepts [25] are as follows. An atom interacting with a near-resonant inhomogeneous laser field experiences a ponderomotive energy shift given by:

$$U(\rho) = \frac{\hbar\Delta}{2k_B} ln\left(1 + \frac{2[\Omega(\rho)]^2}{\Delta^2 + \gamma^2}\right) \tag{1.2}$$

where $\Delta = \omega_L - \omega_0 - k\nu_z$ is the laser detuning from resonance and $k = 2\pi/\lambda$. $\Omega(\rho) = dE(\rho)/\hbar$ is the atomic Rabi frequency in the presence of an oscillating electric field, d is the atomic transition dipole moment, and γ is the spontaneous decay rate. The potential has been written as an equivalent temperature, as

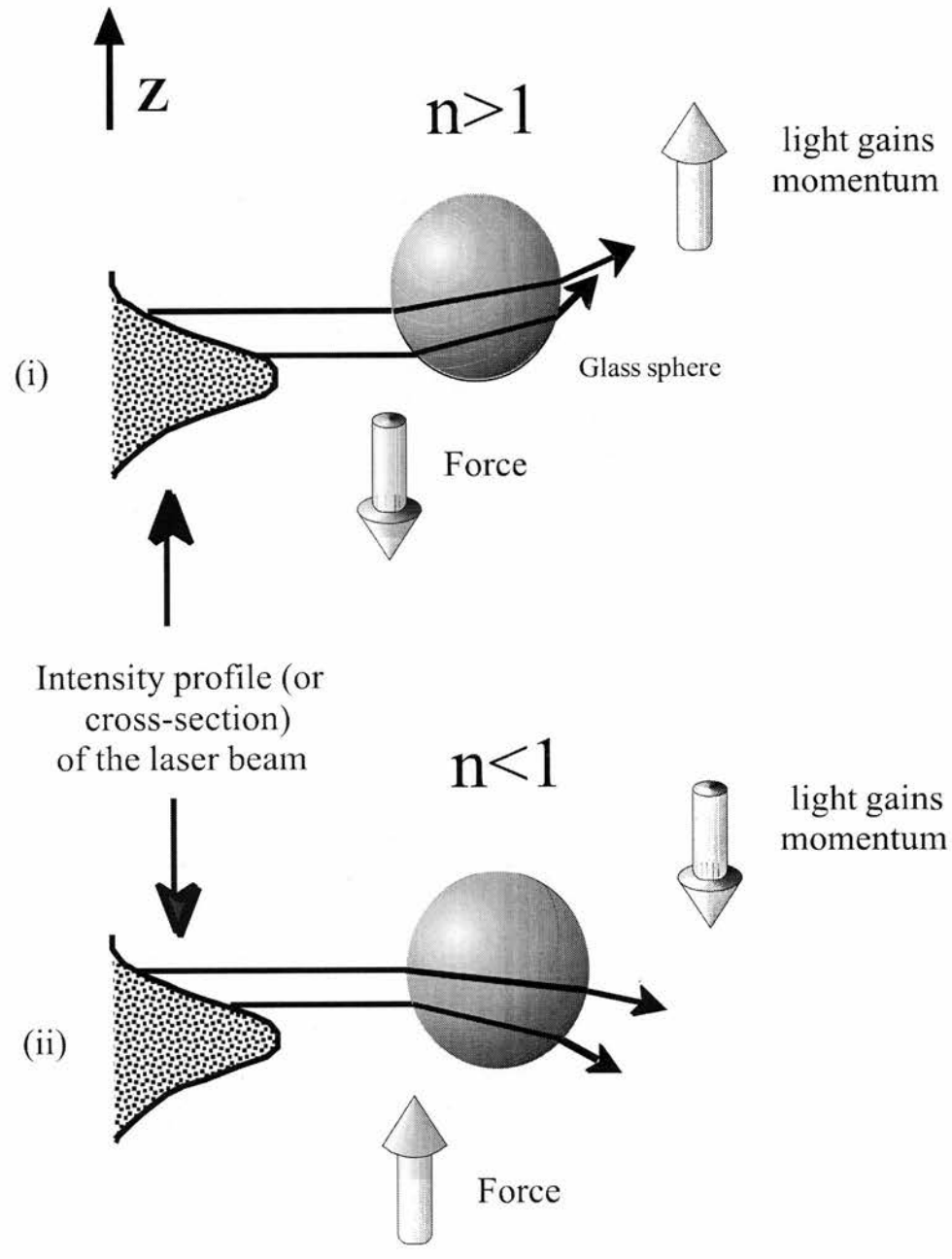

Figure 1.7: *The dipole force*

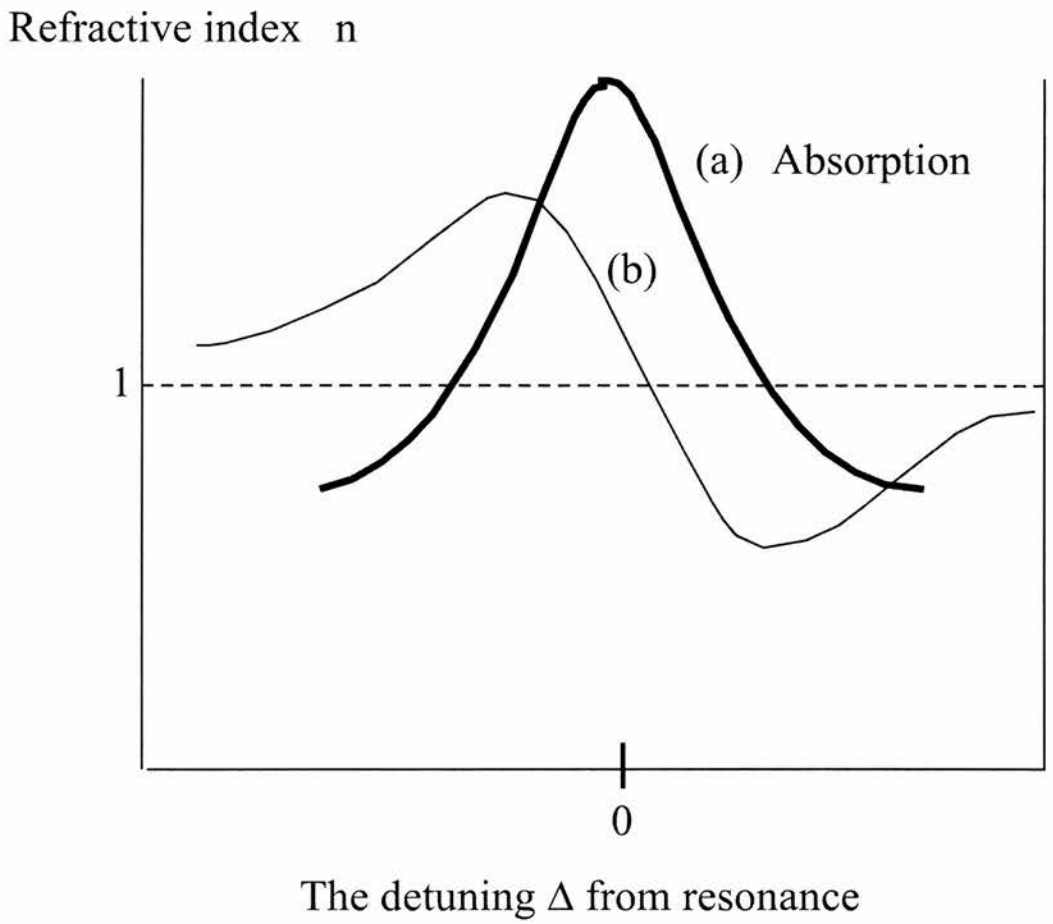

Figure 1.8: *a)Atomic absorption plotted against frequency of incident; b)refractive index*

indicated by Boltzmann's constant k_B. For large detuning from resonance and weak fields, equation 1.2 reduces to the familiar form $U(\rho) = \hbar\Omega^2(\rho)/\Delta k_B$. With positive detuning from resonance (blue-detuning), the positive potential shift acts to repel atoms from high-intensity regions. Conversely, atoms are attracted to high-intensity regions of light having negative detuning from resonance (red-detuning). Atoms move to minimize their energy in the light field gradient.

The Van der Waals potential between wall and atoms is given by

$$U_{VdW} = -\frac{1}{4\pi\epsilon_0}\left(\frac{\epsilon - 1}{\epsilon + 1}\right)\frac{\langle g|d^2|g\rangle}{8k_B x^3} \tag{1.3}$$

where ϵ is the dielectric constant, $\langle g|d^2|g\rangle$ is the matrix element of the square of the dipole operator, and x is the distance from the wall. The effective potential, given by the Van der Waals and evanescent potentials (see blue-detuned light explanation) is everywhere attractive for small intensities. The intensity above which an atom will experience a positive potential is called the threshold intensity. Slightly above threshold the potential is positive throughout the hollow region, except very close to the wall where the Van der Waals potential dominates. Just above threshold the potential exceeds zero at a distance $x = 3/2k$ from the fibre wall and occurs when $U_{ev}(0) = 10^{-4}K$. The corresponding intensity threshold is $I_{th} \sim 10^5 W/m^2$ for a 1GHz detuning from resonance.

Red and blue guiding; evanescent waves

This was first suggested by Ol'Shanii *et al* in 1993 [12], and independently by Savage *et al* [13,14]. Both used slightly different approaches. Ol'Shanii suggested guiding atoms along light beams propagating through the hollow central region of a fibre (red-detuned guiding). Savage, on the other hand, discussed filling the outer (glass) region of a fibre with light and repelling atoms from the walls

using evanescent waves leaking into the hollow region (blue-detuned or evanescent guiding).

Red-detuned light (whose frequency is lower than resonance) can be sent down the centre of the hollow region and atoms will be attracted to the beam and away from the walls, as given in the above theory. However, there are several reasons why this might be undesirable. Firstly, since the atoms are in the laser beam, they will gain energy from it as they scatter photons from it and recoil randomly in the process. Since the aim if this research is to guide *cold* atoms, then this would partially defeat the object. Also, the light is coupled into grazing incidence modes which are leaky, having an intensity attenuation length $L_e \simeq 2.4a^3/\lambda^2 = 3.8mm$, where $a = 10\mu m$. The guiding beam would therefore not be present after a short distance (a few centimetres) and the atoms would again be free to stick to the walls. Since the attenuation length scales as the radius cubed, this is a severe limitation on using small-diameter long fibres, which are practical in laser guiding.

Blue-detuned light (whose frequency is higher than resonance), however, can be coupled into the glass part of the fibre, where it propagates in lossless guided modes. The glass surface surrounding the hollow region will have an evanescent light field. Atoms will be repelled from the high-intensity-field region near the fibre wall. This intensity is significant at a distance of $\sim \lambda/2\pi$ into the hollow region. The atoms are thus nearly specularly reflected from the potential walls. The atom beam can therefore propagate through the fibre in a manner similar to that of light in a multimode, step-index fibre. See figure 1.9, which shows blue-detuned or evanescent guiding. This type of guiding has several advantages over red-detuned guiding. There is very little heating of atoms due to spontaneous scattering of photons, since the atoms spend most of the time in a dark region away from the high intensity at the wall. Also, the light travels in lossless modes

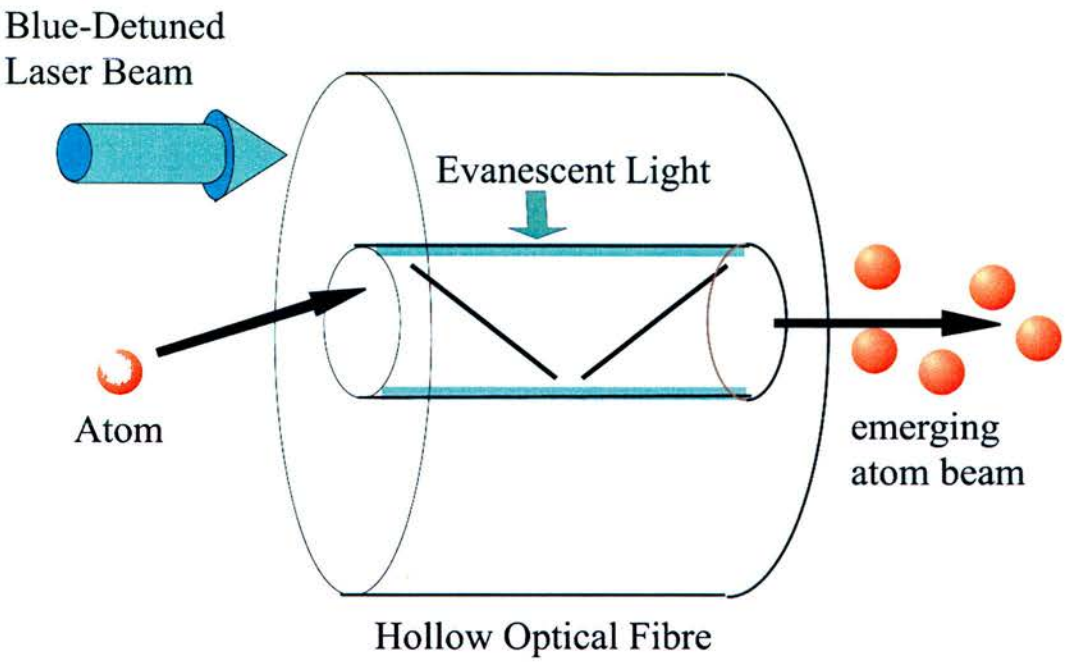

Figure 1.9: *Blue-detuned or Evanescent atom guiding in a hollow fibre*

with no adverse effects due to small-diameter long fibres, contrasting with the red-detuned case.

In blue-detuned guiding, typically some of the laser light scatters from the fibre and couples into grazing incidence modes in the hollow region. A small amount of light in the hollow region can easily dominate the evanescent portion and drive the atoms to the walls. A rough estimate of the mode-matching constraints is obtained by assuming that efficient guiding is possible only when the laser intensity at the wall exceeds the intensity coupled into the EH_{11} grazing incidence mode by approximately a factor of 10. The scattered light must therefore be reduced to 0.05% or less in a fibre with a $144\mu m$ outside diameter and a $20\mu m$ inside diameter. The problem can be alleviated by using a second laser to escort atoms through the spatial transient region where the evanescent potential is dominant. This escort laser is coupled into the lowest order EH_{11} grazing incidence mode and red-detuned from atomic resonance. The atoms are thus attracted to the high-

intensity region along the axis and initially guided into the fibre. Since these grazing incidence modes are leaky (as shown in the discussion of red-detuned guiding above), the escort beam and scattered blue-detuned beam both decay within a few centimetres of the fibre input. Atoms with the highest transverse energy will be lost from the atomic beam as the escort potential decays. However, with the evanescent potential present, these atoms may be retained and guided through the remaining distance. In this way, atoms are escorted by the red-detuned laser into the region where only an evanescent potential exists [25].

There are several ways of coupling light into the fibre. Figure 1.10a) shows the use of a polarizing beam-splitter (PBS) in order to couple both escort and 'evanescent' laser beams. Figure 1.10b) shows a fibre with a critically angled end plane enabling light to be coupled from an orthogonal direction.

It would be useful to have a laser beam with a hollow centre (with a torus cross-section) for either coupling into the glass part of a hollow-core fibre, or guiding an atomic beam alone. Laguerre-Gaussian (LG) beams can fulfil this criterion. The LG_p, l beams possess orbital angular momentum along the optical axis when l is not zero, where p and l are the radial and azimuthal indices of the LG modes [27, 28]. Also, the $LG_{p,l\neq 0}$ beams have a spiral phase structure, so that the phase is undefined on the optical axis, where radiation intensity must be zero. A certain class of LG beams, $LG_{0,l\neq 0}$, in cross section has a dark spot enclosed by a bright ring. This intensity distribution in conjunction with the optical dipole force provides a line of potential extremes along the optical axis. It is also useful to use these LG beams in a dark-spot MOT [29] as mentioned above. Laguerre-Gaussian beams are discussed in chapter 4.

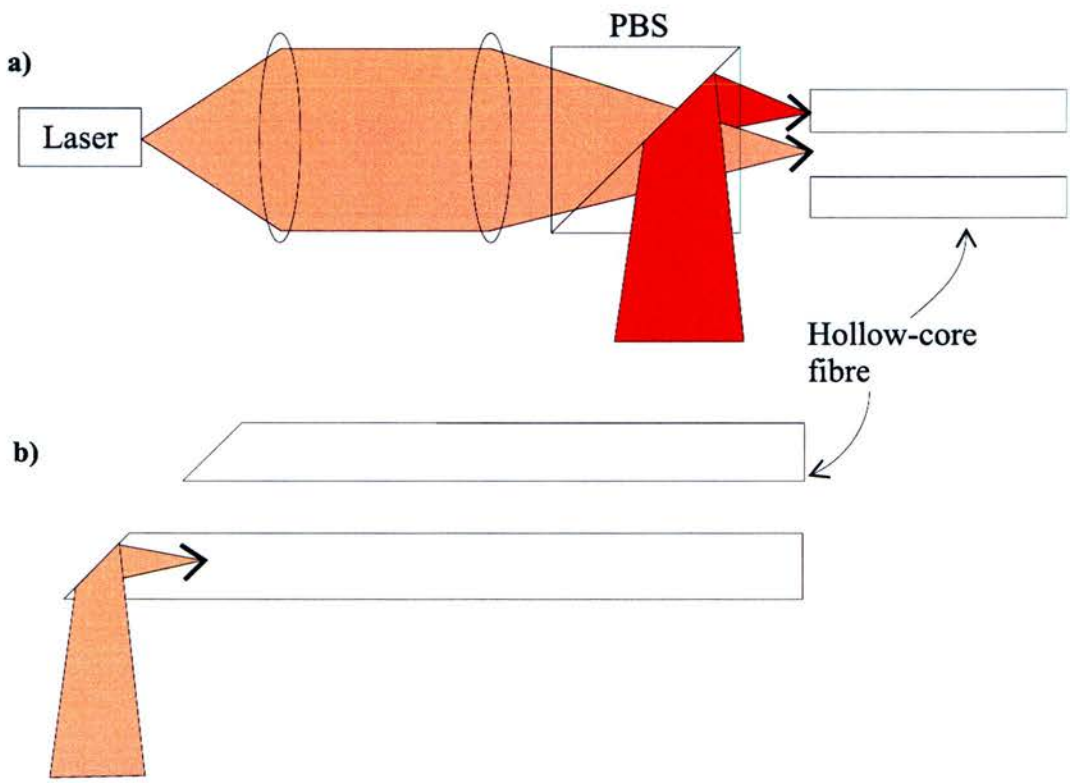

Figure 1.10: *a)Optical coupling with escort and 'evanescent' laser beams combined on a polarizing beam-splitter (PBS) and separately focused onto the fibre's hollow and glass regions; b)Critical angled fibre end plane, allowing coupling of light from the side.*

1.4.4 Spectroscopy & Atom interferometry

Renn and co-workers used red-detuned guiding in their experiments [26]. In their study in 1995, two separate vacuum chambers were connected by a 3.1cm long hollow-core fibre with a hole diameter of $40\mu m$. Light from a Ti:Sapphire standing wave laser was coupled primarily into the EH_{11} mode with an aspheric lens. The coupling efficiency was measured to be 50%, with an attenuation loss of 7% every centimetre of the fibre for the EH_{11} mode. Rubidium vapour was created in one chamber by heating rubidium metal. The guided atoms were detected by surface ionization on a heated platinum or rhenium wire in the second chamber. A channeltron electron multiplier detected the resulting ions which were recorded with a pulse counter. The zero point of the laser detuning, δ, was taken to be the average transition frequency of the $5s_{1/2}(F) - 5p_{3/2}(F')$ multiplet of ^{85}Rb and ^{87}Rb. It was noted that there was a particularly striking sharp turn-on of the guided atom signal. The signal rose to half maximum at $\delta \approx -2GHz$ and full maximum at $\delta \approx -3GHz$. For any larger detunings, the guided atom signal fell off approximately as δ^{-1}, as expected from an expansion of equation 1.2. However, by increasing the intensity the signal increased and the position of maximum flux shifted to larger negative detunings. It was noted that transverse heating of the atoms by spontaneous scattering of photons limited the distance that atoms would be guided through fibres. However, since the scatter rate falls from the saturated value as Δ^{-2} while the potential scales as Δ^{-1}, the guidance distance can be extended by detuning the laser farther from resonance.

The JILA group have also experimented with the evanescent guiding method [25]. The apparatus was similar to their red-detuned guiding work, with two vacuum chambers connected by a short (3cm) hollow glass fibre. Thermally produced rubidium vapour was again present in the first chamber. 500mW laser

light was coupled into the fibre at the entrance using a polarizing beam splitter. Unfortunately, some of the guiding laser light leaked into the hollow region and excited blue-detuned grazing incidence modes in the hollow region. As discussed previously, this would repel atoms onto the walls, since its effect is stronger than any evanescent potential. The group used a second, ~19mW escort laser to circumvent this problem, as descrbed above. They then proceeded to show that there was a threshold effect for the guiding that was indicative of the light potential required to overcome the attractive van der Waals interaction.

Ito *et al* performed spectroscopy of guided atoms in 1996 [31]. A Rb beam was guided in hollow fibres by blue-detuned laser light. The long-range dispersive properties of dipole interaction between guided atoms and evanescent waves was shown. Guidance efficiency was estimated to be above 40%. With proper frequency detuning of the guide laser, in-line spatial separation of two stable isotopes of Rb were realized. The experiment was performed using a thermal beam of Rb guided down a fibre of 3cm in length by a Ti:Sapphire laser. For the spectroscopy, the two-step photoionization technique of overlapping two lasers near the exit of the fibre was used. The ions thus produced were detected by a channel electron multiplier.

In a later experiment (1997), Ito *et al* demonstrated the use of guided atoms as a novel scheme of optical atom deposition [32]. By measuring the spatial distribution of the guided atom flux with a hot-wire detector, it was shown that micron-sized structures with nanometre depth on a substrate could be fabricated. Precise control of the deposition rate with a $1.4\mu m$ hollow fibre was illustrated with the technique of photoionization spectroscopy mentioned above. It was seen that tilting the fibre slightly enhanced the ration of guided atom flux relative to the background transmission.

1.4.5 Magnetic guiding

Another method of confining and guiding atoms is to use magnetism. The first time that a tubular magnetic guide was employed was in Friedburg and Paul's experiment [33] of 1951. Six bars carrying several hundred ampères each were used to produce a large hexapole field such that the gradient focused a beam of atoms by deflecting them towards the axis. The focal length was velocity dependent, but by varying the current in time a pulsed achromatic focusing was possible. Permanent magnets were later used in the same way. The magnitude of the magnetic field within the hexapole increases quadratically with distance from the axis. The solution of Laplace's equation in cylindrical coordinates shows this quite well, giving a magnetostatic potential conveniently expanded in multipole terms of the form:

$$\Phi_n \propto r^{n-1} \cos(n\theta). \tag{1.4}$$

Near the axis, the lowest multipole dominates, which for a six-pole array is given by the magnetostatic potential Φ_3, giving a magnetic field of magnitude $B_3 \propto |\nabla \Phi_3| \propto r^2$. Choosing the right shape for the pole faces will cause higher multipoles to be suppressed. This field structure will cause any atom with a linear Zeeman shift to oscillate around the axis in the harmonic confining potential thus formed. The acceptance of such a magnetic guide is limited by the field strength near the pole tips to an angle of approximately $(\mu_B B/k_B T)^{1/2}$, which is usually about 10 mrad. However, with the thermal energy of atomic beams being reduced by six orders of magnitude using laser cooling, it is now possible to make guides, using only modest magnetic fields, which can completely contain the atomic beam. This was demonstrated by Meschede's group, using permanent rare-earth hexapole magnets [34]. It has even been possible to guide cold atoms using simple kitchen refrigerator -magnets! [35] M.Key *et al* [36] produced a miniature waveguide by embedding four current-carrying wires in a silica fibre. In the

25mm-long tube were drilled five parallel holes, running the length of the fibre. Figure 1.11 illustrates the guide. Each hole had a radius of $261\mu m$. The central,

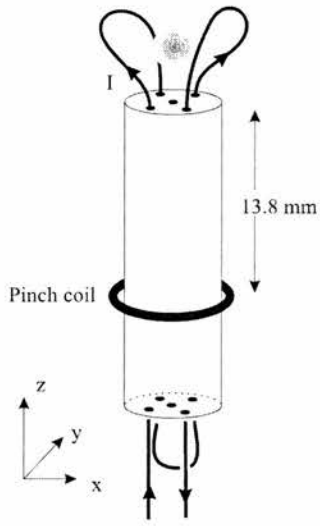

Figure 1.11: *Schematic view of the quadrupole guide. A cloud of cold atoms falls into the central hole where it is guided down to the pinch coil, reflected, and guided back up to the top. The diameter of the guide is greatly exaggerated.*

on-axis hole was for transporting atoms, whilst the outer ones, at the corners of a $1044\mu m$ ($a = 522(10)\mu m$) square, contained copper wires carrying a current I and thus producing a magnetic field. The magnetic field vector is a good approximation to a quadrupole, i.e. $\mathbf{B} = (B'x - B'y)$ with $B' = \mu_0 I/\pi a^2 = 1.46(6)I$ T/m. At the top of the guide, the wires spread out to form a magnetic funnel (of apex angle $\sim 90°$). By wrapping a "pinch coil" around the outside of the fibre, a field could be added in the z direction to close off the guide. Atoms cooled in a standard MOT were in the form of a $T = 23\mu K$ cloud with rms radius $\sigma = 0.72mm$, which was optically pumped into the $(F = 3, m_F = 3)$ ground-state sublevel relative to a uniform magnetic field $B_x\hat{\mathbf{x}}$. As the atoms fell into the dark region, $\mathbf{B}_x$ was reduced to zero and the guide current turned on adiabatically. The centre of the pinch coil had a field of $40G$, the atoms travelling down the guide were seen to have been reflected to re-emerge from the entrance

aperture using a $2ms$ pulse of laser light and a CCD camera. The fact that the atoms were reflected and rose to their original height demonstrated that they had indeed been guided. With a total drop height of $2.38cm$, the round-trip time of $139ms$ indicated that the vertical motion was close to free fall, with the atom's velocity being approximately $45cm/s$ near the top and $65cm/s$ near the bottom. It was also measured that funnel gave an optimum coupling efficiency of 11% (for a guide current of $4.68A$. Any higher current, and hence field strength, would narrow the funnel aperture and reduce coupling efficiency. Conversely, as smaller current (and field) would not overcome the centrifugal force of the atoms around the guide at the wall.

In a proposed guide [37] similar in cross-sectional potential to the previously mentioned blue-detuned/evanescent hollow-fibre guide, two helical solenoids could be interleaved on the same radius and carry equal but opposite currents. This would generate a low field in the centre, which would rise exponentially near the walls at a rate determined by the pitch of the windings.

In another scheme, it possible to use the magnetic field around a current-carrying wire, which increases towards the wire as r^{-1}. This geometry will hold high-field-seeking atoms in Kepler orbits around the wire, kept at small radii by the angular momentum barrier [38]. Although this has been demonstrated in the laboratory [39], it hasn't been widely used because of the inconvenience of having the wire along the beam axis.

Hänsel *et al* used a microscopic magnetic strip (or 'magnetic conveyor belt' [40]) on a chip to form a Bose-Einstein condensate (BEC) and transport it [41]. A sample of laser-cooled atoms is provided, less than 1mm above the substrate surface, using a mirror-MOT (see chapter 5). This enables an *in situ* transfer into the magnetic microtrap. By rapidly increasing the external bias field $\mathbf{B}_y$, a

strong compression occurs in the transverse (y,z) plane, with very little change longitudinally. Following this, immediately the atoms are evaporatively cooled, which reduces the number of atoms by a factor of ten. BEC can now be attained by either reducing the external field $\mathbf{B}_0$, causing a trap decompression and an elongated condensate, or the wire currents can also be modified to move the trap centre position and give a more spherical condensate. By now modulating the currents periodically in the two wires, with a relative phase shift of $\pi/2$, the BEC is 'conveyed' over a distance of 1.6mm along the chip surface. The expanding cloud was seen to have the bimodal distribution of a BEC even after transport, which bodes well for applications like trapped-atom interferometry with condensates.

Ed Hinds speculated in his Physics World article [42] that the development of atom chips and evaporative cooling had brought us close to being able to build quantum circuits wherein cold atoms flow and interact within the guides and traps of the device. Such a chip is Hänsch's variation of the magneto-optical trap, the "mirror-MOT" [43]. Atoms are cooled and trapped just above the surface of a chip using laser cooling and large magnetic coils (see chapter 5). Once the atom cloud has formed, these coils are switched off and a magnetic field produced instead by the currents on the chip. A coarse U-shaped loop brings the atoms from the mirror-MOT to the surface, where they encounter traps and guides formed by thinner wires. A bias field added to that generated by the current in the wire forms the main guide. "Pinch wires" perpendicular to the central wire create a field along this guide that is able to push atoms away from the ends, in a similar way to that described in the previous paragraph. Two further wires in a 'square-wave' pattern enable to the atoms to be guided along the main guide when given alternating currents out of phase by 90°. This 'motor' has been used to carry out collision experiments in the main guide. Ed Hinds states in his article that a

simple quantum circuit might be such an atom guide that splits a single beam of atoms into two beams and then recombines them. The groundstate wavefunction breaks into two parts at the split. When recombined, the final state of the atom cloud depends on the phase difference accumulated by the de Broglie waves along each path. If there is no phase difference, then the atoms recombine in the ground state of the guide. However, a phase difference of π will cause the two parts to recombine to form the first excited state. This kind of interferometer would be exceptionally sensitive to slight differences in gravitational fields between the arms, or rotations, which would be useful in oil and mineral prospecting or navigation. If Bose-Einstein condensates were used in quantum circuits, it is expected that the BEC would behave like a frictionless macroscopic fluid. This would thus be similar to the current in a superconductor, so that effects such as Josephson junctions and superconducting quantum interference devices (SQUIDs) might be seen in analogues with BECs. Quantum computers become more of a possibility with atom chips, when each atom suspended above the chip can store a quantum bit or "qubit" that can represent logical 0 and 1 simultaneously. Using an array of n qubits, any or all of the numbers between 1 and 2^n can be stored at the same time. These so-called entangled states would allow a quantum computer to perform an astronomical number of calculations simultaneously.

1.4.6 Comparison of laser vs. magnetic guiding

In a hollow fibre guiding system with a fibre radius of R, the energy required for quantum confinement is $\hbar^2/2mR^2$. Using rubidium as an example in a tube of $1\mu m$ radius, the energy is equivalent to a temperature of 3nK, which is far below the photon recoil temperature. Therefore, for more likelihood of achieving single-mode propagation of the de Broglie wavelength it might be better to consider

multipole guides, where the atoms can be held by the curved potential. The diameter of the physical opening can also be much larger than the size of the ground-state wavepacket.

However, using funnel-shaped (focused) light beams with a hollow centre, the physical entrance to either hollow-fibre guides or hollow-beams can also be large. Light beams cannot have a dark region as small as hollow fibres can be, since light is diffraction limited to diameters of $lambda/2$ where $lambda$ is the wavelength. For this reason, it might sometimes be better to use magnetic guiding.

The physical manufacture of any device can always have its problems. Thus uniformity of wires and other devices for magnetic guides will always be open to error. With light, though, once the beams have been produced, they will propagate in straight lines (assuming there are no nearby large gravitational forces!). This can make hollow light beams more reliable in some cases. Also, a current passing down a wire will produce some heat, however minimal, which could be transferred to guided atoms, and when working with cold atoms that is not ideal. Although atoms can be heated by random recoils in a light field, most cold atoms schemes use dark regions so this is less likely to happen. On the whole, optical and magnetic guiding can be seen as complementary in many cases.

Bibliography

[1] T.Hänsch, A.Schawlow, Opt.Commun. **13**, 68 (1975)

[2] Physics Today, June 1987, p34

[3] K.Dholakia, Contemp.Phys. **39**, 351 (1998)

[4] C.S.Adams, E.Riis, Prog.Quant.Electron. **21**, 1 (1997)

[5] S.L.Gilbert and C.E.Wieman, Optics and Photonics News **4**, 8 (1993)

[6] C.E.Wieman, G.Flowers and S.Gilbert, Am.J.Phys. **63** (4), April 1996

[7] E.L.Raab, M.Prentiss, A.Cable, S.Chu and D.Pritchard, Phys.Rev.Lett. **59**, 2631 (1987)

[8] A.M.Steane, M.Chowdhury and C.J.Foot, J.Opt.Soc.Am.B **9**, 2142 (1992)

[9] D.Sesko, T.Walker and C.E.Wieman, J.Opt.Soc.Am.B **8**, 946 (1992)

[10] C.Monroe, W.Swann, H.Robinson and C.E.Wieman, Phys.Rev.Lett. **65**, 1571 (1990)

[11] M.Kasevich and S.Chu, Phys.Rev.Lett. **67**, 181 (1991)

[12] M.A.Ol'Shanii, Yu.B.Ovchinnikov, V.S.Letokhov, Opt.Comm. **98**, 77 (1993)

[13] C.M.Savage, S.Marksteiner, P.Zoller, In '*Fundamentals of Quantum Optics III: Proceedings of the fifth meeting on laser phenomena*, University of Innsbruck (F.Ehlotzky, Ed.), p60, (Berlin: Springer-Verlag)

[14] S.Marksteiner, C.M.Savage, P.Zoller, S.L.Rolston, Phys.Rev.A **50**, 2680 (1994)

[15] K.Gibble and S.Chu, Phys.Rev.Lett. **70**, 1771 (1993)

[16] D.S.Weiss, B.C.Young, S.Chu, Phys.Rev.Lett. **70** 1771 (1993)

[17] C.S.Adams, M.Sigel, J.Mlynek, Phys.Rep. **240**, 143 (1994)

[18] R.J.Celotta, R.Gupta, R.E.Scholten, J.J.McClelland, J.App.Phys. **79**, 6079 (1996)

[19] Harold J.Metcalf & Peter van der Straten, "Laser Cooling and Trapping," Springer (1999)

[20] K.Lindquist, M.Stephens and C.E.Wieman, Phys.Rev.A **46**, 4082 (1992)

[21] J.Lawall, S.Kulin, B.Saubamea, N.Bigelow, M.Leduc, C.Cohen-Tannoudji, Phys.Rev.Lett. **75**, 4194 (1995)

[22] C.N.Cohen-Tannoudji, W.D.Phillips, Phys.Today, October 1990, 33

[23] M.H.Anderson, J.R.Ensher, M.R.Matthews, C.E.Wieman, E.A.Cornell, Science **269**, 198 (1995)

[24] Z.T.Lu, K.L.Corwin, M.J.Renn, M.H.Anderson, E.A.Cornell, C.E.Wieman, Phys.Rev.Lett. **77**, 3331 (1996)

[25] M.J.Renn, E.A.Donley, E.A.Cornell, C.E.Wieman, D.Z.Andrerson, Phys.Rev.A **53**, 648 (1996)

[26] M.J.Renn, D.Montgomery, O.Vdovin, D.Z.Anderson, C.E.Wieman, E.A.Cornell, Phys.Rev.Lett. **75**, 3253 (1995)

[27] L.Allen, M.W.Beijersbergen, R.J.C.Spreeuw, J.P.Woerdman, Phys.Rev.A **45**, 8185 (1992)

[28] M.A.Clifford, J.Arlt, J.Courtial, K.Dholakia, Opt.Comm. **156**, 300 (1998)

[29] T.Kuga, Y.Torii, N.Shiokawa, T.Hirano, Y.Shimizu, H.Sasada, Phys.Rev.Lett. **78**, 4713 (1997)

[30] M.Kasevich, E.Riis, S.Chu, R.DeVoe, Phys.Rev.Lett. **63**, 612 (1989)

[31] H.Ito, T.Nakata, K.Sakaki, M.Ohtsu, K.I.Lee, M.Jhe, Phys.Rev.Lett. **76**, 4500 (1996)

[32] H.Ito, K.Sakaki, M.Ohtsu, M.Jhe, App.Phys.Lett. **70**, 2496 (1997)

[33] H.Friedburg, Z.Phys. **130**, 493 (1951); H.Friedburg, W.Paul, Naturwissenschafen **38**, 159 (1951)

[34] W.G.Kaenders, F.Lison, A.Richter, R.Wynands, D.Meschede, Nature **375**, 214 (1995); A.Goepfert, F.Lison, R.Schütz, R.Wynands, D.Haubrich, D.Meschede, Appl.Phys.B **69**, 217 (1999)

[35] C.J.Myatt, N.R.Newbury, R.W.Ghrist, S.Loutzenhiser, C.E.Wieman, Opt.Lett. **21**, 290 (1996)

[36] M.Key, I.G.Hughes, W.Rooijakkers, B.E.Sauer, E.A.Hinds, Phys.Rev.Lett. **84**, 1371 (2000)

[37] J.A.Richmond, S.N.Chormaic, B.P.Cantwell, G.I.Opat, Acta Phys.Slov. **48**, 481 (1998)

[38] L.V.Hau, J.A.Golovchenko, M.M.Burns, Phys.Rev.Lett. **75**, 1426 (1995); K.Berg-Sorensen, M.M.Burns, J.A.Golovchenko, L.V.Hau, Phys.Rev.A **53**, 1653 (1996)

[39] J.Schmiedmayer, Phys.Rev.A **52**, R13 (1995)

[40] W.Hänsel, J.Reicher, P.Hommelhoff, T.W.Hänsch, Phys.Rev.Lett. **86**, 608 (2001)

[41] W.Hänsel, P.Hommelhoff, T.W.Hänsch, J.Reichel, Nature **413**, 498 (2001)

[42] E.A.Hinds, Physics World, 39, July 2001

[43] J.Reichel, W.Hänsel, T.W.Hänsch, Phys.Rev.Lett. **83**, 3398 (1999)

Chapter 2

Diode Lasers for Spectroscopy and Atom Trapping

2.1 Introduction - what is a laser?

Atom energy levels and transitions

Atoms can be thought of as consisting of a central nucleus and a surrounding cloud of electrons. Each atom can be in either a ground state (relaxed) or an excited state, or in other words, they can have different energies. Simplistically, if energy is given to an atom, we can think of an electron in a low energy level being pushed up to a higher energy level further from the nucleus. This is called a transition. The excited atom will eventually decay to a lower energy state and it will emit a photon of energy as it makes this transition. In a laser, atoms are 'pumped' with energy so that they are in a state two or three levels above the ground state. This can be done by applying intense flashes of light or electrical discharges into the lasing medium. The atoms are now in a state of *population*

inversion, with more excited state atoms than ground state atoms. As the excited atoms relax, they emit energy as photons with a specific wavelength related to the energy difference between the two states involved in the transition. The laser light will be monochromatic, coherent and collimated. This light is the result of 'stimulated emission', as opposed to random spontaneous emission such as occurs in a light bulb. Stimulated emission occurs when an emitted photon of a certain energy and phase encounters an atom in the same excited state. The first photon can stimulate or induce the second atom to emit a photon with the same frequency and phase as the first. Using a pair of mirrors around a lasing medium causes photons of very specific wavelength and phase to reflect back and forwards through the medium, stimulating more and more photons of the same wavelength and phase in a cascade. With one of the mirrors being 'partially-silvered', some laser light escapes as a laser beam.

2.1.1 Laser sources

There are various ways of producing laser light, dependent on the gain medium used. Some examples follow:

- *Solid-state lasers* have lasing material distributed in a solid matrix, e.g., the ruby or neodynium-yttrium aluminium garnet (YAG) lasers. The neodynium-YAG laser emits infrared light at 1,064nm. The titanium-sapphire ($Ti : Al_2O_3$) laser [1] is the most widely used tuneable solid-state laser. It can be operated over a wavelength range of 660nm-1,180nm, which gives it the broadest gain bandwidth of any laser. Commercial Ti:sapphire lasers are normally pumped with argon ion lasers for continuous wave (cw) operation.

- *Gas lasers* such as helium-neon (HeNe) are the most common gas lasers

and have a primary output of visible red light. CO_2 lasers emit energy in the far infrared, and are used for cutting hard materials.

- *Excimer lasers* (the name is derived from the terms excited and dimer) use reactive gases such as chlorine and fluorine mixed with inert gases such as argon, krypton, or xenon. When electrically stimulated, a pseudo-molecule or dimer is formed, which produces laser light in the ultraviolet range.

- *Dye lasers* use complex organic dyes, like rhodamine 6G in liquid solution or suspension, as lasing media. They are tuneable over a broad range of wavelengths.

- *Semiconductor lasers*, or diode lasers, differ somewhat from other solid-state lasers. These electronic devices are generally very small and use low power. They come in an ever-increasing range of wavelengths, from violet to infrared, and are tuneable over a small range.

Before diode lasers were improved to an acceptable level, Ti:sapphire lasers were the source of choice for atom cooling/trapping use.

2.2 Criteria of laser needed to trap cold atoms

In order to be able to cool and trap atoms, a laser must conform to a few basic criteria. It should be stable, so that it will not waver by more than two wavelengths once the atomic transition of interest has been found. It should be smoothly tuneable around that region in order to be used as a spectroscopic source. A single mode laser of course means a smaller frequency spread than multimode and is preferable for 'focussing' on just one atomic transition. The natural linewidth of the ^{85}Rb transition (used for trapping and cooling) is 6.1MHz. Therefore, the

linewidth of the laser must be much less than this (less than 1MHz) so as to be able to resolve its transition features.

Power required

For both the trapping laser and hyperfine (repumping) lasers, only a few milliwatts are required to cool and trap a cloud of atoms. A visible cloud (viewed with infrared viewer or CCD camera) can be obtained with as little as 1.5mW of trapping laser power [2]. However, since the number of atoms trapped is proportional to the laser power, using at least 5mW makes setting up the trap much easier.

2.3 Introduction to Diode Lasers

Diode lasers have been progressively improving in reliability, power and wavelength coverage while their cost has been conversely reducing. Therfore they are now a cheap alternative to tuneable dye lasers for use in atomic physics. They are widely available in a range of frequencies at a much lower price and a fraction of the size of dye or Ti-sapphire lasers. However, and unfortunately, 'off-the-shelf' laser diodes tend to have tens of MHz linewidth and are continuously tuneable over only certain limited regions. Their laser frequency is also extremely sensitive to changes in temperature and current and also to optical feedback. This latter sensitivity can be used to good effect, though. These characteristics can be improved a lot by using judicious optical feedback techniques to control the laser frequency. This will be discussed in more detail later in this chapter.

2.3.1 How diode lasers work

Most single-mode diode lasers used in the near infrared region are made of AlGaAs (750-890nm) or InGaAsP (1300-1500nm). The best overall spectral characteristics are found in the 750-870nm region. This is ideal for rubidium and caesium (852nm). These lasers have output powers of 5-15mW, but can produce more than 50mW if the back facet of the diode is coated with a high reflector, and the front facet has a reduced reflectance coating. A typical semiconductor diode laser is shown schematically in figure 2.1. As the illustrative dimensions show, these

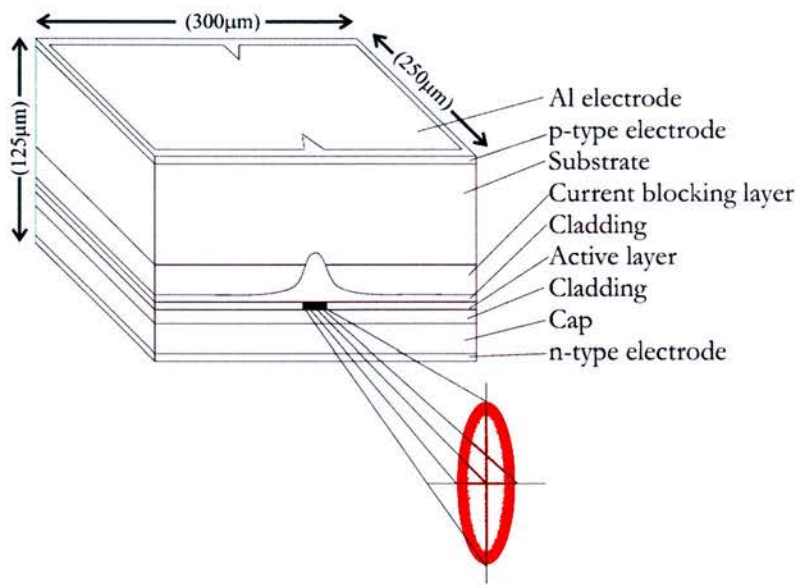

Figure 2.1: *The different layers of a semiconductor diode laser (adapted from Sharp Corporation manual)*

devices are very small. An 'injection current' is sent through the active region (between the *n*- and *p*-type cladding layers). Electrons and holes are created which recombine and emit photons. The wavelength of this light is defined by the band gap and then by the junction temperature and current density. Diode lasers will only tune over about 20nm in wavelength. Compared to atomic transitions, the light has a very broad linewidth. There is a narrow groove in the

active region which confines the light, defining the spatial mode. This region is usually produced by using materials of different refractive index.

As the injection current is increased, the output power increases. At the threshold current, the laser action suddenly starts (figure 2.2). Changes in current will affect the diode temperature (Joule heating at junction) and the carrier density, which changes the index of refraction. The wavelength is thus also changed. For timescales longer than about $1\mu s$, the change in temperature outweighs any refractive-index change due to carrier density change. A tuning curve of wavelength versus current therefore looks similar to that for temperature.

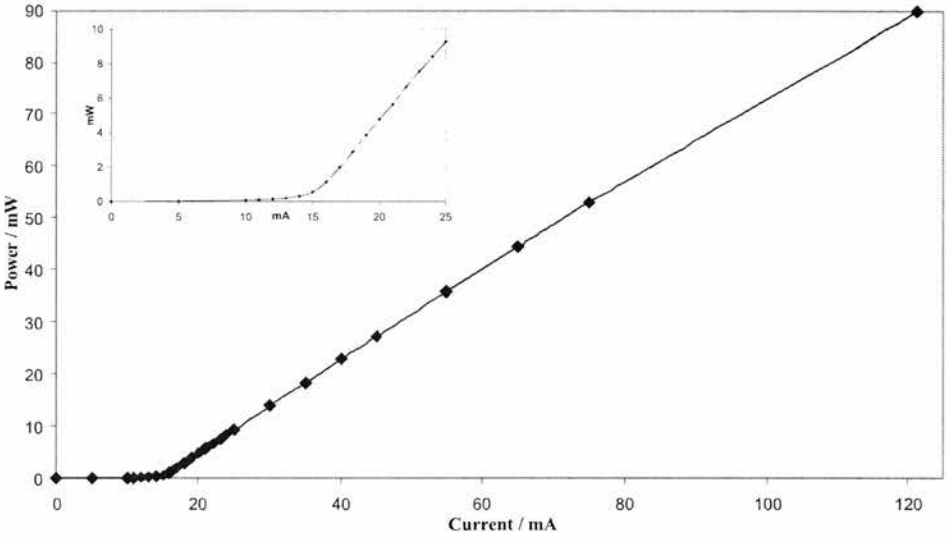

Figure 2.2: *Power versus Current for free-running 852nm diode laser. The insert shows the threshold in detail*

However, if the temperature is decreased while the current remains fixed, the output wavelength will also increase. As temperature changes, both the optical path length of the cavity and the wavelength dependence of the gain curve change. These are both different, however, so that a graph of temperature tuning will be a staircase with sloping steps [3]. For example, in an AlGaAs device, the optical

length of the cavity changes about +0.06nm/K, while the gain curve shifts about +0.25nm/K. Each 'step' is the changing cavity mode, while the difference between steps is due to hopping from one longitudinal mode to the next (≈0.35nm). It is better to run a diode at lower temperatures, since a typical lifetime of about 10^5 hours is reduced by a factor of 5 when the temperature is increased by 10K [4]. The output of diode lasers tends to have a large divergence. This is due to the small rectangular region from which it is emitted. The beam profile is thus elliptical (figure 2.1), with an aspect ratio of about 3:1. The beam is generally also astigmatic, but with a suitable collimating lens and spatial filtering a good, non-diverging Gaussian profile can be obtained.

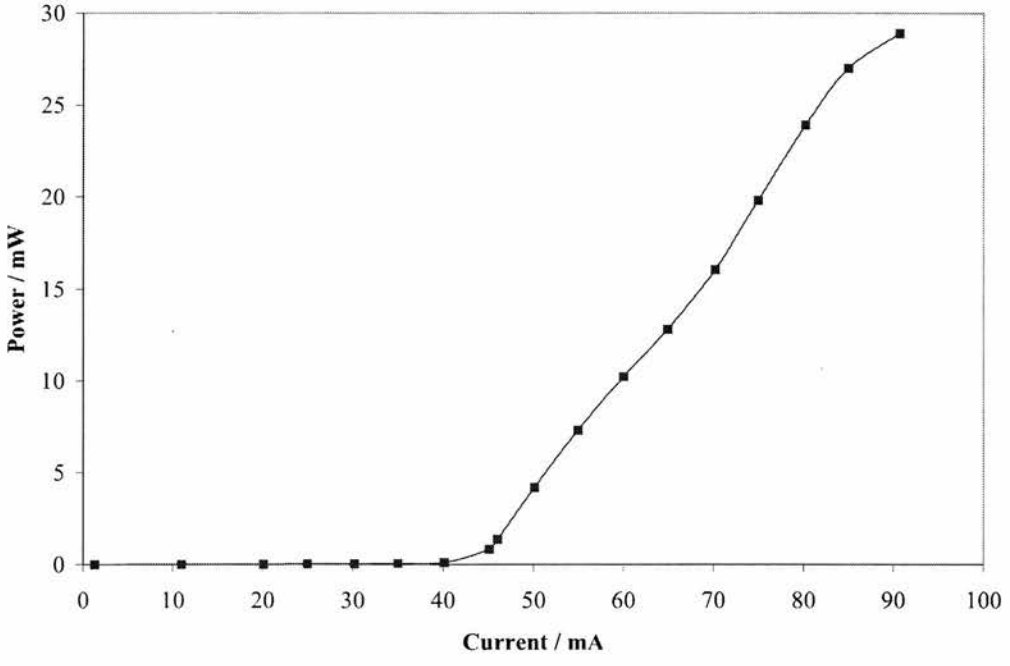

Figure 2.3: *Power versus Current for free-running 780nm diode laser.*

2.3.2 Characterisation of a 780nm Laser Diode

Before using any diode laser experimentally, it is good practice to find out its characteristics. We used Hitachi HL7851G diode lasers in our cooling and trapping apparatus. They were measured to have a lasing threshold at about 45mA input current (figure 2.3). Using a monochromator, we also measured the change in wavelength of the laser light as the temperature of the laser was changed (using a Peltier, of which more detail is given below).

The optical characteristics given in the manual for the diodes are given below (figures 2.4 and 2.5).

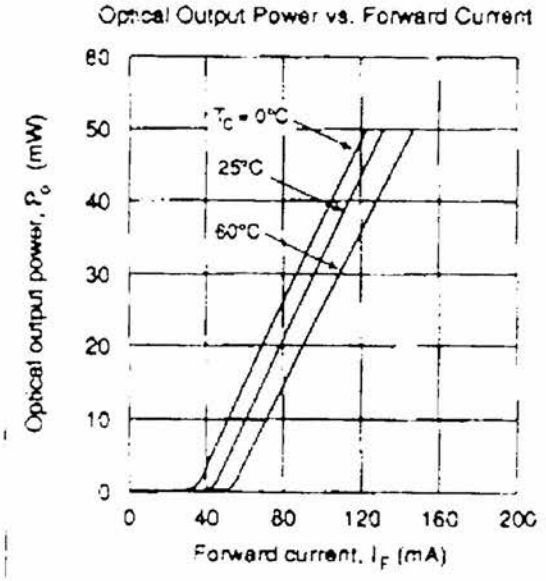

Figure 2.4: *Typical characteristic curves. P_o is optical output power.*

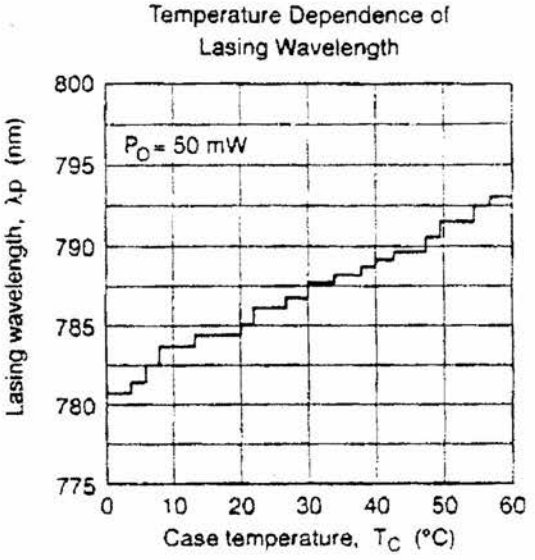

Figure 2.5: *Typical characteristic curves, continued, showing temperature dependence.*

2.4 Feedback of light into a diode laser

As mentioned earlier, optical feedback can be used judiciously to improve on some of the characteristics found in 'off-the-shelf' laser diodes. Firstly, I shall discuss why laser diodes are susceptible to feedback.

Diode lasers are sensitive to optical feedback for a number of reasons, which work in combination. Firstly, when plotting gain against wavelength it can be seen that the curve is quite flat. Secondly, the cavity finesse is quite low; and thirdly the cavity is very short. These combine to give an extremely weak dependence on wavelength and relatively few photons in the cavity during operation. This means that any photons introduced into the cavity can have a majority effect and perturb the frequency easily. That is, if photons of a different frequency (determined by an external cavity, for example) are introduced into the cavity,

they will be amplified by the laser, increasing their number. The laser is acting like a photodetector in this case, generating more carriers in the junction and affecting the net laser gain. The laser favours the 'new' frequency photons and thus the output will be selected to be at that frequency.

Unfortunately, any feedback can have this effect on the laser, so it is important to keep stray reflections to a minimum. If the beam is going through a focus, then a larger proportion of scattered light will be returned to the cavity, increasing sensitivity. Optical isolators can be used to reduce unwanted feedback, ranging from the simple (attenuator or circular polariser) to the more complex and expensive (Faraday isolator)[1].

Several methods can be used to introduce frequency-selected feedback light into the laser cavity in a controlled manner. The two most common are the Littman-Metcalf [5] and Littrow [6] configurations. These both utilise the manner in which a diffraction grating affects incident light. It is dispersed away from the grating surface at an angle, which depends on its wavelength. Thus, a grating can be used to select a narrow spectral band from a much wider band. The grating equation:

$$m\lambda = d(\sin\alpha + \sin\beta)$$

(see figure 2.6) can be differentiated to give the angular spread (dispersion) of

[1]Laser light is first linearly polarized, e.g. at 0°. As this linearly polarized light enters the Faraday rotator rod, the plane of polarization rotates as the light propagates along the axis of the rod. The Faraday rotator has to be tuned to rotate the plane of polarization by 45°. The light then passes through an output polarizer whose transmission axis is also at 45°. Thus, most of the light intensity emerges from the output of the Isolator. Any backward light re-enters the isolator through the output polarizer and becomes polarized at 45°. It then passes through the Faraday rotator which produces another 45° of rotation and is now polarized at 90° or horizontally, and is stopped by the input polarizer, still at 0°. Thus, the laser is isolated from its own reflections which may occur in the application part of the optical apparatus.

the spectrum:

$$\frac{d\beta}{d\lambda} = \frac{\sin\alpha + \sin\beta}{\lambda\cos\beta}$$

When the grating is operated in the Littrow configuration (in which the light is retro-diffracted; see figure 2.9), the equation for the dispersion simplifies to:

$$\frac{d\beta}{d\lambda} = \frac{\tan\beta}{\lambda}$$

.

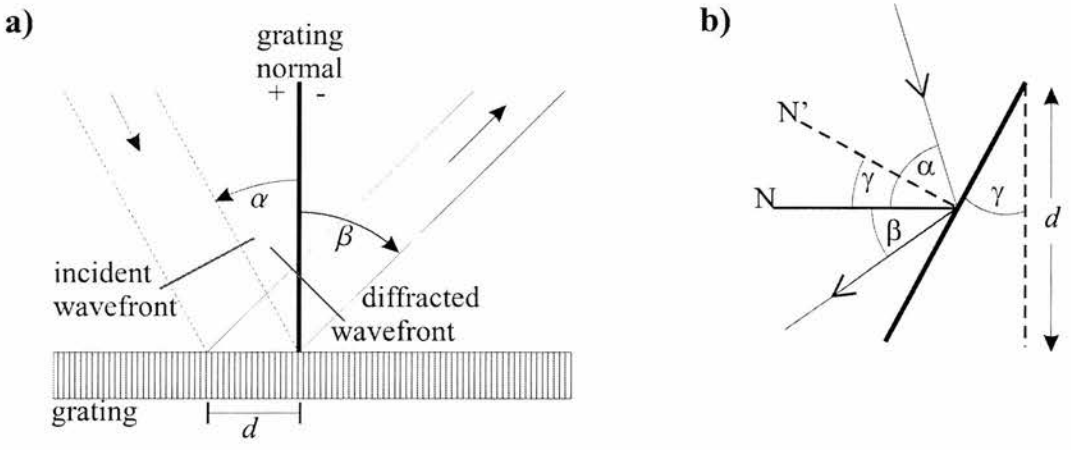

Figure 2.6: *The Grating Equation, with a) α =incidence angle, β =diffraction angle, m =(integral) diffraction order, λ =wavelength of light and d =groove spacing; b) grating normals N and N' and grating angle γ*

2.4.1 The Littrow and Littman configurations

In the Littman configuration a grating is used near to grazing incidence (figure 2.7). This method of tuning the laser frequency offers high angular spread and consequently narrower spectral feedback. However, as the angle of incidence approaches 90°, the efficiency of the grating drops significantly.

The Littman configuration (figure 2.7) has a better immunity to optical feedback and directional stability (with frequency tuning). It also has a large tuning

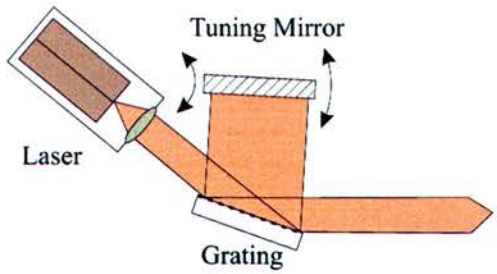

Figure 2.7: *Littman tuning using a grating near grazing incidence*

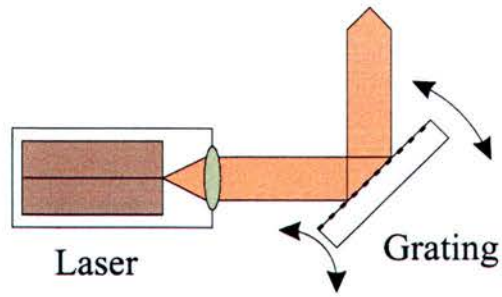

Figure 2.8: *Laser tuning using a grating in the Littrow configuration as the feedback element*

range but at the expense of power. Alignment and positioning of pivot points is extremely critical too.

The Littrow configuration (figure 2.8) is the simpler of these two, requiring fewer parts and less critical alignment. Unfortunately, as the frequency is tuned, the beam direction rotates with the grating position. As discussed later, this is not generally a problem in a trapping enviroment. A diffraction grating reflects, in its first order, a small proportion of the output light back into the laser. The output of this compound system is the zero order of the grating. This sets up a lasing cavity with the extremities being the back facet of the diode and the grating 'mirror'. This system is commonly known as an extended cavity diode laser (ECDL). The larger cavity means that the linewidth of the output laser light will be smaller. By changing the cavity size (by applying a voltage to the piezoelectric disk[2] which varies the grating position) it is possible to tune the laser smoothly over about 5-8GHz. This limit is imposed by the external cavity mode spacing. There will also be mode hops at about 50GHz due to the free spectral range of the diode laser.

[2]Piezoelectric disks are also known as piezoelectric actuators or PZTs. A current applied to a quartz crystal or barium titanate ceramic causes a deformation which is used here to translate the grating holder.

2.5 The Extended Cavity Diode Laser (ECDL)

We designed and built a simple, cheap and very compact ECDL, which can be seen in figure 2.9.

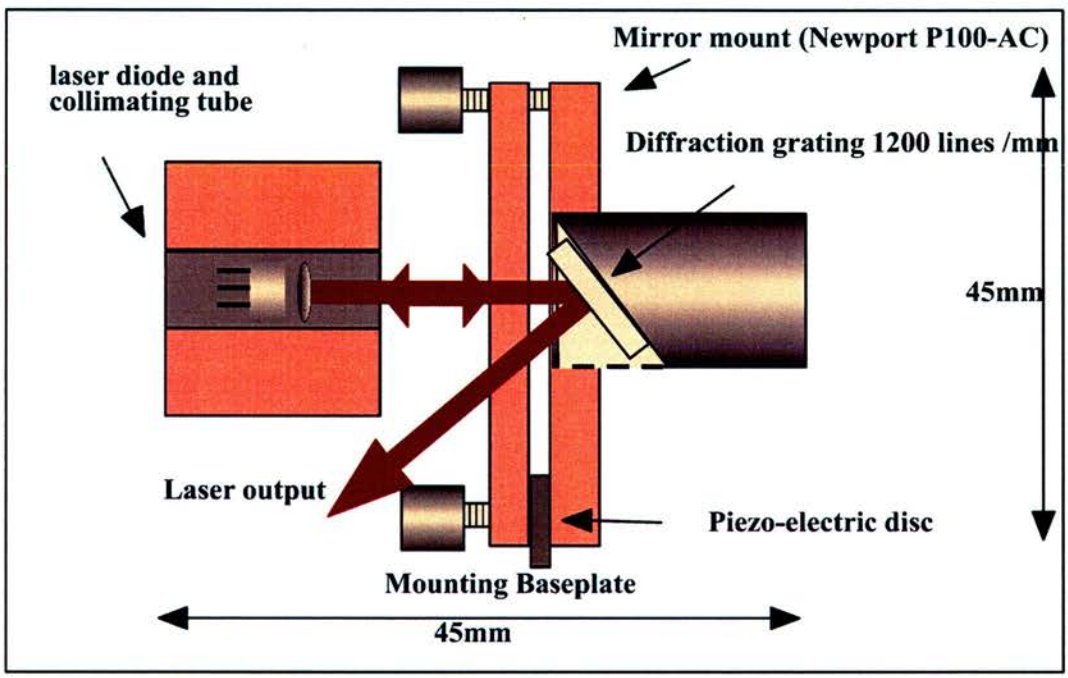

Figure 2.9: *The extended-cavity diode laser, using the Littrow configuration*

Basically, the system consists of a diode laser, a collimating lens and a diffraction grating. We have constructed systems using various frequency lasers, but have concentrated mainly on 780nm and 852nm[3] for trapping rubidium and caesium respectively. For the 780nm system we used a 1200 line-per-mm diffraction grating. A base-plate was machined to mount components such that proper collimation could be achieved. The layout can be seen in figure 2.9. The diffraction grating is mounted in a Littrow configuration, as previously discussed, so that the light diffracted into the first order returns to the laser. The grating is acting as one "mirror" of the external cavity, with the back facet of the diode being the second

[3]The 852nm ECDL is discussed in detail in the following chapter

mirror. The grating must therefore be very stable and carefully aligned. It was mounted on a commercial mirror-mount attached to the base-plate. Alignment can be achieved more easily by turning the input current of the laser up so that the laser light is quite bright. The diffracted beam can then be seen as the two orders (zero and first) and the first order directed back into the laser quite easily. When this has been done roughly, the current can be turned down to just below threshold for the free-running laser and the grating position adjusted more finely using the mirror-mount controls. This is done relatively quickly by gradually adjusting the vertical control and then manually scanning the horizontal position of the mount (swinging it around its hinge) and looking for a bright flash of the zero order beam on infrared (IR) card as the external cavity is setup. When this is seen, the vertical position is correct (although fine adjustments can improve it slightly), and the piezoelectric disk can be now inserted in front of the horizontal mount control. This control is now adjusted until the brighter spot is seen on the IR card, showing that the system is now running in external cavity mode. The cavity length is fine-tuned by using the piezoelectric speaker disk (such as those used in musical birthday cards) to move the grating when a voltage is applied.

The correct angle of the grating for the Littrow configuration can be calculated as follows. The grating angle γ can be seen (figure 2.6b) to be:

$$\gamma = \frac{\alpha - \beta}{2}$$

and since for the Littrow configuration $\alpha = \beta$ and using the grating equation, this implies that:

$$\gamma = sin^{-1}\left(\frac{m\lambda}{2d}\right)$$

Given that we are considering the first order ($m = 1$), $\lambda = 780nm$ for our laser and $1/d = 1200$ lines/mm:

$$\gamma = sin^{-1}\left[\frac{1 \times 780 \times 10^{-9}}{2} \times \frac{1200}{10^{-3}}\right] \simeq 27.9^{\circ} \simeq 27^{\circ}54'16''$$

Unfortunately, extended cavity diode lasers tend to be easily affected by acoustic, mechanical and thermal noise. These effects can be minimized as described below. In order to be used for 'long term' projects, such as atom trapping, an ECDL must be locked to an external, stable reference source. This will ensure that the frequency remains stable for long periods. Some methods of stabilising the frequency are polarisation locking, current modulation and saturated absorption spectroscopy. These techniques are discussed briefly below. It is also possible to take advantage of the Zeeman effect in an atomic vapour cell, as is discussed in the next chapter.

2.5.1 Characterisation of the extended-cavity diode laser

With the diode laser in the extended cavity geometry, the lasing threshold was measured to be about 35mA (figure 2.10). For the ECDL to be usable as a

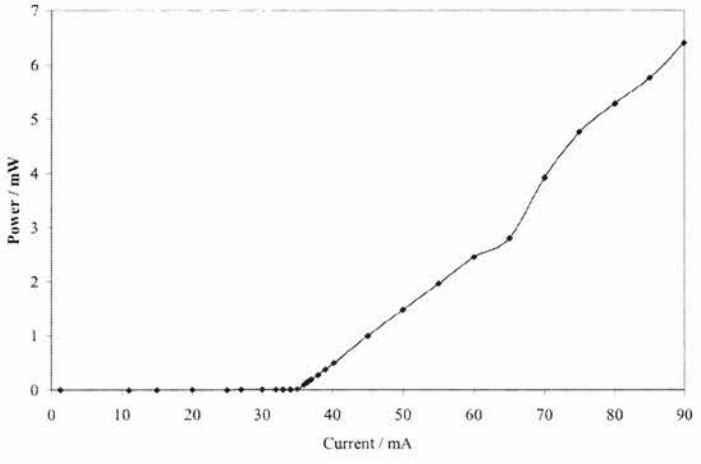

Figure 2.10: *780nm ECDL lasing threshold (Power/Current)*

spectroscopic source, it must be running as a single mode. This was checked using an optical spectrum analyser (OSA), consisting of a high finesse ($\sim$ 600) etalon with a free spectral range of 300MHz. The frequency of the output light was

measured using a monochromator, and then tuned (discontinuously) by rotating and translating the grating with the horizontal control of the mirror mount. Turning the screw approximately an 8th turn at a time gave frequency tuning of up to 13nm, see Figure 2.11. By changing the voltage to the piezoelectric disk,

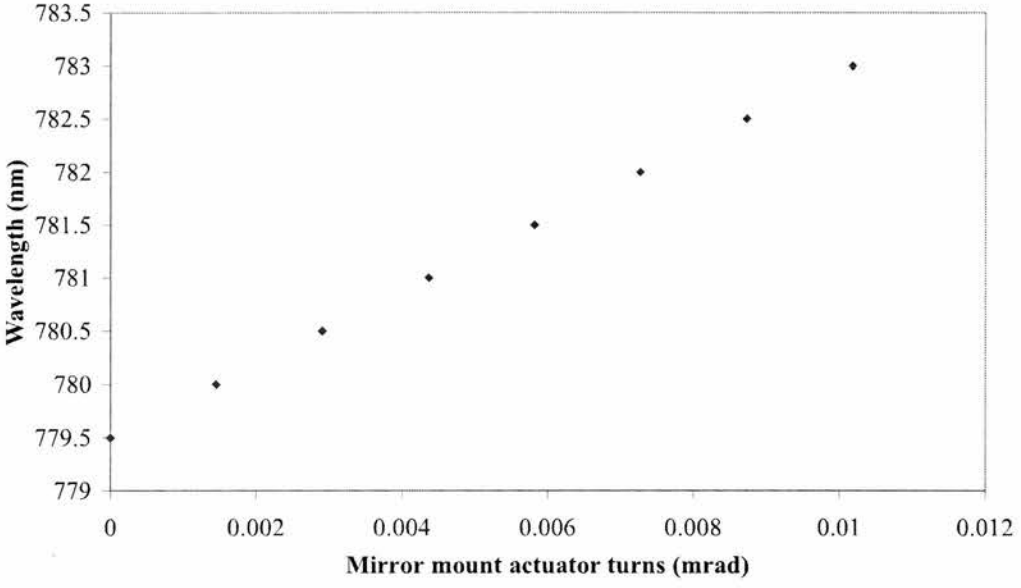

Figure 2.11: *Discontinuous tuning of 780nm diode*

it was possible to tune the ECDL smoothly over 8GHz, as measured using the OSA. The linewidth was also measured with the OSA to be between 1.5MHz and 375kHz, see Figure 2.12. The finesse (200) and free spectral range (300MHz)of the optical spectrum analyser give the minimum linewidth measureable as 1.5MHz. We need a linewidth of less than 1MHz, as mentioned above, so that transition features of about 6.1MHz can be resolved. It can be assumed that the values given by the OSA manufacturer are 'worst case' values, and the device is actually better than advertised! The finesse is more likely to be about 600, for example. Jitters in the laser can cause it to look as though it has a larger linewidth, since it is averaged over time on an oscilloscope. Thus, by taking a snapshot a more true reading can be made. The value of 375kHz was measured using a snapshot

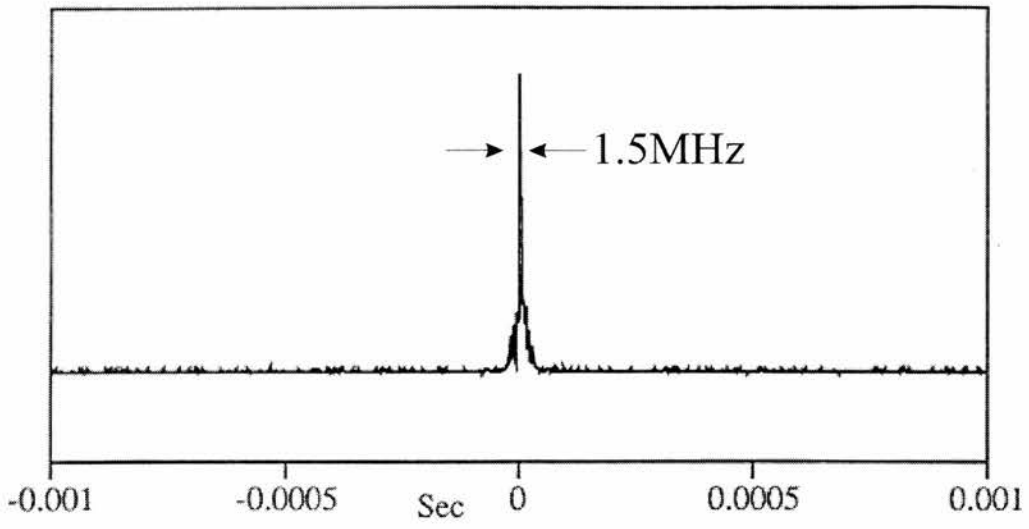

Figure 2.12: *Linewidth of the 780nm ECDL measured with the OSA*

in about 200ms.

Heterodyning two lasers for a more accurate linewidth

By setting up two ECDL's at almost exactly the same wavelength it is possible to align the two beams spatially so that they are interacting over a large distance. The light beams will interfere and cause beats at twice the linewidth of the individual lasers. By directing the two beams into a fast photodiode, these beats can be measured on a radio-frequency (rf) spectrum analyser. The alignment of the interacting lasers is very critical, so we aligned them along the length of the laboratory before inserting the photodiode into the beams. See figure 2.13 for the arrangement we used. Each laser must be at the same wavelength (to within 3GHz). Thus, a saturated absorption spectrum was taken from each laser (see Section 2.5.2) and both were 'zoomed in' on the same feature. The output of the spectrum analyser is shown in figure 2.14 and can be seen to be approximately

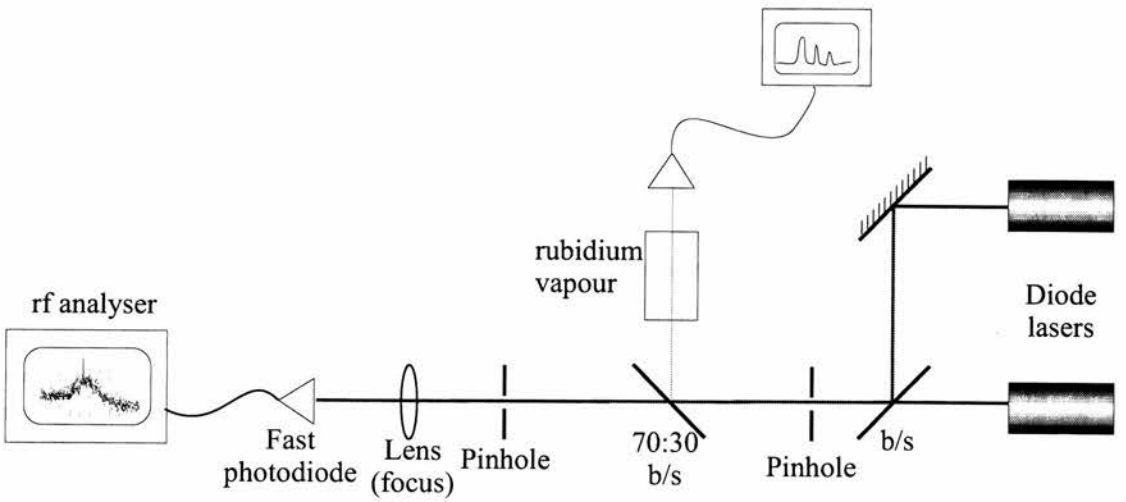

Figure 2.13: *Geometry used for heterodyne experiment*

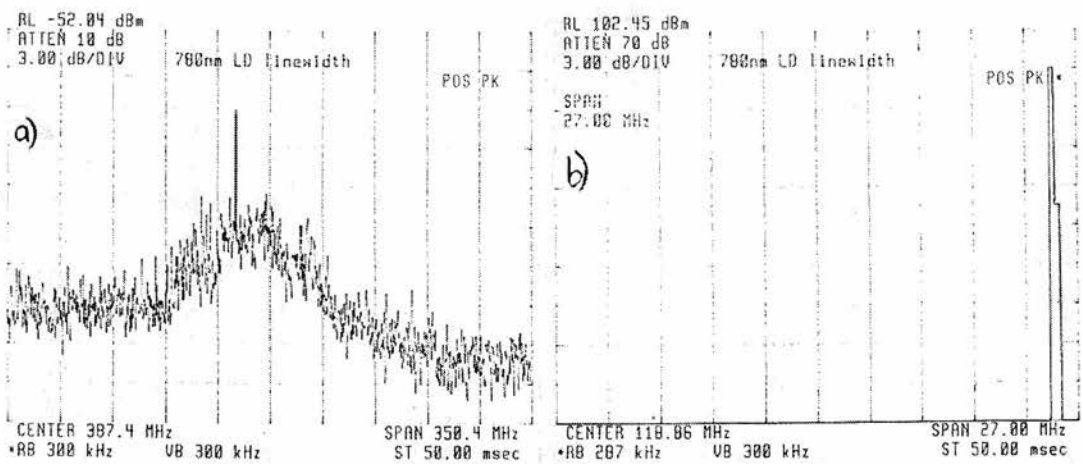

Figure 2.14: *Linewidth of the 780nm ECDL measured from two heterodyned lasers. b) is a closeup of the peak in a)*

this, it must be locked to some fixed frequency, that is the transition frequency of the atom that is to be trapped. An atomic resonance/transition is obtained by taking a small percentage of the laser beam away from the trapping route and through a cell of atomic vapour. Photons are absorbed by the atoms and this change in power can be measure with a photodiode. There are several methods for firstly getting this frequency and then locking on to it. Generally, an electronic 'lock-box' is used into which an atomic spectrum signal is fed and 'zoomed-in' on the required transition feature (seen on an oscilloscope). This is the locking signal. The box detects whether the laser has drifted from this frequency and sends feedback to the laser to shift its frequency up or down as appropriate. Different methods of achieving the locking signal are given below. Another method, dichroic atomic-vapour laser lock (DAVLL) is given in the next chapter.

An absorption spectrum is observed when light passes through some material which absorbs certain frequencies, showing up as dips in a continuous spectrum recorded by a photodetector from the exiting light. The absorbed light provides energy for an atom to undergo a transition from a ground state to an excited state. In practice, the frequency of the (laser) light is scanned over a particular range around a known set of absorption frequencies for the material. We use a glass cell of atomic vapour. The atoms are moving at different speeds within the cell, so that atoms moving towards the incoming light beam see a decrease in its wavelength, and atoms moving away see increased wavelength. This is the well-known 'Doppler effect'. However, this leads to Doppler broadening of absorption features in a spectrum, and will obscure the hyperfine dips caused by atomic transitions. Since we want to lock to these small features, we must try and get Doppler-free absorption spectroscopy. This can be achieved with a counterpropagating stronger 'pump' beam (from the same laser, thus the same frequency) through the vapour cell and overlapping with the weaker 'probe' beam.

Both these beams will interact with the same group of atoms, those moving parallel to their direction. The stronger beam will saturate the absorption of these atoms, reducing that experienced by the weaker probe beam over a very narrow range of frequencies. This gives fine dips in the spectrum recorded from the probed. By subtracting a Doppler broadened (unsaturated) spectrum from this, just the dips can be seen, relating to particular atomic transitions (with some crossover resonances [4] between these). See Figure 2.15.

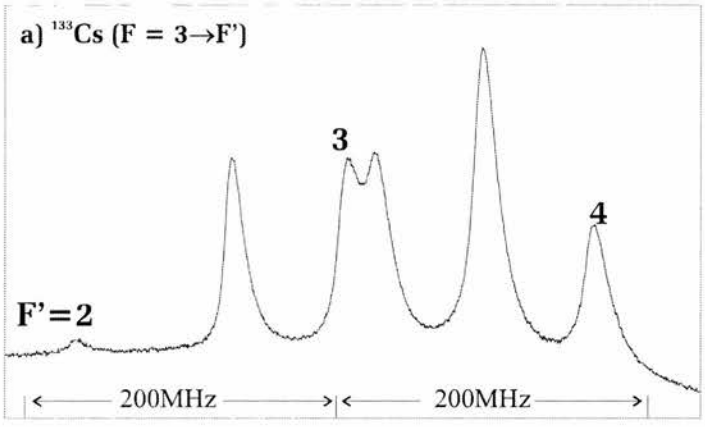

Figure 2.15: *Saturated absorption features for caesium, showing transitions and crossover peaks.*

Polarisation spectroscopy can provide a locking signal which can be used to stabilize an ECDL too [7]. This method is similar to saturated absorption techniques, but the polarisation rotation of the probe is monitored rather than the change in the absorption. The apparatus is essentially the same as for saturated absorption except that the pump beam passes through a quarter-wave($\lambda/4$) plate before interacting with the weaker probe beam. The probe then passes through a linear polariser, crossed with respect to the original light beam, before striking a

[4]Crossover peaks are formed when the bandwidth of the laser is wide enough to affect two transitions at the same time. Thus a peak is formed halfway between the two 'real' transitions, made up from the addition of those two.

photodiode (see figure 2.16). Anisotropy is introduced by the circularly polarised

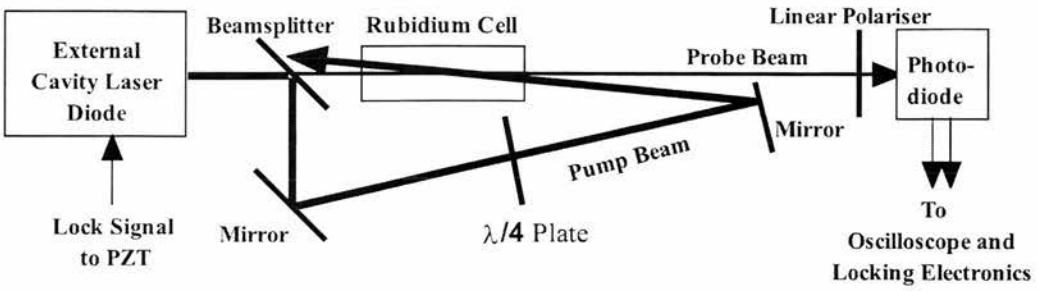

Figure 2.16: *The polarisation spectrometer apparatus layout*

pump beam which counter-propagates through the vapour cell. The linear probe can be considered as being the addition of two oppositely sensed circularly polarised beams (left and right circularly polarised). The pump beam introduces a difference in absorption and refractive index in each of these two beams because of the non-uniform pumping of the sublevels. After passing through the cell, the recombined beams give a beams whose plane of linear polarisation has been rotated. This will pass partially through the linear polariser and give and increased signal on the photodiode. As the frequency of the laser is scanned over an atomic transition, the signal detected by the photodiode will be a dispersion shape (if the angle between the polariser and the linear polarised probe is large). This allows easy location of the correct hyperfine transition using the background absorption profile. Also, the dispersive slope crosses zero, which can be locked onto with suitable feedback electronics.

In current modulation, the equipment and layout are the same as for saturated absorption spectroscopy. The current is dithered at the same time as the PZT current is scanned. Whereas the PZT runs at a relatively low frequency, the current can be modulated much faster (kHz), although not so fast as to produce sidebands. Since it is much faster, higher frequency noise can be filtered out more

easily, just as the PZT can filter out low frequency noise.

Wieman and colleagues suggest using two levels of stabilisation in their paper [2]. They are using current feedback for eliminating the effects of high frequency noise and PZT feedback for low frequency noise.

2.5.3 Overcoming inherent problems

Acoustic, mechanical and thermal noise

Unwanted changes in cavity length due to thermal expansion can be avoided by stablising the temperature of the diode and base-plate to within a few mK using a Peltier.The temperature stabilisation components were connected as given in the manual for the MPT temperature controller[5] (see figure 2.17). The TE module

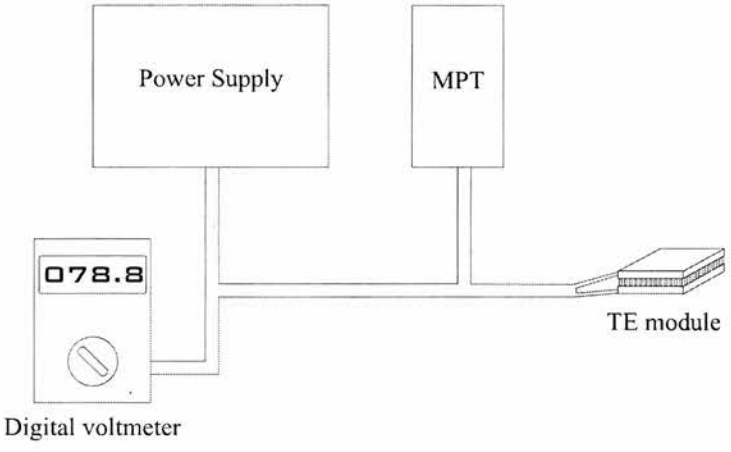

Figure 2.17: *Connecting the Peltier/TE module*

was sandwiched between two blocks of metal in the baseplate using heatpaste to conduct temperature. A thermistor was also inserted into a hole drilled into the

[5]I cannot find what the acronym MPT stands for, but assume it is something like "Module for Peltier Temperature (control)", since the MP*C* controls *current*.

mirror mount along with some heatpaste[6]. This provides feedback to the MPT temperature controller. Controls on the MPT include a temperature setpoint adjuster (turning clockwise reduced temperature) and a damping adjuster, which can be set to provide optimal damping as the temperature oscillates around the setpoint. The setpoint was varied (and given time to settle) and the wavelength of the free-running laser measured using a monochromator.

To reduce unwanted effects of mechanical noise on the optical table, a layer of Sorbothane® was placed under the baseplate to absorb some vibration and shocks. The whole laser set-up was also enclosed in a draft-proof metal box.

Wavelength and angular scanning

Once the laser is working in the external cavity mode, it can be scanned across a range of frequencies by ramped voltage signal to the piezoelectric disk. There is a defect of this geometry in that the output beam is deflected horizontally as the wavelength is scanned. The angular rate for this is approximately

$$\frac{d\theta_{beam}}{d\lambda} = \left[d^2 - (\lambda/2)^2\right]^{1/2} \simeq 0.08°/nm$$

for grating constant d. However, for saturated absorption spectroscopy or neutral atom trapping, e.g. for rubidium where the $5s_{\frac{1}{2}} - 5p_{\frac{3}{2}}$ hyperfine multiplets of the two naturally occuring isotopes span less than 0.014nm, this is no bother.

Grating quality and ECDL power

If a high quality grating is used in the Littrow geometry, then the percentage of light being retroreflected into the diode could be relatively large. For this reason,

[6]Heatpaste is a good conductor of heat and thus transmits the heat with little loss to the thermistor.

a grating blazed for 300nm was used with both 780nm and 852nm extended cavity diode lasers. In this way, only a small quantity of light is reflected into the first order and thus back into the laser. This is enough to set up the extended cavity and means that more power goes into the zeroth order, that is the output of the whole system. Gratings were made by Optometrics USA, Inc., and an efficiency graph for a grating blazed at 300nm can be seen in figure 2.18.

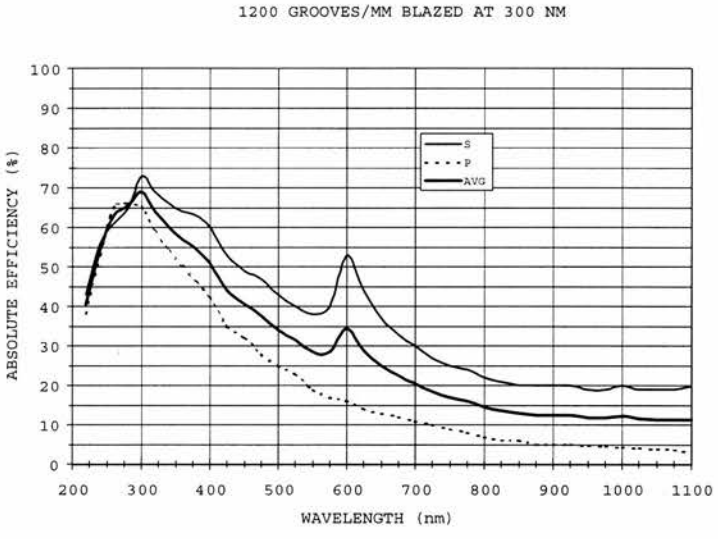

Figure 2.18: *Optometrics Catalogue graph of grating efficiency.*

Beam shaping

A normal diode laser emits a beam which is strongly divergent. By using a collimating lens this can be overcome, but the cross-sectional shape of the beam is still elliptical, as can be seen in figure 2.1. This is due to the shape of the output facet of the chip and cannot be changed without redesigning the chip

itself. However, there are a number of ways in which this can be overcome. One method is to use anamorphic prisms which can be adjusted to give a circular cross-sectional area. Another way is to use cylindrical lenses in a telescope formation. Since they only affect magnification in one dimension, they can be used to either increase the minor axis or decrease the major axis of the ellipse. The final shape can be adjusted to be circular. More recently, a novel way of producing a circular output 'directly' from the diode laser has been developed. A cylindrical microlens has been attached directly to the output facet of the diode so that beam becomes circular immediately, although it is still divergent and needs to be collimated [8]. This so-called circulase has the added benefit that a minute amount of light feeds back from the microlens into the laser cavity which stabilises it somewhat more than standard diode lasers. Since fewer optical components are needed when using this device, there is also less power lost in beam shaping. The anamorpic prisms caused a reduction of about 20% in power, whereas the cylindrical lenses lost about 15%.

2.6 Conclusions

Diode lasers are a very small and inexpensive source for use in atom trapping experiments. Although they do not produce as much power as a Ti-Sapphire laser, for example, this is not a hardship, since relatively little power is needed to trap atoms. Setting them into the Littrow configuration makes them easily tuneable and more stable. Using various simple techniques it is possible to lock the laser frequency so that they can be used for cooling, trapping and guiding atoms. There are some inherent problems with diode lasers, but these can be overcome without much bother. In all, laser diodes in an extended cavity geometry are a good compact source for use in various cold atom situations.

Bibliography

[1] 'Laser Fundamentals' by William T. Silfvast describes $Ti : Al_2O_3$ lasers quite well (p.458) and mentions ring lasers (p.387).

[2] C.E.Wieman, G.Flowers, S.Gilbert, Am.J.Phys. **63**, 317 (1995)

[3] C.E.Wieman and L. Hollberg, Rev.Sci.Instrum. **62**, 1 (1991)

[4] Hitachi Optodevice data book 1993, p116

[5] K.C.Harvey and C.J.Myatt, Opt.Lett. **16**, 910 (1991); M.Littman, Opt.Lett. **3**, 138 (1978)

[6] M.A.Clifford, J.Arlt, J.Courtial and K.Dholakia, Opt.Comm. **156**, 300 (1998)

[7] G.P.T.Lancaster, R.S.Conroy, M.A.Clifford, J.Arlt and K.Dholakia, Opt.Comm. **170**, 79 (1999)

[8] G.P.T.Lancaster, W.Sibbett, K.Dholakia, Rev.Sci.Instrum. **71**, 1 (2000)

[9] M.A.Clifford, G.P.T.Lancaster, R.S.Conroy and K.Dholakia, J.Mod.Opt. **47**, 1933 (2000)

[10] R.S.Conroy, A.Carleton and K.Dholakia, J.Mod.Opt. **46**, 1787 (1999)

[11] K.B.MacAdam, A.Steinbach, C.E.Wieman, Am.J.Phys. **60**, 1110 (1992)

[12] L.Ricci, M.Weidemüller, T.Esslinger, A.Hemmerich, C.Zimmermann, V.Vuletic, W.König, T.W.Hänsch, Opt.Comm. **117**, 541 (1995)

[13] A.S.Arnold, J.S.Wilson, M.G.Boshier, Rev.Sci.Instrum. **69**, 1236 (1998)

[14] G.N.Rao, M.N.Reddy, E.Hecht, Am.J.Phys. **66**, 702 (1998)

Chapter 3

852nm extended cavity diode laser - Performance and Stabilisation

3.1 Introduction

Diode lasers are now used extensively for high-resolution spectroscopy [1]. However, there are drawbacks due to at least two points necessary for a spectroscopic source. They cannot normally provide a narrow linewidth nor a smoothly frequency-tuneable light beam. Diode lasers are also very susceptible to optical feedback [2], which can be detrimental to the output of the laser, but can be used to one's advantage in making a suitable spectroscopic source. By judicious use of optical feedback, the Q factor of the cavity can be increased and the linewidth reduced dramatically, as discussed in a previous chapter.

3.2 The Zeeman Effect for stabilising an ECDL

3.2.1 Introduction

For this stabilisation method [3], a weak magnetic field is applied to an atomic vapour cell, in the case of the 852nm laser this is a caesium cell (Figure 3.1). Laser

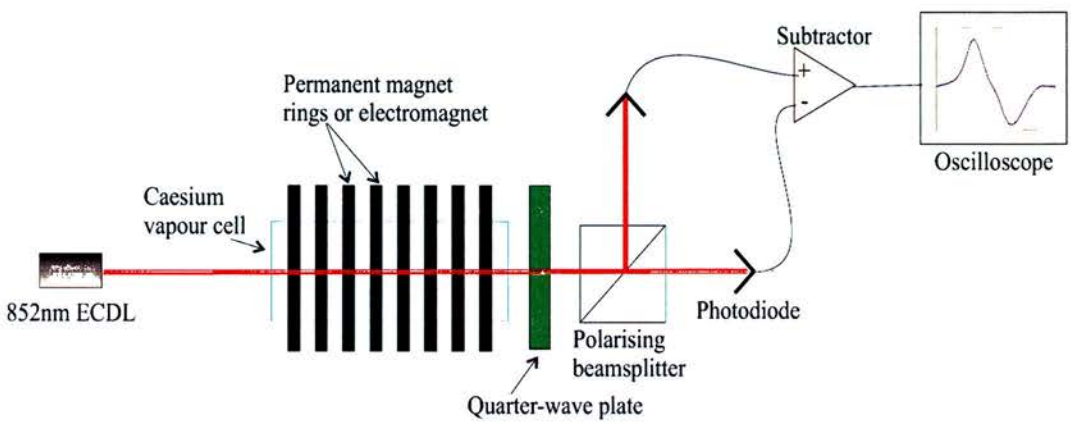

Figure 3.1: *Arrangement of apparatus for achieving a DAVLL signal*

light passing through the cell is absorbed by the caesium if it is at a transition frequency. This would be seen as a dip in a continuous spectrum about that particular frequency. However, because the atoms are moving, the absorption signal is Doppler-broadened. In the presence of a magnetic field, the Zeeman components of that signal are split into two. The linearly polarised light can be thought of as the addition of two equal circularly polarised components of opposite handedness. For σ^+ polarised light propagating in the z-direction in a B-field with the same direction, the central frequency of the absorption increases. The frequency decreases for the opposite polarisation, σ^-. See Figure 3.2(a). Subtracting the absorption profiles for the two polarisations gives a dispersive error signal. This is required for locking. The act of subtraction actually reduces fluctuations that may arise in the error signal due to variations in lineshape or absorption. This is because the locking point is at zero, when the light incident

on both photodiodes is the same. This locking scheme has been called a dichroic atomic-vapour laser lock (DAVLL) [4].

The magnetic field can be produced by two methods, both of which we have tried. Firstly, a series of rings cut from rubber embedded with magnetic material [4], and secondly a normal electromagnet. The variation of the magnetic field along the length of the cell was measured to be less than 9% for both systems (Figure 3.3 shows variation for annular disks). The light exiting the cell is immediately incident on a quarter-wave plate, with both its fast and slow axes at 45° to the plane of the incident linearly polarised light. A polarising beam-splitting cube after this separates the two orthogonal components, which are then directed onto two photodiodes. Subtracting these two signals gives a dispersive signal passing through zero. A typical dispersive DAVLL curve generated for caesium is shown in Figure 3.2(b). The capture range of the signal is over 500MHz wide, which allows the laser to be generally unaffected by large jumps of frequency. Using this signal and an electronic locking circuit, feeding back to the PZT, the laser system with caesium was recorded to drift about 5MHz per hour.

To model the transition frequencies of the DAVLL signal, one must take into consideration the strength of the magnetic field relative to the splitting of the hyperfine levels. Figure 3.4 shows the D1 and D2 levels for sodium, together with the splitting caused by a weak and a strong magnetic field respectively [7]. Splitting for rubidium is similar. The equations governing the effect can then be simplified as follows. A field is considered weak if the energy level splitting is small compared to fine structure splitting. Coupling between orbital and spin moments (spin-orbital coupling) is stronger than either coupling of spin or orbital moment alone to the external magnetic field. In other words, $g_F \mu_B B << A$, where A is the hyperfine splitting constant for the level under consideration g_F is the Lande g-factor, μ_B is the Bohr magnetron and B is the external magnetic field.

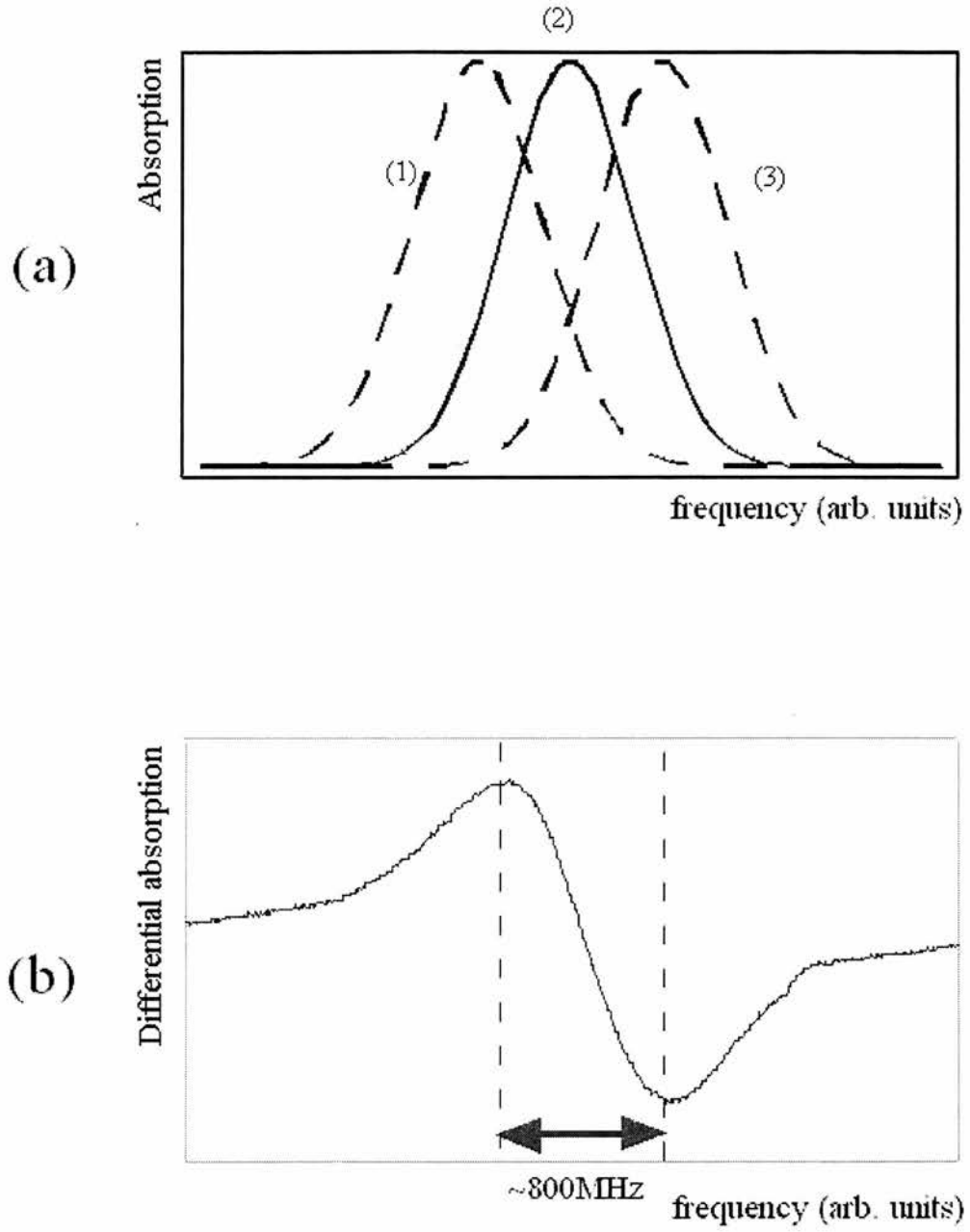

Figure 3.2: ***(a)****The origin of the DAVLL error signal. Peaks (1) and (3) are Doppler broadened features for both senses of circularly polarised light incident on the vapour.* ***(b)****Subtraction of peaks (1) and (3) gives a DAVLL signal. This is recorded from caesium*

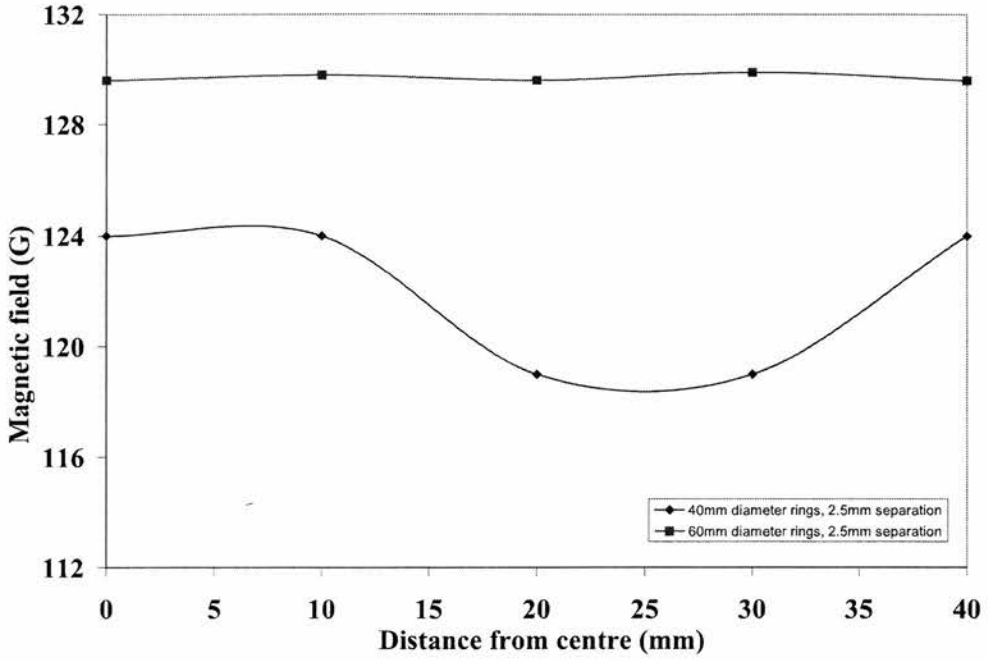

Figure 3.3: *Variation of magnetic field horizontally through annular disks of magnetic embedded material*

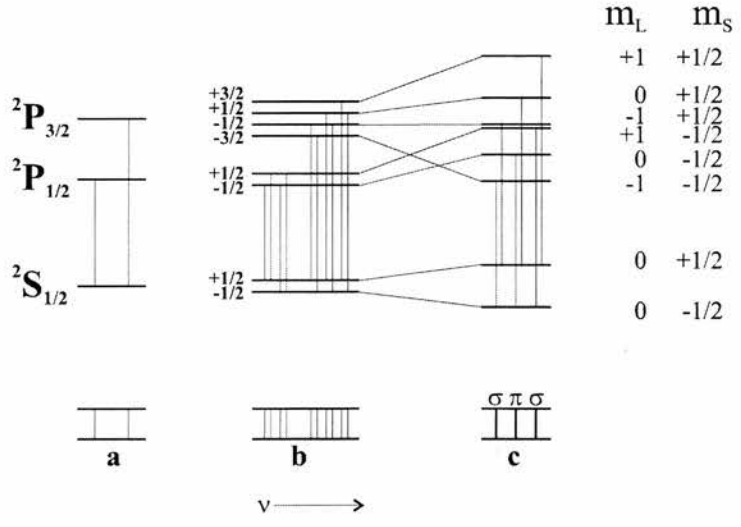

Figure 3.4: ***(a)****Atomic D1 and D2 levels in Na; Splitting of energy levels in presence of* ***(b)****a weak magnetic field,* and **(c)**a strong magnetic field, showing the magnetic quantum number m_L and magnetic spin quantum number m_S

Normal Zeeman equations can then be used. On the contrary, if $g_F \mu_B B >> A$ then the field is considered strong. The magnetic field dissolves the fine structure coupling. In this case the Paschen-Back equations are used. For intermediate cases, the Breit-Rabi equations are used for levels with $J = 1/2$, and equations for other levels can be calculated from the diagonalised hyperfine Hamiltonian [8]. Spin-orbit coupling increases rapidly with increasing nuclear charge. Therefore, the conditions for a 'strong' field are met at much lower field with lighter atoms than with heavy ones. The small splitting of the P-levels of the isotopes, shown

Energy Level	**Hyperfine Splitting Constant, A**	**Intermediate Field Strength (T)**
$^{133}Cs\ ^6P_{3/2}$	50.5 MHz	0.0036
$^{133}Cs\ ^6S_{1/2}$	2.298 GHz	0.154
$^{85}Rb\ ^5P_{3/2}$	25.03 MHz	0.0018
$^{85}Rb\ ^6P_{3/2}$	3.035 GHz	0.217
$^{87}Rb\ ^6P_{3/2}$	85.8 MHz	0.0061
$^{87}Rb\ ^6P_{3/2}$	6.834 GHz	0.489

Table 3.1: *Hyperfine splitting constants and field strengths for* ^{133}Cs, ^{85}Rb *&* ^{87}Rb.

in Table 3.1, illustrates how only a relatively weak external field is required to change from the normal weak Zeeman splitting into the Paschen-Back effect, with a magnetic field of the order of 100 Gauss. The magnetic sublevels of the hyperfine levels are normally degenerate, but they can be split noticeably when an external field is applied. Different polarisations of incident light will give different transition frequencies. For example, π (plane polarised) radiation excites $\Delta m_F = 0$ transitions, whilst σ^+ and σ^- circularly polarised light excites $\Delta m_F = \pm 1$ transitions.

3.2.2 Why use DAVLL? Comparison with other locking methods

As previously mentioned, other methods for stabilising a diode laser's frequency are current modulation, saturated absorption spectroscopy and polarisation spectroscopy. These methods lock the ECDL to an atomic resonance, which is essential when cooling and trapping atoms. Most locking techniques use feedback from Doppler-free signals to control the current and/or PZT voltage, which thus maintains the laser frequency at the required value. Dithering of, or rapidly controlling, the laser current is used to reduce rapid fluctuations in laser frequency, which contribute to the laser linewidth [4].

In saturated absorption spectroscopy, a Doppler-free signal is obtained by looking at only the atoms moving perpendicular to the probe laser beam. This will give a series of peaks relating to the atomic transitions occuring as photons are absorbed and emitted. Using suitable feedback electronics, the laser can be locked to the side of one of the transition peaks. However, as can be seen (figure 2.15), the peaks are very narrow with a large gradient slope. When the laser jumps frequency (due to noise or other disturbances), it is often with a greater frequency change than that of one of these slopes. The locking circuitry is unable to recover the original frequency position, and so the laser becomes unlocked quite easily. The large recapture range (large slope) of DAVLL means that the laser is more likely to return to its locked position after a frequency jump.

Polarisation locking is a similar method to saturated absorption techniques, but the polarisation rotation of the probe beam is monitored rather than the change in the absorption. The slope of the signal is about seven times larger than that of the saturated absorption signal over a range of about 100MHz, making this

locking technique more sensitive than saturated absorption. The signal-to-noise ratio is also much better, since the larger slope allows for bigger jumps of the laser frequency (e.g. by knocking the optical table) without losing the lock. In this respect, polarisation locking is comparable to DAVLL.

In current modulation, the basic equipment and geometry are the same as for saturated absorption spectroscopy. The current is dithered at the same time as the PZT is scanned. This allows high frequency noise to be filtered out, while the PZT filters out low frequency noise. However, a lot of (expensive) electronics is needed to modulate the diode current, and also adds to the amount of equipment needed to run just the laser system(s).

3.3 Equipment Used

A standard Littrow configuration [5] is used to produce an external cavity diode laser (see Chapter 3). Two single longitudinal mode laser diodes were used with caesium and rubidium respectively. For use with the caesium cell, a SDL-5410-G1 laser diode operating at 852nm with a maximum output power of 100mW was chosen. A Hitachi 7851G laser diode operating at 780nm with a maximum output power of 50mW was used with a rubidium cell. A diffraction grating with 1200 lines/mm blazed at 300nm and held at the Littrow angle was used for each diode to achieve feedback. The diffraction grating is mounted on a machined holder inserted into a clear quadrant design commercial mirror-mount (Newport P100-AC). The mirror-mount design allows easy access to the laser and also the freedom to use the laser with diffraction-gratings of both 1200 lines/mm and 1800 lines/mm (Optometrics UK). The laser diode is mounted in a commercial collimating tube (Thorlabs LT110P-B) which is mounted on a baseplate. This

whole is affixed to a large cylindrical base that is temperature-stabilised to a few mK. A piezo-electric element (PZT) placed between the horizontal adjustment screw and the main plate of the mirror-mount allows the position of the grating to be adjusted minutely. Mostly, experiments were carried out at 852nm, using a cylindrical vacuum cell of caesium atomic vapour. To create a magnetic field, a set of permanent magnets in the form of iron impregnated rubber were cut into rings. The central hole was large enough to fit around the glass vapour cell, and the outer diameter could be varied. We used two sets of eight rings, with outer diameters of 40mm and 60mm respectively. The field produced was about 100 Gauss. The separation of the rings was kept the same by using non-magnetic spacers; we used thick cardboard. We also used an electromagnet in place of the permanent magnets so that we could vary the magnetic field. However, it was noted (by mistake) that the photodiodes used to detect the light beams should not be too close to the electromagnet, since it will affect them and lead to spurious results! To complete the DAVLL apparatus, there was a quarter-wave plate and a cubical polarizing beam-splitter. Two photodiodes were used to intercept the beams from the beam-splitter, and these in turn sent their signals to an oscilloscope.

3.4 Using the DAVLL system

3.4.1 The 852nm Extended-Cavity Diode Laser

As in our other experiments, we had chosen to use an extended cavity diode laser since it is so easy to tune its frequency. However, previously we had been working with rubidium vapour, with its transitions around 780nm. With the DAVLL system, we had chosen to use caesium, which is same group as rubidium

and is able to be used in cooling, trapping and guiding situations. Caesium has one natural isotope with atomic weight of 133 and transition frequencies around 852nm. This is further into the infrared region than the rubidium systems, so it was harder to see the beam for alignment purposes, although of course infrared viewers and cards were used.

Before setting the diode into an extended cavity geometry (exactly as with the 780nm diode lasers), it was characterised. The threshold of lasing was at about 15mA input current (figure 3.5). The diode laser was then put into the extended

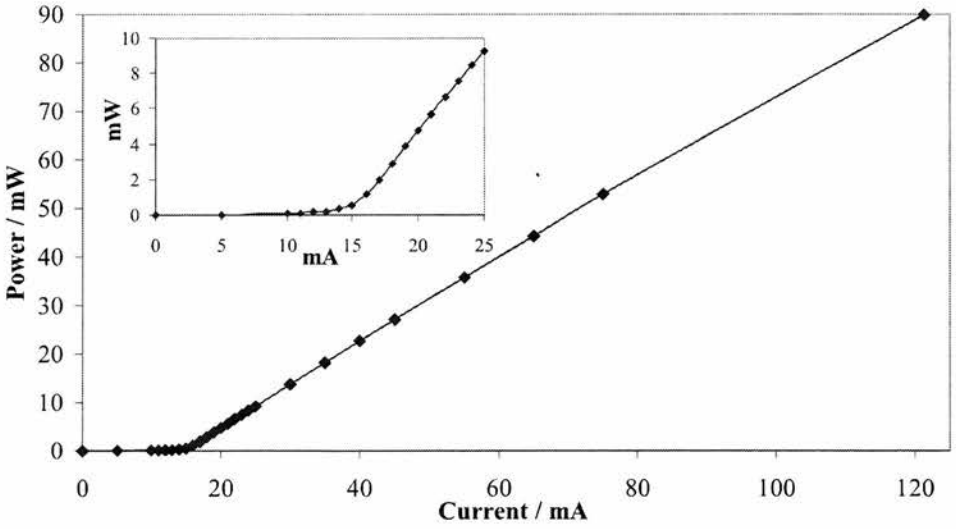

Figure 3.5: *Power versus Current for free-running 852nm diode laser. The insert shows the threshold in detail*

cavity geometry. Two different blazed gratings were tried, to see which gave the best results. Firstly a 750nm blazed grating was used (figure 3.6) and then 300nm (figure 3.7). This latter should be better, since it should be less efficient in its first order, i.e. the light sent back into the diode and thus should give a

higher power in its zero order output. Above the threshold, the graph appears

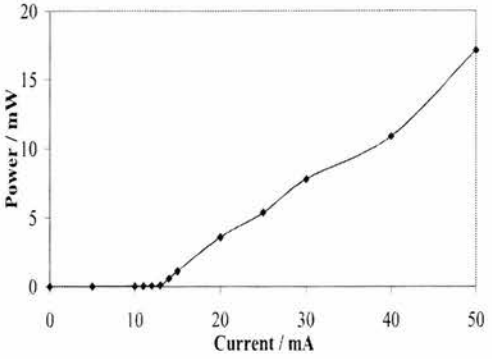

Figure 3.6: *852nm ECDL with 750nm blazed grating*

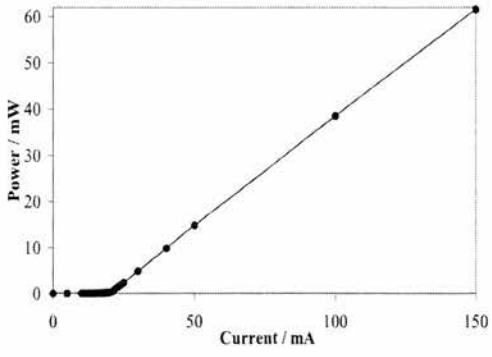

Figure 3.7: *852nm ECDL with 300nm blazed grating*

uneven, and it is not known for certain what caused this. It is probably because of uneveness of the power meter, since the signal becomes obviously more unstable if the light beam is incident near the edge of the detector. For the ECDL to be usable as a spectroscopic source, it must be running as a single mode. This was checked using an optical spectrum analyser (OSA), consisting of a high finesse ($\sim$ 600) etalon with a free spectral range of 300MHz. The frequency of the output light was measured using a monochromator, and then tuned (discontinuously) by rotating and translating the grating with the horizontal control of the mirror mount. Turning the screw approximately an 8th turn at a time gave frequency tuning of up to 13nm, see Figure 3.8. By changing the current to the PZT, it was possible to tune the ECDL smoothly over 8GHz, as measured using the OSA. The linewidth was also measured with the OSA to be about 520kHz, see Figure 3.9. This represents possibly the simplest high performance ECDL operating at 852nm.

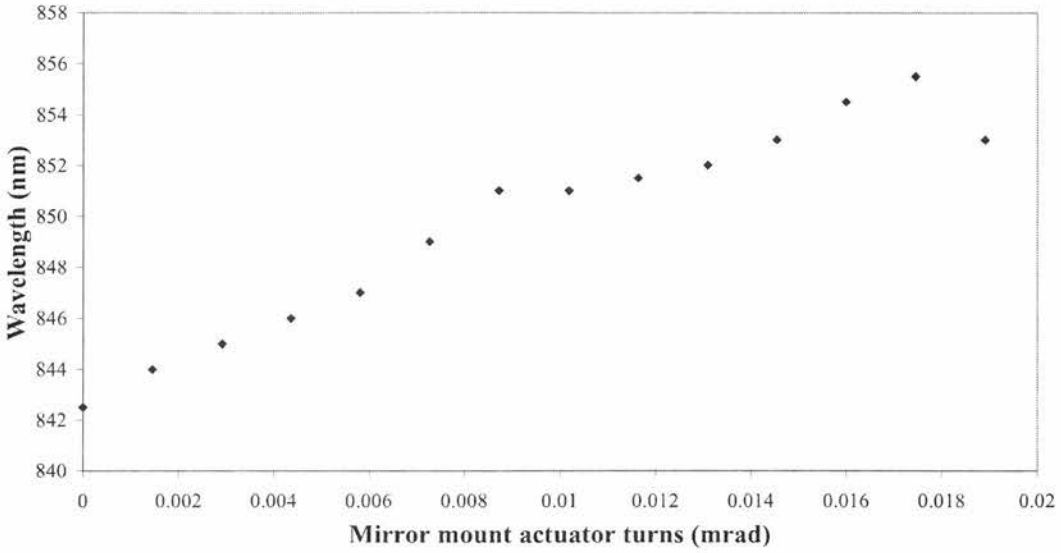

Figure 3.8: *Discontinuous tuning of 852nm diode (750nm blazed grating)*

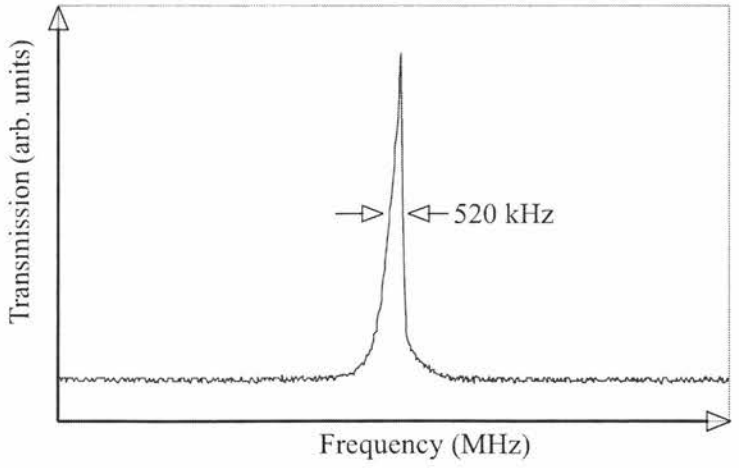

Figure 3.9: *Linewidth of the 852nm ECDL measured with the OSA*

3.4.2 The DAVLL system

Linearly polarised light, which as mentioned previously can be considered to be made up of equal proportions of left- and right-circularly polarised light, passes through the vapour cell in the presence of a magnetic field. The variation of the magnetic field (for both annular disks and the electromagnet) was less than 9%. Upon exiting the cell, the light beam is immediately incident on a quarter-wave plate with both its fast and slow axes orientated at 45° to the plane of incidence of the linearly polarised light. The following polarising beam-splitting cube then separates the light into two components of orthogonal polarisation. These are each incident on a different photodiode. Subtracting these two signals gives a dispersive signal passing through zero, as can be seen in the DAVLL curve generated for caesium (Figure 3.10). If the frequency separation of the two signals is too great, then a 'kink' appears in the DAVLL dispersive curve. This is not actually a problem, since a lock can still be produced. The capture range of the

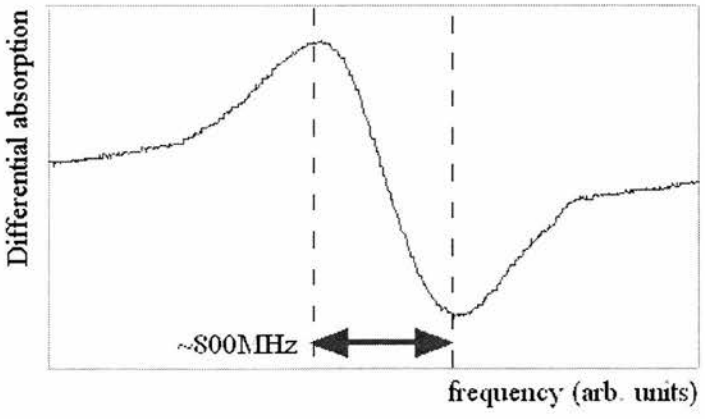

Figure 3.10: *A DAVLL signal recorded for caesium*

locking signal is large (500MHz), which means that the laser can recover from most jumps in frequency (which are generally much less than 500MHz).

In order to ensure that the laser was at the correct atomic transition frequency, a saturated absorption signal was also taken. However, the peaks did not look as they appeared in print elsewhere. It was decided that this was because there was too much power in the beams. Using too high value a neutral density filter made the photodiodes more sensitive to mains ripple, though. A compromise of ND 1 in the probe and ND 0.2 in the pump gave the best results. Use of ND filters also reduced feedback, since light reflecting back would be attenuated a second time by the filter. This helped to stop the diode laser from going multimode. The current into the diode laser was also increased (from about 59mA to about 100mA), which gave a better signal.

The laser was locked to the caesium transition line using the DAVLL signal as input into the locking circuit. A small fraction of the locked laser light was split off and sent into an optical spectrum analyser (OSA) and seen to be quite steady, Figure 3.11(a). Causing perturbations to the optical table (by hitting it) made the signal jump, but it quickly returned to its locked position. The system was then left for several hours while a Tektronix digital oscilloscope recorded the output signal from the OSA. The drift of the system could be seen by the 'thickness' of the recorded lines and was measured to be about 5MHz/hour, Figure 3.11(b). For the unlocked system, the drift was much larger over a shorter time, as seen in Figure 3.11(c). This can be readily improved by stabilising the temperature of the system [4].

In the original method [4], it was stated that the locking point of the ECDL can be tuned whilst retaining the lock. Corwin *et al* [4] briefly mention that rotating the waveplate imbalances the signals at both photodiodes and enables one to tune the locked laser. However, no details for tuning were given. A simpler and more flexible way to tune the locked laser frequency is to place either a rotatable polariser or variable neutral density (ND) filter in front of one of the

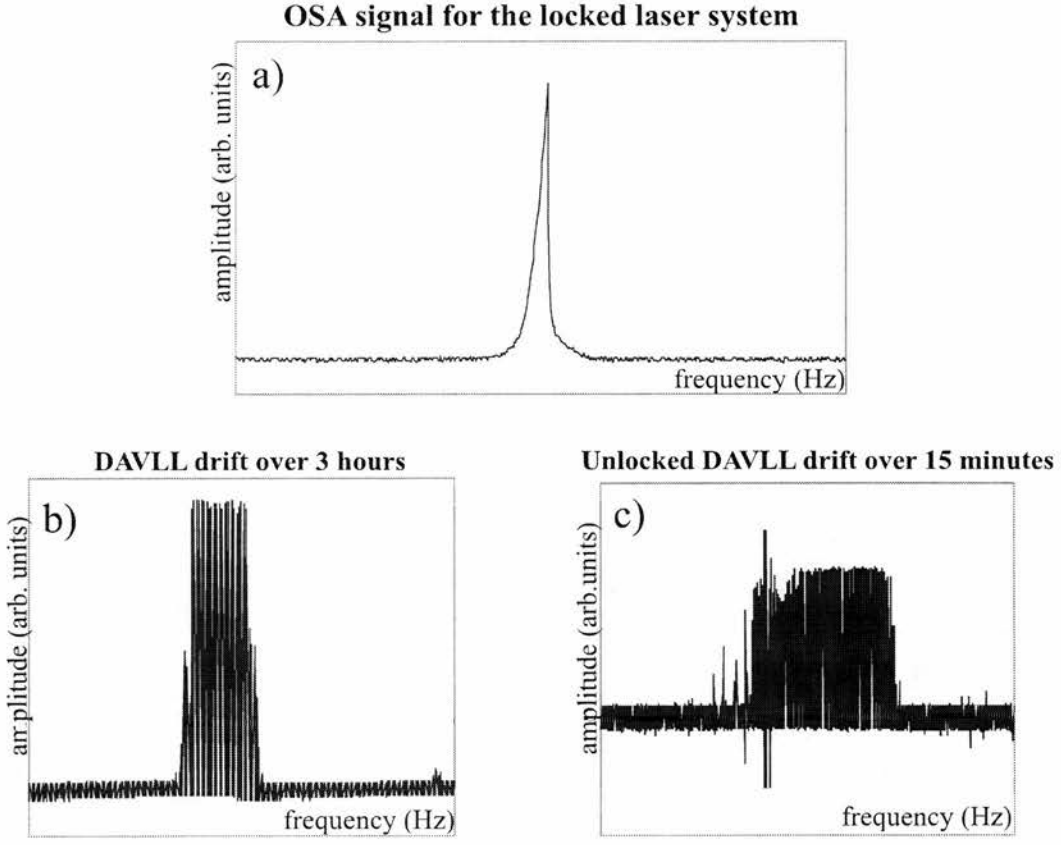

Figure 3.11: ***(a)****Signal from the OSA for the locked laser system; Drift of the laser system over:* ***(a)****3 hours, Locked, and* ***(b)****15 minutes, Unlocked*

photodiodes. This allows for much greater control in varying the locking point. Rotating the polariser or varying the value of ND filtration changes the amount of light reaching that photodiode and thus imbalances the signal of the two Doppler broadened peaks. A numerical model of this superimposed with experimental data for frequency tuning using the rotating linear polariser is shown in Figure 3.12. A very good fit is seen between theory and experiment. The lock point

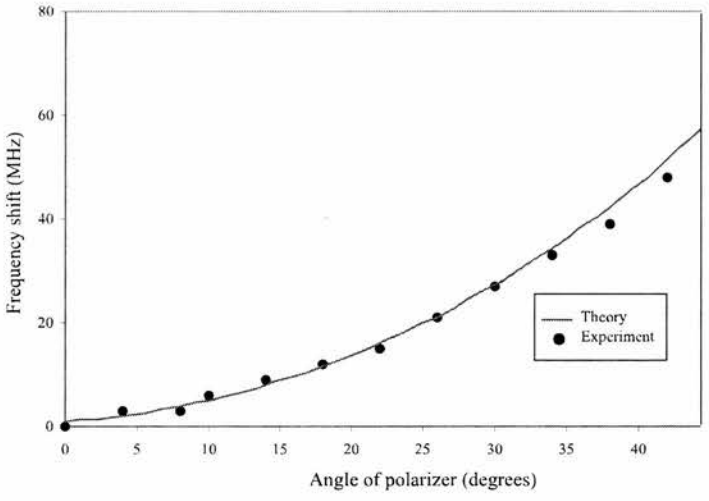

Figure 3.12: *Tuning the frequency by rotating a linear polariser in front of a photodiode. A good fit to theory is shown.*

is a zero in net photocurrent. Experimentally, it can be seen that this method offers greater flexibility over the rotation of the waveplate and the ability to tune both up and down in frequency (by placing the polariser/ND filter before either photodiode) from the original lockpoint.

3.5 DAVLL signal modelling for rubidium

To see how DAVLL works, a computer model was made. First an 'ideal' Doppler broadened signal[1] was taken as a Maxwell-Boltzmann distribution. This is given by the equation:

$$I_\nu = I_0 e^{\frac{-c^2(\nu_0-\nu)^2}{\nu_0^2\alpha^2}}$$

where the most probable atomic velocity, $\alpha = (\frac{2kT}{m_A})^{\frac{1}{2}}$, m_A is the atomic mass, k is Boltzmann's constant and T the temperature. Next we need two of these distribution signals separated by some frequency. Take one signal as centred on ν_0, the other centred on ν_1. Thus the dispersive signal will be given by subtracting one from the other:

$$I_\nu = I_0 \left(e^{\frac{-c^2(\nu_0-\nu)^2}{\nu_0^2\alpha^2}} - e^{\frac{-c^2(\nu_1-\nu)^2}{\nu_1^2\alpha^2}} \right)$$

For a magnetic field of about 120G, the separation of the peaks is about 800MHz, so that $\nu_1 = \nu_0 + 800MHz$. The relative size/power of each peak is affected by the rotation of the quarter-wave plate. The zero-point on the resultant dispersive slope is therefore affected by this.

The central intensity of one peak $I_0 = cos^4(\theta) + sin^4(\theta)$, so that the relative intensity of the other peak is given by $2.sin^2(\theta).cos^2(\theta)$. The zeropoint (locking position) is given at frequency ν when $I(\nu) = 0$, that is

$$I_0 \left(e^{\frac{-c^2(\nu_0-\nu)^2}{\nu_0^2\alpha^2}} - e^{\frac{-c^2(\nu_1-\nu)^2}{\nu_1^2\alpha^2}} \right) = 0$$

However, turning the quarter-wave plate causes both peak amplitudes to vary at once. By rotating a linear polariser in one beam varies the amplitude of one peak only, and by changing which beam is attenuated, the zeropoint can be moved up

[1] "Spectrophysics" by Anne Thorne (Chapman & Hall) covers this quite well

and down in frequency from the original centre. The amount by which a beam is attenuated by the rotating polariser is given by Malus' law: $I(\theta) = I_0.cos(\theta.\frac{\pi}{180})^2$.

MathCad was used to model DAVLL for rubidium and caesium (see Appendix).

3.6 Conclusions

Stabilisation of an extended cavity diode laser at 852nm using the Zeeman effect in caesium vapour has been studied. This is the first known time that this method of frequency locking has been applied to a simple ECDL at 852nm. Whilst studying this system, a method of tuning the locked ECDL using an optical offset has been used and the frequency shifts recorded. The Zeeman (DAVLL) method is versatile and simple. The resulting stabilised ECDL is suited for many applications, including laser cooling of caesium. The same system can be used with other elements to lock lasers to other atomic transition frequencies. Rubidium has been used to lock an ECDL to 780nm.

Bibliography

[1] C.S.Adams and E.Riis, Prog.Quant.Elec. **21**, 2 (1997)

[2] C.E.Wieman and L. Hollberg, Rev.Sci.Instrum. **62**, 1 (1991)

[3] M.A.Clifford, G.P.T.Lancaster, R.S.Conroy, K.Dholakia, J.Mod.Opt. **47**, 1933 (2000)

[4] K.L.Corwin, Z.T.Lu, F.Hand, R.J.Epstein, C.E.Wieman, Appl.Optics **37**, 3295 (1998)

[5] M.A.Clifford, J.Arlt, J.Courtial and K.Dholakia, Opt.Comm. **156**, 300 (1998)

[6] G.P.T.Lancaster, R.S.Conroy, M.A.Clifford, J.Arlt, K.Dholakia, Opt.Comm. **170**, 79 (1999)

[7] Haken & Wolf, The Physics of Atoms and Quanta, fifth edition, [Springer]

[8] E.M.Arimondo, M.Inguscio, P.Violino, Rev.Mod.Phys. **49**, 31 (1977)

Chapter 4

Laguerre-Gaussian Light Beams

4.1 The need for hollow light beams

It has already been discussed (in chapter 2) that atom density in a normal magneto-optical trap (MOT) is limited by light assisted collisions between the atoms. As mentioned, a dark-spot MOT, where repumping light is excluded from the centre of the trap, results in a dramatic reduction in the light-induced loss. A hollow-core beam used for repumping only those atoms outside the trap centre would have this effect.

Similarly, atom guiding has been mentioned previously. When atoms need to be guided from one place to another, hollow fibres can be employed, but light must be used to prevent the atoms from sticking to the glass walls of the 'tube' due to the Van der Waal's force. However, it would be useful to have a laser beam with an annular cross section for either coupling an atom beam into the fibre, or replacing the fibre altogether. This latter case would mean that the Van der Waal's force which caused problems in the fibre could be overcome.

4.2 Various hollow light beams

There are several ways of producing 'hollow' light beams, some better than others. The easiest method might seem to be to shine a normal Gaussian beam through a glass slide with a dot printed onto it. This has been used by at St. Andrews as a quick method of seeing atoms being guided out of a MOT. Another way would be to couple light into the glass part of a hollow-core fibre. The light exiting from the other end of the fibre would be in the form of an annulus. Other light beams are more complex to produce, but are preferential for a number of reasons, as shall be discussed below. These include Laguerre-Gaussian and Bessel modes, both of which can be produced with a central dark region surrounded by one or more bright concentric rings.

4.3 What are Laguerre-Gaussian beams?

The usual output of a laser, in terms of transverse modes, can be described as a product of a Hermite polynomial and a Gaussian polynomial and is known as a Hermite-Gaussian (HG) modes. These modes are rectangularly symmetric. There is another class of paraxial light beams which are circularly symmetrical, usually denoted LG_p^l, where l and p are the two integer indices that describe the mode. l is the number of 2π cycles of phase in the azimuthal direction around the circumference of the mode, while $(p+1)$ gives the number of nodes across the radial field distribution. These are known as Laguerre-Gaussian modes and are of interest because the azimuthal phase term indicates the presence of orbital angular momentum. More importantly for atom trapping and guiding are the modes where the radial term (p) is zero, which gives a dark central 'hole' surrounded by a single bright annulus. The analytic form of their amplitude is [1]:

$$E(LG_p^l) \propto \exp\left[\frac{-ikr^2z}{2(z_r^2+z^2)}\right] \exp\left[\frac{-r^2}{w^2}\right]$$
$$\times \exp\left[-i(2p+l+1)\arctan\left(\frac{z}{z_r}\right)\right]$$
$$\times \exp[-il\phi](-1)^p \left(\frac{r\sqrt{2}}{w}\right)^l L_p^l\left(\frac{2r^2}{w^2}\right) \quad (4.1)$$

where z is the distance from the beam waist, z_r is the Rayleigh range, k is the wave number, w is the radius at which the Gaussian term falls to $1/e$ of its on-axis value, r is the radius, ϕ is the azimuthal angle and L_p^l is the generalised Laguerre polynomial. The term $\arctan(z/z_r)$ is the Gouy phase of the mode.

4.4 Generation of Laguerre-Gaussian modes

A simple method for obtaining Laguerre-Gaussian modes is to convert the Hermite-Gaussian mode output from a conventional laser. This can be performed by using a spiral phase plate (not described here), a hologram, or cylindrical lenses. The first two introduce a screw-phase dislocation in the centre of the beam, which on propagation causes destructive interference and leads to the characteristic annular intensity pattern. Using cylindrical lenses, it is possible to convert Hermite-Gaussian modes of all orders into corresponding Laguerre-Gaussian modes. Unlike spiral phase plates and holographic converters, this method can, in principle, produce pure Laguerre-Gaussian mode. However, it needs an open-cavity laser, which rules out laser-diodes.

4.4.1 Holograms

A hologram is a record of the diffraction pattern formed between a reference field at an electromagnetic of interest. Thus, to holographically recreate a Laguerre-

Gaussian mode, the diffraction pattern needs to be recorded onto film. In this case, the pattern takes the form of a diffraction grating with l dislocations or 'forks'. Laser light passing through this receives a screw phase dislocation on the beam axis, giving the characteristic $exp(-il\phi)$ phase structure of a Laguerre-Gaussian beam. In the far field an annular intensity pattern (for $p = 0$ modes) is obtained.

The formula for determining the form of the forked hologram is straightforward. Using polar coordinates, a binary grating will be produced by [1]:

$$l\frac{\phi}{\pi} = n + \frac{2r}{\Lambda}cos\phi \tag{4.2}$$

Where $n = 0, \pm1, \pm2, \ldots$ and Λ denotes the grating period. This formula relates the boundaries between the transparent and opaque areas of the hologram. High efficiency holographic elements may be obtained by converting such an amplitude hologram into a phase hologram and blazing it to maximise the light in the first diffracted order. In this case, the transmittance function of the hologram may be written as [2]:

$$T(r, \phi) = \exp(i\delta H(r, \phi)) \tag{4.3}$$

δ denotes the amplitude of the phase modulation. The holographic pattern H is given by:

$$H(r, \phi) = \frac{1}{2\pi}mod\left(l\phi - \frac{2\pi}{\Lambda}rcos\phi, 2\pi\right) \tag{4.4}$$

where $mod(a, b) = a - int(a/b)$.

Generally, when a fundamental Gaussian mode (TEM_{00}) shines through such a hologram, the output is a superposition of an infinite number of LG modes, each having the same l index but with a range of values for the p index. An analytical decomposition of the output beam shows that the $p = 0$ mode contributes 78.5% of the intensity in the first diffracted order. Higher order LG modes have

contributions of $p \neq 0$ which may be simply determined:

$$E_{lp} = \sqrt{\frac{p!}{(p+1)!}} l\Gamma\left(p + \frac{l}{2}\right)/2p! \tag{4.5}$$

For a given azimuthal index, the above formula can be used to determine the contribution E_{lp} of each radial index p to the field amplitude. This formula assumes identical input and output beam waists.

The holograms used in my studies were made (by J.Arlt) in the following manner. A computer-generated pattern was printed directly onto colour film (Kodak Ektachrome Professional 100) using a slide writer film recorder. Contact prints were then made onto standard holographic film (Edmund Scientific Ltd.). The film was developed and bleached using a rehalogenation bleach as detailed by Kim [4]. This allowed diffraction efficiencies of approximately 40% into the first order. Higher efficiencies can be achieved by using specialist holographic glass plates and compensating for the non-linearity of the film. However, using the method described, it is simple to make efficient holograms which are then easy to use and take up very little space. They are particularly useful for use with diode lasers, from which it would be impossible to obtain high-order Hermite-Gaussian modes for producing high-order Laguerre-Gaussian modes as in the following method. The same fundamental Gaussian mode can be used with different holograms to create a range of Laguerre-Gaussian modes. High l modes are particularly useful for transporting atoms, for example because they can be focussed much more than low l modes. This and other matters will be discussed later.

4.4.2 Mode-conversion of Hermite-Gaussian modes

The cylindrical lens mode converter is manufactured from two identical cylindrical lenses of focal length f, separated by $\sqrt{2}f$. The input beam is focussed at the midpoint of the lens system with a beam waist of $w_0 = \sqrt{(1+1/\sqrt{2})f\lambda/\pi}$. It should be possible to convert any Hermite-Gaussian mode with indices m and n (denoted $\mathrm{HG}_{m,n}$), aligned at 45° to the principal axes of the lenses, into a Laguerre-Gaussian mode with the same beam waist.

For example, a $\mathrm{HG}_{1,0}$ mode, aligned at 45° to the axes of the lenses, can be thought of as two in-phase modes, $\mathrm{HG}_{1,0}$ and $\mathrm{HG}_{0,1}$, aligned with the principal axes of lenses. The separation of the two lenses is such that these two orthogonal modes undergo Gouy phase shifts that differ by 90°. After the lenses, their superposition is a Laguerre-Gaussian mode with $l = 1$ and $p = 0$ (denoted LG_p^l). The same principles apply for higher-order Hermite-Gaussian modes, although the expansion and transformation is more complex. The Hermite-Gaussian mode is transformed into a corresponding Laguerre-Gaussian mode with $l = m - n$ and $p = \min(m, n)$.

As mentioned above, it is not possible to use this method with a diode laser as the light source. Also, using holograms takes up much less space on an optical table. In use it is not necessary to focus the beam as accurately as in the cylindrical lens method, making it simpler to use. For these reasons, and the fact that the laser diode is now established as a workhorse tool for high-resolution spectroscopy, this method is simply the best one to use.

4.5 Why use Laguerre-Gaussian beams?

Azimuthal phase and Angular momentum

In previous experiments, the angular momentum of Laguerre-Gaussian modes has been transferred to particles trapped in an optical tweezer, causing them to rotate [3].

However, the real use of Laguerre-Gaussian modes in atom-trapping and guiding is due to the radial term. As mentioned previously, with $p = 0$, there will be a dark central minimum in the beam. As will be seen later, the inner dark region gets larger and the out ring of light gets narrower as the azimuthal phase index l increases.

A dark hole in bright ring

For guiding atoms along a hollow 'tube' of light, it is of course necessary that this tube doesn't constrict (to the point of closing completely). It is possible to create a 'hollow' beam from a normal Gaussian beam by introducing an opaque disk or point into the beam, for example a dot on a glass slide. However, due to the effects of diffraction, the dark central region created will soon disappear. This does not happen in the case of Laguerre-Gaussian or Bessel beams; the dark central regions will continue theoretically forever. In the case of Bessel beams, the hole is "non-diffracting"; that is, it remains the same size over space. For Laguerre-Gaussian beams, however, although the hole remains a hole over distance, its size will change with focusing.

The Rayleigh range Z_R is used as a measure of the amount a monochromatic Gaussian light beam spreads as it propagates in space. It gives the distance over

which a Gaussian beam increases its cross-sectional area by a factor of 2, and can be defined with the following formula:

$$Z_R = \frac{\pi w_0^2}{\lambda} \tag{4.6}$$

where w_0 is the width of the beam waist and λ is the wavelength of the light beam.

The dark region of a 'hollow' beam can be utilised in a number of ways with regards to atom trapping and guiding. By using a combination of standard TEM_{00} light beams and LG_0^1 beams, Snadden and coworkers made a magneto-optical trap [6]. The number of atoms trapped was increased, because the Laguerre-Gaussian beams reduce the AC Stark shift and broadening transitions at trap centre. Kuga and coworkers trapped atoms along the centre of a Laguerre-Gaussian beam [7]. For guiding of cold atoms, it is the repulsive optical dipole force of blue-detuned laser light that allows atomic motion to be restricted to the inner, dark region of a laser beam, where photon scattering and the associated heating are minimised[1]. By focusing a Laguerre-Gaussian beam down to the open end of a hollow-core optical fibre, it is possible to guide cold atoms into it and thence guide them.

4.5.1 LG modes compared with other hollow beams

Bessel beams

As stated above, Gaussian light beams diffract as they propagate through space. The Helmholtz equation governs this phenomenon in every area of physics:

$$[\nabla^2 + \kappa^2]\phi(r, \kappa) = 0 \tag{4.7}$$

[1]G.P.T.Lancaster, R.S.Conroy, M.A.Clifford, J.Arlt, K.Dholakia, "Channeling of cold atoms along a Laguerre-Gaussian light beam" Conference paper presented at *Quantum Electronics and Laser Science*, San Francisco, 2000

However, Durnin [8, 9] pointed out that there is a class of diffraction-free mode solutions. The zeroth-order Bessel beam is one such solution and results in a beam with a narrow central region surrounded by a series of concentric rings. For an ideal Bessel beam, the electric field is proportional to the zeroth-order Bessel function J_0:

$$E(r, \phi, z, t) = E_0 \exp(i(-\omega t + k_{\|} z)) J_0(k_{\perp} r) \tag{4.8}$$

where $k_{\|} = (2\pi/\lambda)\cos\theta$ and $k_{\perp} = (2\pi/\lambda)\sin\theta$ and θ is a fixed angle [10].

For propagation in the z direction, these Bessel solutions have the property that the intensity $I(x, y, z) \propto |E(x, y, z)|^2$ obeys

$$I(x, y, z \geq 0) = I(x, y) \tag{4.9}$$

This means that the intensity profile does not change as the beam propagates through space. The Bessel beam has an intensity distribution proportional to $J_0^2(k_{\perp} r)$ with a central spot size equivalent to $2.405/k_{\perp}$. Both of these are independent of z, which implies that the central maximum propagates in a 'non-diffracting' manner. To practically realize such a beam would require that it be of infinite extent. Equation 4.8 shows that this would require a beam of infinite energy, since the electric field amplitude is not square integrable (unlike a Gaussian beam).

By Fourier transforming equation 4.8, it can be seen that the Bessel beam can be considered as a superposition of an infinite number of plane waves with their wave-vectors distributed on a cone centred along the axis of propagation. This knowledge helps to design methods of approximating a Bessel beam. One such method is to place an annular slit in the back focal plane of a lens [9]. Other methods involve using axicons or holographic techniques.

4.6 LG beams for atom guiding

4.6.1 LG guiding compared with Fibre guiding

Having cooled and trapped a sample of atoms in a magneto-optical trap, it might now be useful to move them somewhere else (for further cooling, a cleaner vacuum, etc.). This can be down a hollow fibre or a 'hollow' laser beam, as previously stated.

In the case of a hollow-core optical fibre, atoms are likely to stick to the walls of the tube because of the Van der Waals forces between atom and wall. To overcome this problem, the outer annular glass region is filled with laser light that repels the atoms from the walls by the dipole or 'gradient' force. This is the same way that atoms can be guided down 'hollow' light beams (e.g. Laguerre-Gaussian, Bessel) to create 'atom hosepipes' [11].

4.7 Experimental results

Using our external cavity diode laser with very simple holographic elements, Laguerre-Gaussian modes with azimuthal indices ranging from 1 to 6 have been generated. The laser system readily gives upto 30mW of tunable narrow linewidth laser light at 780nm. With a hologram efficiency of about 40%, 10mW of laser light in a Laguerre-Gaussian mode was obtained. This is sufficient for many cooling and trapping experiments.

The optical table was laid out as shown in figure 4.1. Anamorphic prisms were used to shape the beam so as to have a circular cross-section, since the output

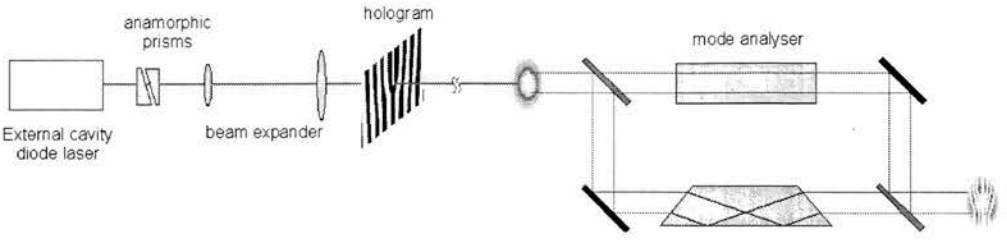

Figure 4.1: *Experimental layout for production of Laguerre-Gaussian modes using a hologram*

of the laser diode is elliptical[2]. The circular beam was then expanded so as to illuminate a larger area of the hologram and thus give a cleaner Laguerre-Gaussian mode. An aperture was used to separate the first order from the other orders generated. To ensure that this was indeed a Laguerre-Gaussian mode, it was directed into a mode-analyser. The analyser consisted of a Mach-Zehnder interferometer with a Dove prism in one arm, allowing the interference of the Laguerre-Gaussian mode with its mirror image. Figure 4.2 shows the interference patterns obtained with this arrangement for Laguerre-Gaussian modes with $l = 1, 2, 3$ and 6. The figures clearly show additional fringes on one side of each pattern, due to the differing angles of intersection of the light beams on either side of the pattern. From the additional number of fringes, it is possible to determine the mode index l. An extra $2l$ fringes should appear in the pattern for each mode observed. This occurs because the wavefronts of two Laguerre-Gaussian modes of opposite helicity intersect at different angles on either side of the interference pattern. A zeroth order, non-diffracted beam would exhibit straight fringes, showing a plane wave phase structure. The first-order beam exhibits a single fork in the fringes, indicating an $e^{i\phi}$ phase structure. The second-order beam has a double fork, indicating its $e^{i2\phi}$ phase structure, while the third

[2]Now that circulasers are available (having a microlens on the output facet of the diode) which give a circular output beam, the prisms are no longer necessary.

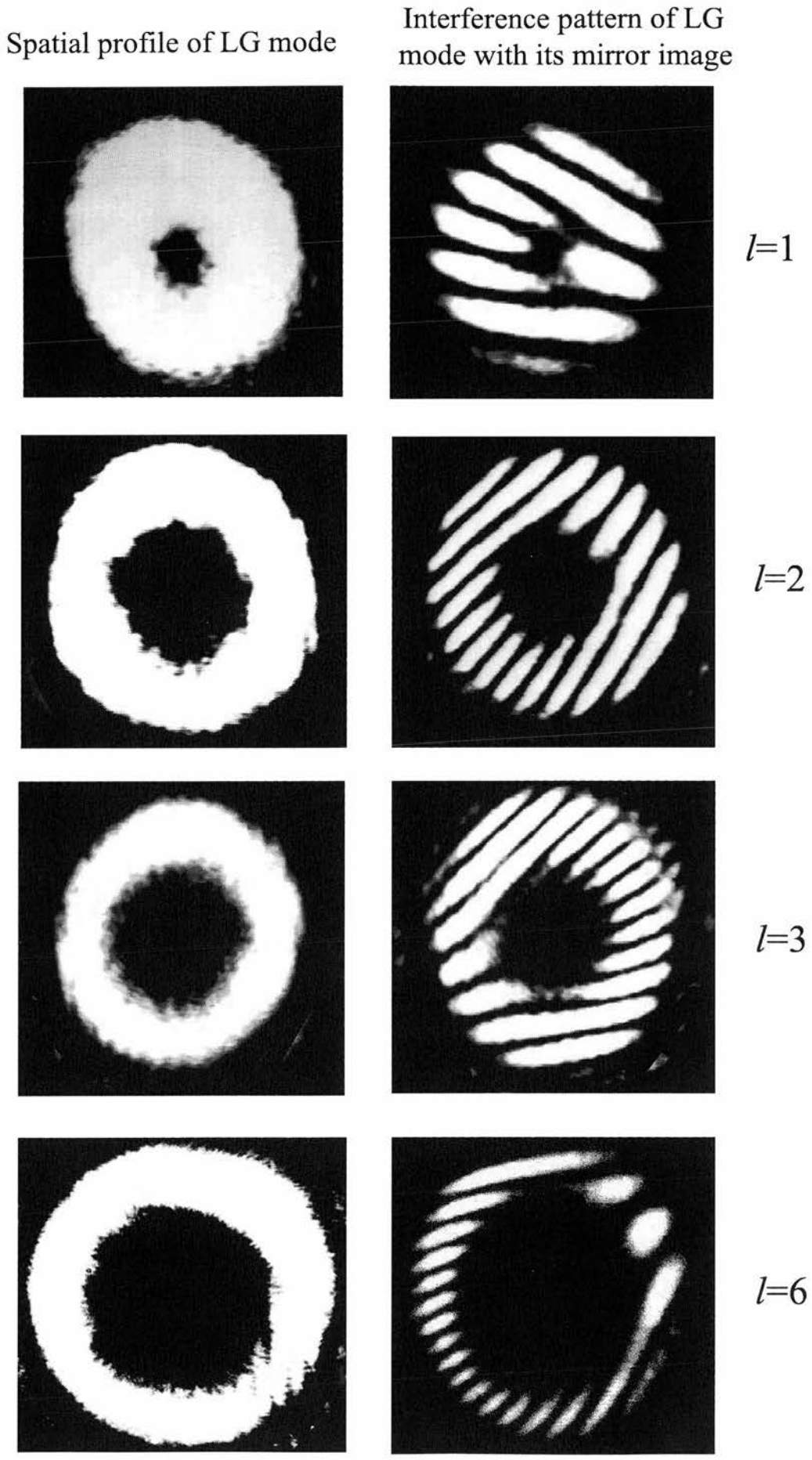

Figure 4.2: *Laguerre-Gaussian modes and interference patterns formed with their mirror images*

and sixth orders show three and six forks respectively for their $e^{i3\phi}$ and $e^{i6\phi}$ phase structures, respectively.

4.8 Hollow fibre studies

The theory of fibre guiding and some earlier experiments are given in chapter 1. Some work was done by me in modelling guiding potential, measuring hollow fibres and coupling light into the glass portion of the fibres.

4.8.1 Fibre characteristics

Guiding potential (modelled)

Previous experiments (Renn, etc.) have used 500mW guiding lasers with a 6cm long fibre, $20\mu m$ core diameter. Ito *et al* say that the depth of potential $\simeq$ $1mK$, corresponding to $30cms^{-1}$ atomic velocity. A collimated atomic beam can have a transverse atomic velocity and transverse velocity distribution of less than $5cms^{-1}$. The Doppler effect can be neglected on interactions with the evanescent wave.

The optical guiding potential is given by:

$$U(r) = \frac{1}{2}\hbar\Delta \ln\left(1 + \frac{I(r)/I_0}{1 + 4\Delta^2/\Gamma^2}\right) \tag{4.10}$$

Where $\Delta = \omega - \omega_0$ (detuning from atomic resonance ω_0)

$I(r)$ = field intensity

I_0 = saturation intensity = $1.6Wcm^{-2}$ for ^{85}Rb D2 line

Γ = natural linewidth = $6.1GHz$ for ^{85}Rb D2 line

r = distance from inner surface

barrier is highest at $\Delta \simeq \frac{1}{4}\sqrt{I(r)/I_0}$

This must overcome the van der Waals potential:

$$U_{vdW} = -\frac{1}{4\pi\varepsilon_0}\left(\frac{\varepsilon - 1}{\varepsilon + 1}\right)\frac{\langle g|d^2|g\rangle}{8k_B x^3} \tag{4.11}$$

Where ε = dielectric constant

$\langle g|d^2|g\rangle$ = matrix element of square of dipole operator

x = distance from the wall.

Assume 40% of light can be coupled into the glass.

The evanescent component extends a distance x into the vacuum, given by

$$E(x) = E_0\alpha\exp(-\kappa x) \tag{4.12}$$

ε =electric field amplitude incident at interface

factors α and κ given in terms of refractive index n, incidence angle θ and wavelength λ

$\alpha = 2\sqrt{n^2/(n^2-1)}\cos\theta$

$\kappa = (2\pi/\lambda)(n^2 sin^2\theta - 1)^{\frac{1}{2}}$

Intensity on the inner wall of the fibre is approximately the total power in the guide / cross-sectional area of the glass. $I(0) = p/A$. Field intensity relates to the electric field strength by $E = \sqrt{2I/n\varepsilon_0 c}$.

$$\therefore I(x) = I(0)\alpha^2\exp(-2\kappa x) \tag{4.13}$$

Assume the incident angle corresponds to the numerical aperture (NA) of the coupling lens, 0.1 giving ~ 0.26.

Our laser has a power $\simeq 30mW$. Cross-sectional area $= \pi(R^2 - r^2)$. Assuming all power coupled:

$$\therefore I(0) = \frac{30 \times 10^{-3}}{\pi(R^2 - r^2)} \tag{4.14}$$

For three hollow fibres made in St.Andrews, this gave the following results: The

Fibre	**Outer diameter** (μm)	**Inner diameter** (μm)	**I(o)**
1	480	10	41.465 kW/m^2
2	60	40	4.775 MW/m^2
4	440	90	51.478 kW/m^2

fibres were ink-filled so that only glass modes could be seen.

Please see the Appendix for Mathcad models of guiding potentials for various atoms and guide sizes.

4.9 Modes transported/coupled

A laser beam was focused with a convex lens of focal length 50mm onto the glass part of a hollow core glass fibre. The hollow part was ink-filled as above. The divergent annular output was collimated with a $\times 10$ microscope objective close to the fibre and a 250mm focal length lens about 200mm away from it. The plan was to couple Laguerre-Gaussian modes into the glass part of these fibres to see how well these were transmitted down the fibres. Also, since the "hole" size into higher l Laguerre-Gaussian beams is larger , could beams of even cross-section but differing angular phase be produced by coupling them through hollow glass fibres. However, since the output of such a system was so divergent and attenuated, it was not possible to interfere a transmitted mode with its mirror image as in the

case with the holographically produced Laguerre-Gaussian beams (chapter 4).

4.10 Conclusion

The ease with which it is possible to create Laguerre-Gaussian modes using a diode laser makes this a very suitable method for use in atom trapping and guiding experiments. In a trapping environment, a dark-spot magneto-optical trap utilising Laguerre-Gaussian beams for repumping leads to higher densities of trapped atoms. Cold atom beams have been guided along the centre of a Laguerre-Gaussian light beam. This is useful for taking cold atoms away from their source trap to another region, for example to be magnetically cooled into a Bose-Einstein condensate. On other occasions it might be more expedient to use the more robust hollow-core fibre. This can be used to transport atoms between different vessels, whilst maintaining the vacuum. Also, the flexible fibre allows atoms to be guided (within limits) around corners.

Bibliography

[1] M.A.Clifford, J.Arlt, J.Courtial and K.Dholakia, Opt.Comm. **156**, 300 (1998)

[2] H.He, N.R.Heckenberg, H.Rubinstein-Dunlop, J.Mod.Opt. **42**, 217 (1995)

[3] H.He, M.E.J.Friese, N.R.Heckenberg, H.Rubinstein-Dunlop, Phys.Rev.Lett. **75**, 826 (1995)

[4] N.Kim, Opt.Comm. **105**, 1 (1994)

[5] J.Courtial, M.J.Padgett, Opt.Comm. **159**, 13 (1999)

[6] M.J.Snadden, A.S.Bell, R.B.M.Clarke, E.Riis, D.H.McIntyre, J.Opt.Soc.Am.B **14**, 544 (1997)

[7] T.Kuga, Y.Torii, N.Shiokawa, T.Hirano, Y.Shimizu, H.Sasada, Phys.Rev.Lett. **78** 4713 (1997)

[8] J.Durnin, J.Opt.Soc.Am.A **4**, 651 (1987)

[9] J.Durnin, J.J.Miceli, Jr., and J.H.Eberly, Phys.Rev.Lett. **58**, 1499 (1987)

[10] C.A.McQueen, J.Arlt, K.Dholakia, Am.J.Phys. **67**, 1 (1999)

[11] K.Dholakia, Contemp.Phys. **39**, 351 (1998)

Chapter 5

Cooling and Trapping Rubidium with a mirror-MOT

5.1 Introduction - Why use a mirror-MOT?

In this chapter, I shall discuss the design, implementation and operation of a mirror-MOT for cooling and trapping rubidium atoms [1]. I shall show how it is possible to trap atoms with only four laser beams in comparison to the usual six (a standard MOT). Atoms are also trapped near to a surface, which is useful elsewhere for loading cold atoms into microfabricated magnetic traps within the surface. Drilling a hole through the mirrored surface (which is on a 45° prism) should allow easy extraction of the atoms for guiding. The position of the rubidium getter/oven near to the trapping region means that fewer atoms are lost to wall pumping and thus the vapour pressure is more controllable. I will also show how the number of atoms trapped were counted to be about 10^8, and the trap lifetime to be about 0.2 seconds.

5.2 Background

5.2.1 The mirror-MOT and surface trapping

As previously mentioned, the standard configuration for a magneto-optical trap (MOT) uses six mutually orthogonal laser beams. This works very well and has been used for numerous experiments, so why is it important establish a different trap?

Matter waveguides require controlled manipulation of the atomic de Broglie wavelength by an external potential, and such manipulation can be achieved by using light forces or the interaction of atoms with magnetic fields. Microscopic control of atoms might lead to quantum logic gates (quantum computing) and atomic optical components. The microtrap consists of a conducting 'wire' embedded within a surface. However, it is difficult to load such a trap with a cold atom cloud, since the microfabricated substrate must be placed very close to the cloud. For a conventional six-beam MOT, this surface would be in the way for one of these beams. The mirror-MOT circumvents this by making the surface into a mirror, so that it is possible to reflect one beam by 45°. This will make the equivalent of four beams (two retro-reflected) in the conventional MOT, as seen in Figure 5.1. Although mention of this novel mirror-MOT was made in Reichel and Hänsch's paper [2], no details were given as to its operation or even construction. The following designs and investigations were carried out at St.Andrews in order to further understand it and assess its suitability for use in various atom-trapping situations. The design will allow replication of this significant new atom trap.

There are other surface traps of interest too, as discussed by Hinds and Hughes [3].

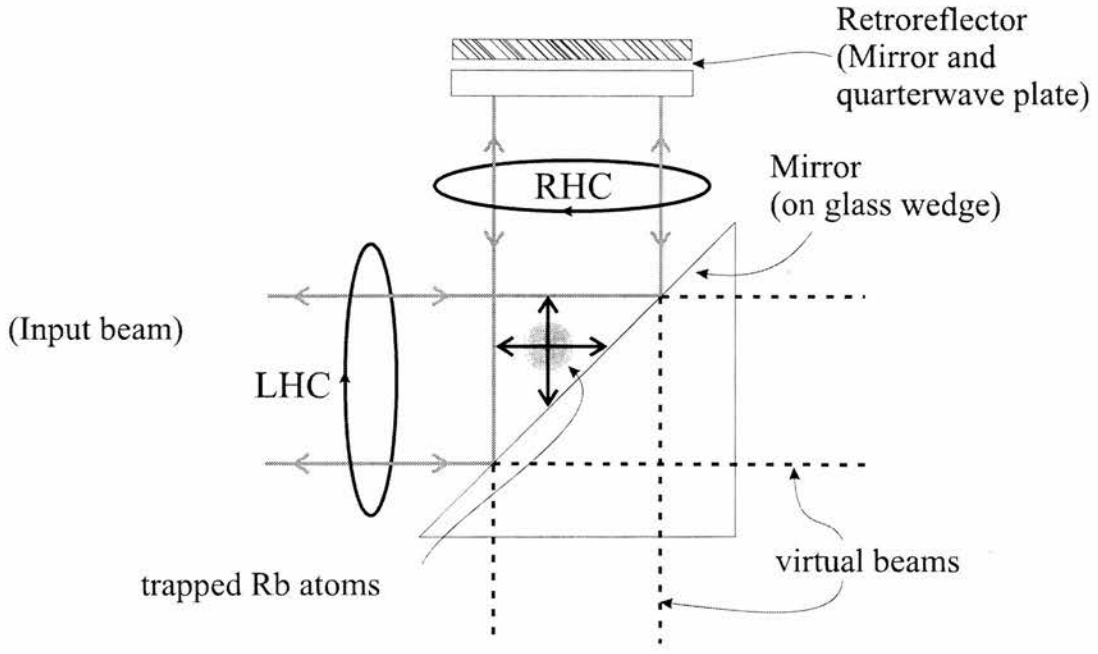

Figure 5.1: *A Mirror-MOT, showing how the two reflected beams are equivalent to four in a conventional MOT.*

In these traps, the magnetic trapping force can be made tight enough to trap individual atoms.

Hinds' own magnetic waveguide uses the Zeeman effect to trap atoms above a magnetic surface [4]. The magnetic field is produced by a surface with varying magnetization and causes a Zeeman shift in the $F = 3, m_F = -2$ sublevel. This can be used to trap ^{85}Rb atoms (within a potential well). Large mode spacing makes this trap/waveguide useful for propagating de Broglie waves in a single mode.

Folman *et al* [5] used atom chips, formed by nanofabricated wire on surfaces, to trap and guide ^{7}Li atoms. The small size of the trap should eventually allow trapping of smaller volumes (e.g. 10nm), which would be useful for manipulation of individual atoms or BEC's, and controlled collisions for atom entanglement.

5.3 Design and Construction of the System

5.3.1 Realisation - Building the mirror-MOT

A mirror-MOT needs only four laser beams in order to trap atoms. Figure 5.1 shows how one retro-reflected beam incident of the mirrored surface at 45° is equivalent to two retro-reflected beams in a conventional MOT. Only one other (retro-reflected) beam is thus needed for trapping to be possible, and this is grazing incidence on the mirror (in/out of the page in the diagram). However, atoms will still occasionally drop down into the lower ground state (in rubidium), so a separate extended-cavity diode laser (ECDL) is used for repumping atoms back into the cooling cycle. Atoms are trapped in the space bordered by the mirror surface (Figure 5.2), equivalent to the usual MOT geometry. The trapping space is half the size of that in a conventional MOT, however.

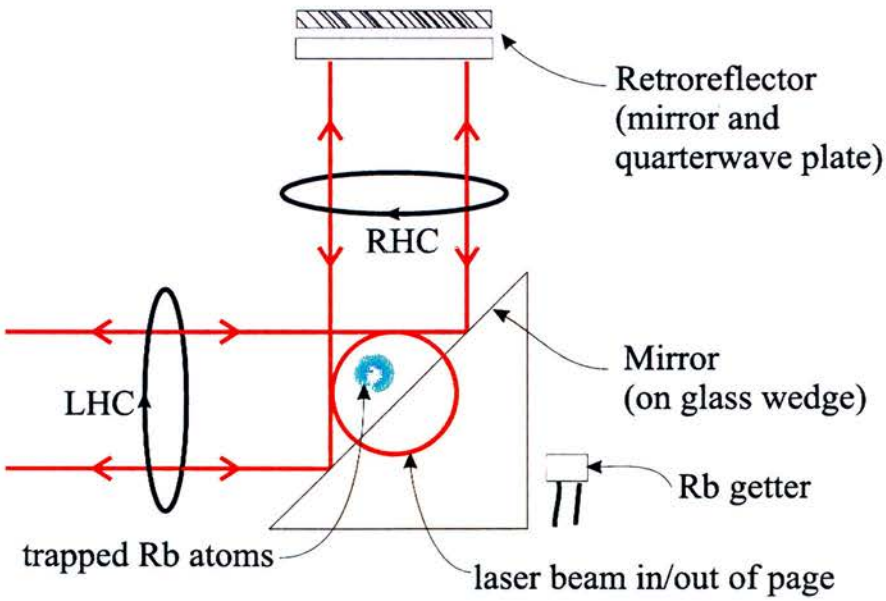

Figure 5.2: *A mirror-MOT, showing the position of the trapped atoms and also that of the Rb source*

Of course, for trapping to occur, the correct beam polarizations must be produced and the magnetic field orientated the right way. The mirrored surface and the retro-reflector produce the required beam polarizations (figure 5.2). The anti-Helmholtz coils were orientated so that their axes were vertical. In this way, by imbalancing the relative coil currents it was possible to move the atom cloud vertically.

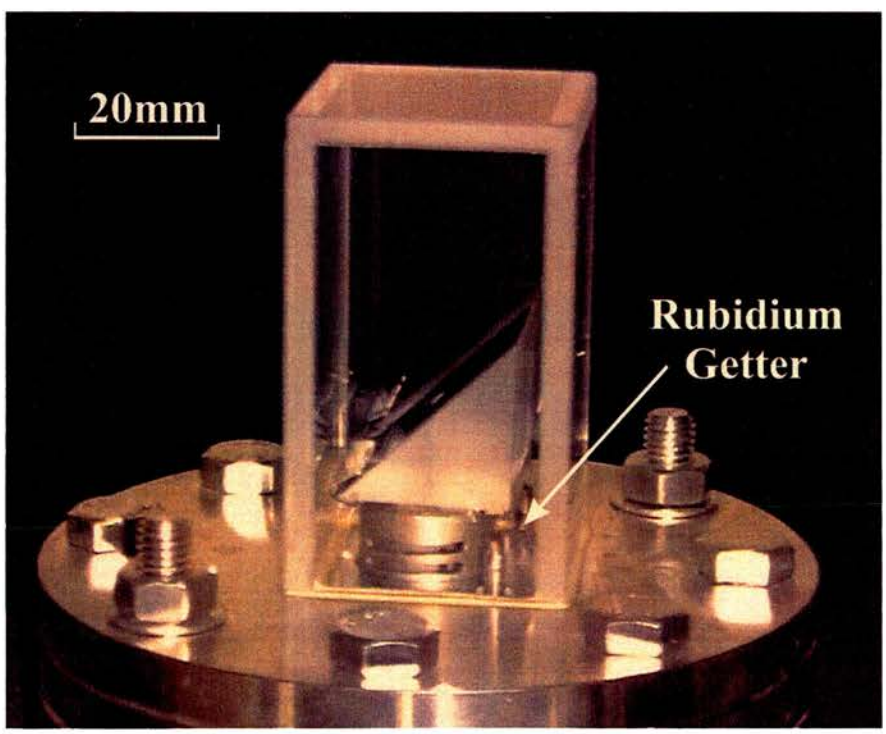

Figure 5.3: *The trapping cell of the Mirror MOT, showing the mirrored prism and the flange which attaches the apparatus to the vacuum system*

Following is a brief summary of trap construction, with more details given below. The Mirror-MOT at St.Andrews was designed and built by G.P.T.Lancaster and K.Dholakia, whereas I worked on the coils, measured the number of atoms, and so on. The trap is mounted on one flange of a standard six-way UHV cross-piece. The whole vacuum system is held at a base pressure of 10^{-10}mbar by a 25l/sec ion pump. A blank flange bored with a 25mm hole is fitted onto a 2cm long

metallic cylindrical holder. The holder has holes cut into its walls, allowing for gas flow. Upon this is attached a right-angled coated prism. Two further small holes drilled in the flange are used for connecting a rubidium getter oven[1]. By having the rubidium source so close to the trapping region, it is easier to accurately control the atomic pressure. Also, since the walls of the vacuum vessel act as pumps for any excess rubidium vapour present, the rest of the vacuum system is not contaminated by rubidium. The Rb oven is connected using kapton wire to an electrical feedthrough placed on one arm of the six-way cross. Running a current of a few amperes through the oven typically generates an adequate amount of rubidium at the trapping region. The prism and Rb getter are covered by a quartz cuboid which is fixed to the flange using low vapour pressure torr seal (Caburn-MDC, UK). The cuboid is inexpensive and commercially made (Hellma, UK), with outer dimensions of $25mm \times 25mm \times 50mm$ and wall thickness of 3mm. One end of the cell is open, and all the other sides are fused. The cuboid is normally used as a cell for spectrometry, so the glass is of high optical quality, so it is thus excellent for use in atom traps. Figure 5.3 shows the trapping cell attached to the flange and containing the mirrored prism.

The vacuum system

In building any vacuum system, ultra-high (UHV) or otherwise, the constructor should wear latex gloves and be sure to keep vacuum components away from sources of dust, vapour and anything which could contaminate a surface and cause leaks later. Copper gaskets are usually fitted into flange joints to make a good join. The copper has a smooth finish and has been treated to reduce the

[1]A Rb getter normally introduces the metal vapour into a vacuum to combine with and removes trace gases from vacuum tubes. The 'oven' heats up when current is passed through it and the rubidium sample is vapourised

amount of outgassing. A gasket is placed on to the knife-edge of a flange, so that when the joint is closed, the edge will push into the copper and make a tight seal. Rubber 'o' rings cannot be used because they outgas a lot, and cannot be baked to any high temperature. After tightening each nut, the opposite nut (with respect to the flange centre) should be tightened. This allows for an even seal by partially closing the gap between the flange faces. Sequential tightening is repeated for two more cycles until the flange faces meet and a pronounced increase in torque is felt. The kapton wire (Caburn-MDC) connecting the RB getter is designed for high and ultrahigh vacuum use to 260°C. Copper wire is dipped/insulated by Kapton Type F film and heat-treated to minimize the amount of gas trapped in it. It has a dielectric strength of 80kV/mm. To connect this to the outside world, an electrical feedthrough (Caburn-MDC) is used, utilising ceramic to metal sealing technology.

The rubidium getter itself is very important, since it must produce the correct pressure of Rb vapour in the cell. The optimum pressure for trapping is between 10^{-8}mbar - 10^{-9}mbar. This is much lower than that of a room temperature sample ($\approx 5 \times 10^{-7}$mbar). In a vacuum system made of stainless steel, Rb vapour will be removed by chemical reactions and absorption. This rate of 'wall pumping' starts off higher than the ion pump and depends on how well coated in Rb the walls are. Eventually an equilibrium will be reached. Removing the Rb source would have little effect initially, as the walls slowly released Rb. Fused silica or Pyrex act similarly, but other types of glass continue to pump Rb even after long term exposure to the vapour. For this reason, our cell was made from fused glass, as discussed below. The Rb source is a Rb getter or oven. In form this is a few milligrams of a rubidium compound within a stainless steel oven. When current (3-5A) is sent through the oven, Rb vapour is produced. A higher current will produce a higher vapour pressure in the cell. However, if any fluorescence is seen

in the background vapour, then there is enough Rb present to cool and trap.

The glass prism and Rb getter are within a fused glass cubical cell[2], as mentioned above. The fact that no epoxy is used means that there will be no outgassing from this part of the system. In previous experiments, five sheets of plate glass were sealed together with epoxy [13]. Our system is improved in that the low vapour torr epoxy is only between the cube's base and the flange, so that there is only one place for leaks to occur. It is also more sturdy and can be baked to higher temperatures, allowing for higher vacuums. The cell dimensions (mm)are: outside $70 \times 40 \times 40$; and inside $66 \times 32 \times 32$. It is made from optical glass with transmittance of over 80%. This allows very good optical access, is quite inexpensive, and needs no glassworking skill.

To check for leaks, a spectrometer tuned to helium is attached to the system. It is first taken down to about 0.1mbar with a 'roughing' pump and then a diffusion pump and backing pump take the pressure to 10^{-6}mbar. If the spectrometer was just detecting air, then it would be impossible to distinguish this from outgassing or leakage. Helium is then released around the system and will show up on the spectrometer if there are leaks. By tying plastic bags around all the joints but the one tested and 'squirting' helium at the flange, it is possible to find out where leaks are precisely. These may be caused by hairline scratches in the gasket or by uneven tightening of the bolts. Finding a leak would normally mean replacing the gasket.

The whole vacuum system now needs to be pumped down to a low enough pressure to start the ion pump. For this, a turbo-backed dry pump (diaphragm) was used. It will take the system down 10^{-2}mbar, after which the turbo starts and takes it to about 10^{-6}mbar. It is a better choice than an oil-sealed pump which can

[2]Data from Hellman Worldwide catalogue

introduce water vapour and oils into the vacuum. The ion pump can then be switched on to further reduce the pressure to about 10^{-8} or 10^{-9}mbar. We have used a Varian VacIon *Plus* 40 Triode pump[3]. The Triode pump allows starting from as high as 6.6×10^{-5}mbar, because ions are prevented from bombarding the system and pump walls at starting pressures, and has high speed for inert gases. It works by ionizing atoms or molecules in its capture range and then they can be taken out of the 'air'. This does mean that as the pressure drops, the chances of any particles drifting into the ion pump decrease. Also, the current produced by the moving ions can be read and the pressure can be determined by reading the current and converting this to pressure with the appropriate pressure versus current graph shown in figure 5.4. The diagram shown in figure 5.5 shows how

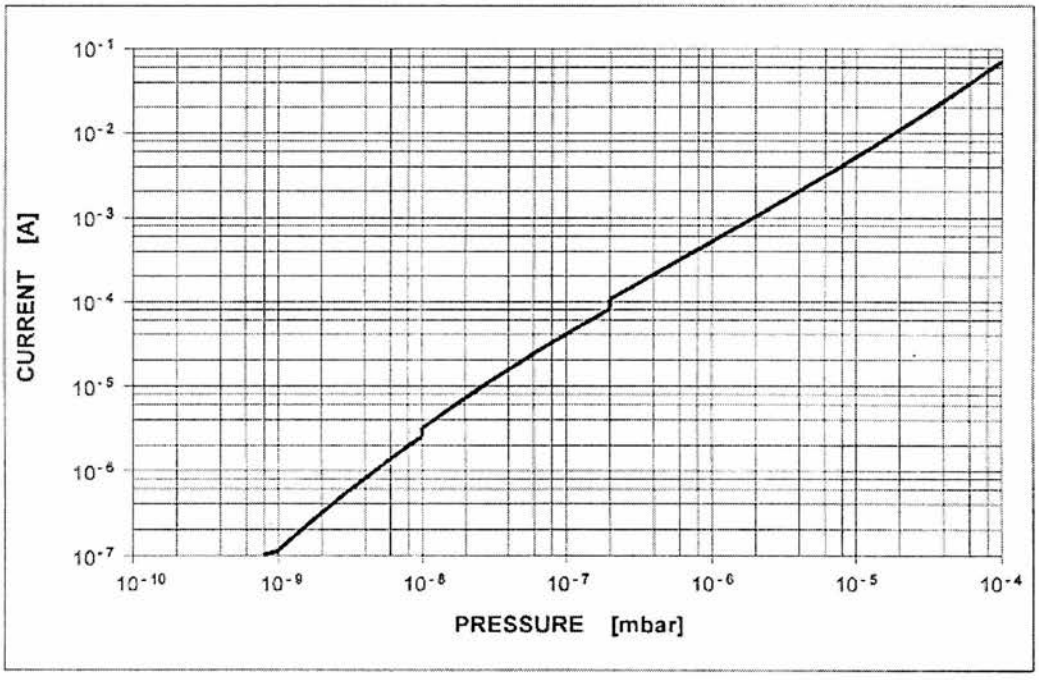

Figure 5.4: *VacIon Plus 40 Triode pump pressure (mbar) vs current diagram*

the ion pump is fitted into a typical system. We do not have the gauges. To achieve the required base pressure (i.e. less than 10^{-8}mbar), it is necessary to

[3]See Varian VacIon Plus 40 manual

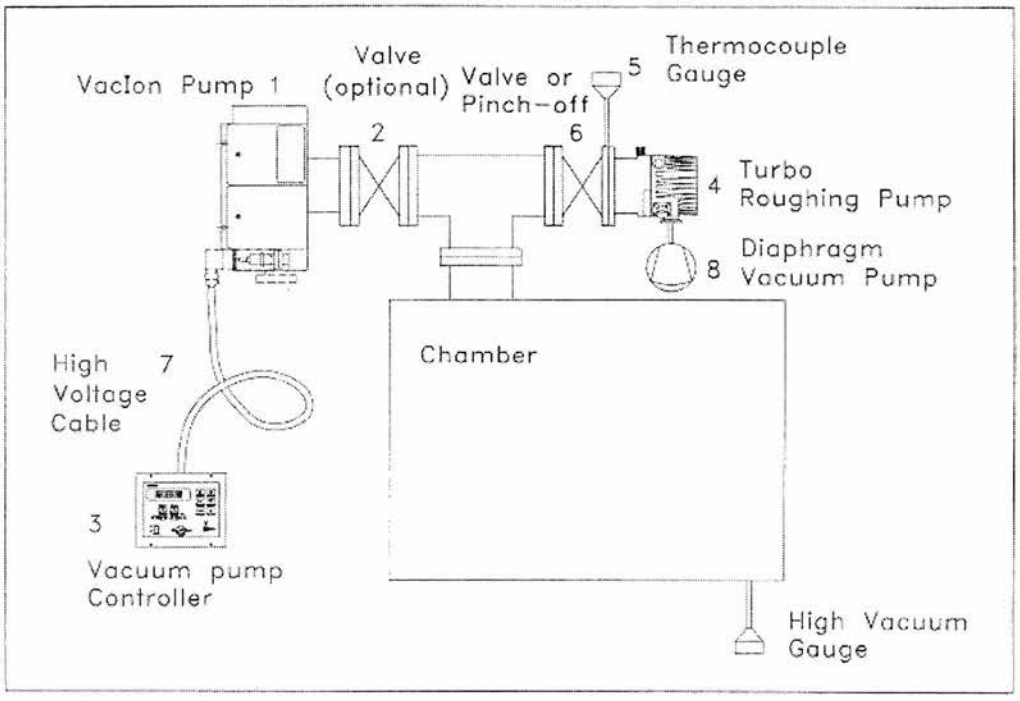

Figure 5.5: *Schematic showing a typical installation with an ion pump*

bake the system, which will get rid of a lot of the water-vapour trapped in the steel and glass walls. Thermal heating tape is wrapped around all parts of the trap system and it is heated to temperatures between 150°C and 250°C within an oven unit. This will remove water vapour from the surfaces without damaging the magnet and high voltage connector of the ion pump. Without baking pressures of $10^{-9}/10^{-10}$mbar cannot be achieved. Bakeout can open up a leak in glass to metal epoxy seals, due to the different thermal expansion coefficients of the glass and metal. However, since the cuboid was placed onto the metal (not sunk into a groove), different expansion rates should not affect the sealant (and have not to date). The low pressure epoxy (Caburn-MDC) we used is bakeable to 150°C, thermally conducting and can be used at pressures of upto 10^{-10}mbar. Thermocouples are placed around the vacuum system to ensure that the heating (and thus expansion) occurs evenly, to prevent leaks forming. The bakeout lasts

for about twenty four hours and then the system is allowed to cool, during which time a drop in pressure should be observed. The turbo pump should be switched off when the system is cool and the pressure is being maintained by the ion pump. We closed the valve to the turbo pump and removed it altogether. The trap could then be moved from the bakeout oven onto the optical table. During this brief time, the ion pump could safely be switched off without the pressure rising enough to cause problems. Of course, it was essential to support all the flange joints when the trap was being carried, so that no strain could cause a leak.

The optical system

Two diode laser systems were used to provide, respectively, the trapping light on the $F = 3 \rightarrow F' = 4$ transition and repumping on the $F = 2 \rightarrow F' = 3$ for rubidium 85. The lasers are set-up in an extended-cavity geometry, as mentioned in previous chapters. However, in this case, the diode lasers used had a virtual point microlens attached to the exit facet[4]. The diodes are available from Blue Sky Research (part no. PS026-00) and consists of a Hitachi HL7851G laser diode which has a microlens placed a few microns from the output facet. The output beam from these 'circulasers' is circularly divergent (compared to a normal elliptical beam). When collimated and in the Littrow geometry with a diffraction grating of 1200 lines/mm , this produces a highly stable, narrow linewidth laser source (<1MHz) with a circular output beam [6]. No further beam-shaping optical components [7] are required, so the trapping experiment is simplified. Additionally, the microlens attached to the diodes facet causes the system to be more stable to long-term drift. In practice, clouds of trapped atoms have been held for several minutes with the ECDL systems *unstabilised* to any

[4]This lens makes the diode laser act like a point source.

external reference. However, for reproducibility, the lasers have been stabilised using polarisation spectroscopy [8].

The whole trap apparatus was raised on a perspex base. This was done so that, in the event that the wire carrying current to the rubidium oven broke, the table would be electrically insulated and the laser diodes would not be destroyed.

5.3.2 Dual purpose - surface trap & guiding source

In a previous section, I have mentioned that the mirror-MOT is of direct interest in the field of microtrapping using magnetic fields. For this situation, a surface trap is absolutely essential. However, we have found that this system is also suitable for use as a source for guiding atoms.

Cold atoms can be guided along both hollow optical fibres and also 'hollow' light beams [9, 10]. These can be thought of as "atom hosepipes". However, first there must be a 'reservoir' of cold atoms, and secondly there must be some way of transferring these atoms into and along the atom hosepipe. The reservoir can be created easily enough, using any of the standard MOT designs. In the case of the mirror-MOT, we had drilled a small (1.5-2mm) hole in the middle of the mirrored surface. The hope was that we could channel trapped atoms into this. Various methods were considered, as laid out below.

Firstly, it was noted that if the retro-reflected beam was incident on the prism from the top, it would force atoms down into the hole. Previously, the beam had been retro-reflected from the top, which meant that there was already a 'shadow' of the hole vertically above it, so that there would be no light pressure pushing the atoms down into the hole. A plug beam sent upwards through the hole would stop atoms falling out until required. See figure 5.6. By sending a Laguerre-Gaussian

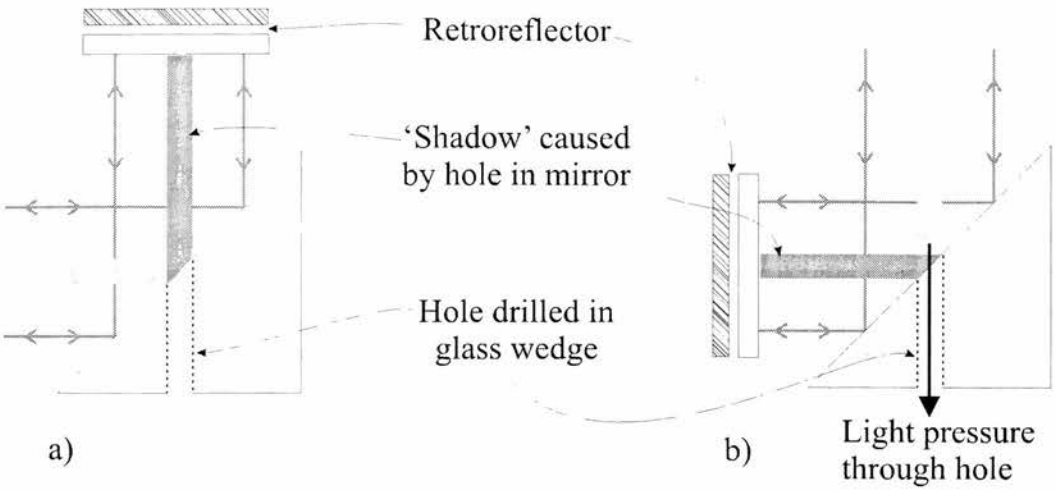

Figure 5.6: *Trap geometry showing* ***a)****vertical retro-reflection and associated 'shadow', and* ***b)****horizontal retro-reflection allowing atoms to 'fall' into the hole*

(LG) beam or a Bessel beam down onto the hole, atoms would already be within a guiding system. By 'filling' the hole in the hollow beam with normal Gaussian light, the atoms would still be cooled and trapped. A polarising beamsplitting cube could be used to effect this (figure 5.7, whilst an acousto-optical modulator (AOM) could be used to blue-detune the Bessel/LG beam so that it would guide the atoms. Another idea would be to send a guiding beam down the face of the prism, forgetting about the hole altogether.

We discussed a normal LVIS (Low-Velocity Intense Source of atoms) [11] and the fact that there is some light preventing atoms leaving the trapping region (between x-x in figure 5.8). Changing frequency detuning of the laser should give optimum atom flux out of the MOT. Also, we asked what the plug beam consists of. A 'sheet' of blue-detuned light might act like a wall, whereas a beam of on-resonance (i.e. not detuned for Doppler reasons) trapping light should push atoms back into the trapping beams and hence into the MOT. Taking this into consideration, in the case of the mirror-MOT it was decided that introducing light vertically would remove any possible 'x-x' plug beam.

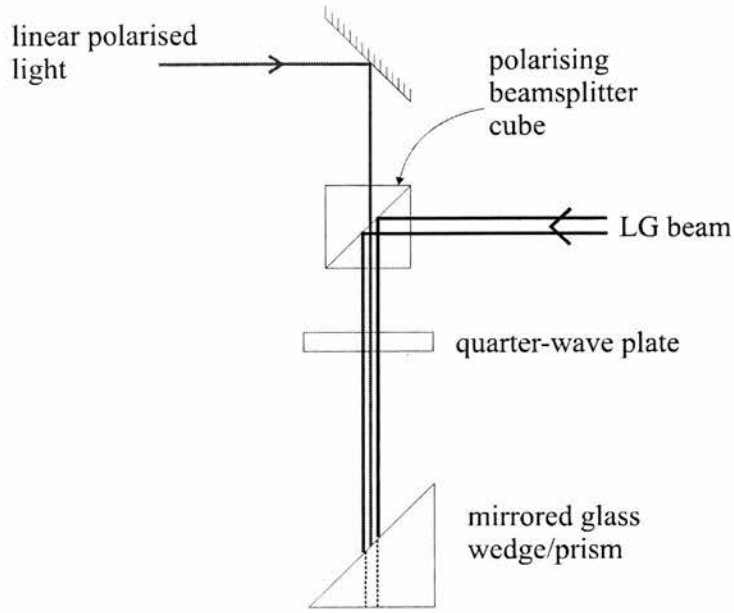

Figure 5.7: *Laguerre-Gaussian (LG) guiding of atoms into the hole of the mirror-MOT, showing normal Gaussian used for cooling/trapping*

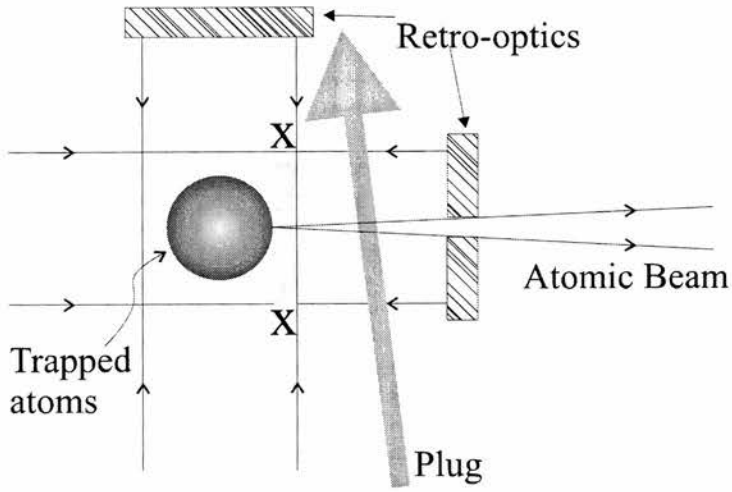

Figure 5.8: *LVIS schematic, showing a 'sheet' of light (**x**-**x**) that might act like a wall for atoms escaping, and also the 'official' plug beam, P*

The exact position of the atoms in the trap was unclear, that is, we could not be sure that they would be trapped over the hole drilled into the prism. Therefore, some method of moving the cloud needed to be incorporated into the MOT. At first, the use of shim coils was discussed. These would be an extra pair of coils (or possibly a single coil) that could be unbalanced so as to force the atom cloud one way or the other. However, by unbalancing the currents in the anti-Helmholtz (trapping) coils already in place, the same effect could be brought about. For better maneuvering, this would mean that the coils' axis need to be horizontal, and shim coils might still be needed so that the cloud could be moved in two dimensions.

5.3.3 Investigation of the electromagnetic coils

For coils of diameter 6cm, width 1cm and current of about 2.5A and separation 3cm, it was calculated that 57 turns would give a field gradient of about 10 Gauss/cm [12]. These were wound (on a lathe) using 0.5mm enamelled wire (RS insulated copper wire). To prevent uncoiling, duct tape was wrapped around the coils.

The equation used to calculate the field due to the coils was:

$$B = \mu_0 N \frac{a^2}{2}\left(I_1\left[\left(\frac{a}{2}+x\right)^2+a^2\right]^{-3/2}+I_2\left[\left(\frac{a}{2}-x\right)^2+a^2\right]^{-3/2}\right)$$

where $\mu_0 = 4\pi \times 10^{-7}$Wb/A.m, N is the number of turns, I_1 and I_2 are the currents in each coil, a is the radius of the coils and x is the distance from the zero-point of the coils.

Upon further thought, it was decided that the coils should have 120 turns each. This was so that the coils wouldn't get so hot[5]. Also, it would be possible to

[5]If the same gauge of wire is kept, then adding turns decreases heat dissipated, but the coil

produce higher magnetic fields (using more current), and thus a greater difference between the coils. The zero point, where the atoms are trapped, could therefore be moved a greater distance. However, when trying to trap with these coils in place we were unable to capture any atoms. Using a Hall probe, it was seen that there was a zero point midway between the coils, as required, and the field appeared to be even around it. After checking that the lasers were running in external cavity mode, the beams were correctly aligned through the trapping cell, the quarter-wave plates were correctly positioned and aligned, and that the coils had the right polarity, there were still no atoms seen. On using the Hall probe on each coil independently, it was noticed that one was much weaker than the other. Removing 15 turns from the stronger coil resulted in both giving approximately 40 Gauss for a current of 2A. The coils were returned to their anti-Helmholtz configuration and the zero point found to be roughly in the centre point. This time, on returning to the trap and realigning the lasers, atoms were captured.

It was seen that the coils needed to be extremely unbalanced for the atom cloud to be in the optimum position. For example, with the cloud at its optimum size, the upper coil was powered by 1.25A whilst the lower coil was at 2.5A, double the amount. The coils were checked with the Hall probe again, but this time the probe was mounted on an X-Y translator to ensure that the field was even. There was definitely an imbalance, and when examined individually, the difference between the two coils was seen to be large (13 Gauss at 2A). This time, the weak (top) coil was completely dismantled and 130 turns of new wire wound onto it. The strength of the field was measured at 2A and 1A and turns removed as necessary until it was similar to the 'bottom' coil. This occured when there were 114 turns on the 'new' coil. Connectors were soldered on and an

takes up more space. However, if *thinner* wire is used to fit the whole into the same space, heat dissipation would be the same as with fewer turns of thicker wire.

anti-Helmholtz configuration set up. Using different coil separations, the central zero position was measured (at 2A), both measured from the leftmost coil on the translator. All the results showed the system to be symmetrical (see table 5.1)

Separation (mm)	**Zero position (mm)**
42	22
51	26
66	32
81	41

Table 5.1: *Position of magnetic field zero compared to coil separation*

With the coils back in place on the trap, the laser beams aligned, and both coils set at 2A, a cloud of atoms was captured almost immediately. The cloud was more-or-less round. However, soon afterwards, it was discovered that the 'bottom' coil's power connector had snapped off and needed to be resoldered. A poor connection previously may have contributed to bad (unreproducible?) readings before. This whole escapade proves that the coils' manufacture is just as important as the ECDLs and other components in the trap system.

5.4 Results - Using the mirror-MOT

5.4.1 Capturing an atom cloud and moving it

The mirror-MOT system is switched on in the following order: Firstly, the two ECDL's are turned on, together with their associated controllers, signal generators, lock-boxes, photodiodes and oscilloscopes. After the lasers have settled, they

are confirmed to be on a rubidium line. This should imply that the lasers are running in external cavity and single mode, but these should be checked occasionally too. The path of the laser beams en-route to the trapping cell is checked to make sure that none are clipping any of the optical components. The electromagnetic coils are ensured to be centred correctly with respect to the centre of the trap. The beams must be aligned correctly with both the trap and coils. The retro-reflected beams are then checked with infrared sensitive card to confirm that they are indeed returning along the same line as the original. However, if they are *too* well aligned, there will be feedback, so it is better to misalign slightly. After degassing, the rubidium oven is switched on and left until enough rubidium vapour has built up in the cell. This is seen on a CCD monitor as the incoming, online laser beams cause the rubidium vapour to glow. The electromagnetic coils (in anti-Helmholtz configuration) are switched on. The two ECDL's are now tuned in to the appropriate hyperfine features, trapping and repumping respectively. Since we sometimes blocked a beam to check alignment, it is essential that all blocks are removed before trapping can occur!

At first, we cooled and trapped the rubidium atoms without locking any of the lasers. As long as the repumping laser was quite close to the correct hyperfine feature, then it didn't matter if it drifted a little in frequency. In practice, it was also possible to trap with that laser scanning over a small range. The trapping laser, however, needed to be very accurate. Therefore, with all the other criteria satisfied, the central frequency was shifted around (using the PZT disk) minutely until trapped atoms were seen on the CCD monitor. Before using circulasers, it was necessary to continually adjust the trapping laser in order to keep a cloud. However, with the slightly more stable circulasers, the cloud would often remain quite steady for any time from a few seconds upto several minutes, although the system still needs locking for long-term trapping. It was easy to see how sensitive

the system was to noise, because the cloud would flare when anyone spoke or gently nudged the optical table.

Now that the atom cloud was visible (see figure 5.9), the system was optimised to get the largest, roundest shape possible. This was achieved by adjusting the

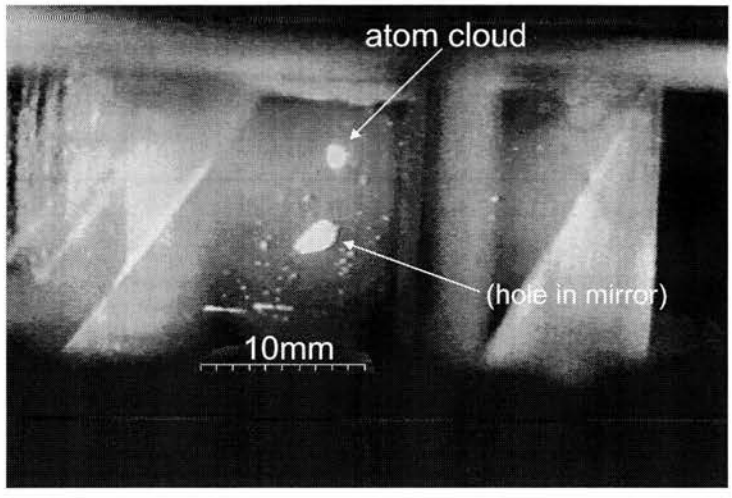

Figure 5.9: *Rubidium atoms cooled and trapped in the Mirror-MOT*

alignment of beams (using the mirrors) and the position of the coils. The position of the cloud within the cell can also affect its shape. For example, if the cloud is *too* close to the mirror surface then it will become unstable and begin to disappear. By imbalancing the currents in the separate coils, it was possible to move the cloud up and down (since their axis was vertical). Thus a stronger top coil or a weaker bottom coil would cause the cloud to move downwards, whilst a weak top coil or strong bottom coil would move the cloud upwards. In other words, by imbalancing the coils, the zero field point was moving towards the weaker of the two coils. This can be seen on a two-dimensional schematic of the fields of the two coils (Figure 5.10) With 2A in the coils to begin with, it was seen that varying one by 0.1A moved the atom cloud by about a millimetre. Since a change of 1A gives approximately 6 Gauss difference in field, it can be calculated that to

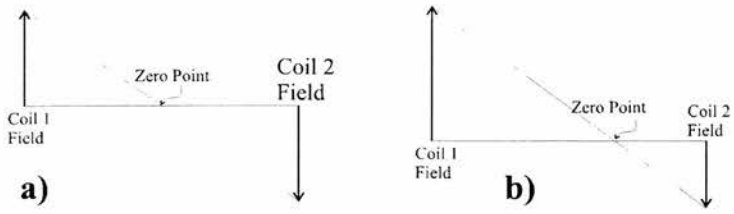

Figure 5.10: *Two-dimensional schematic of the field produced by two anti-Helmholtz coils, showing the position of the zero field point for* ***a)****balanced and* ***b)****imbalanced coil currents*

move the atoms 1mm a change of 0.6 Gauss or 0.6×10^{-4} Tesla is needed in one coil.

5.4.2 Counting the atoms and measuring trap lifetime

The fluorescence from the cloud of cold atoms is used to count the number of them. Thus, a photodiode is needed to measure this light. However, before proceeding, the photodiode must be carefully calibrated by measuring the change in voltage produced for different intensities of laser light. This relationship is then assumed to be linear. In this way it is possible to accurately separate the fluorescence of the trapped atoms from the scattered light and fluorescence of the background vapour.

Calibration

A high index neutral density (ND) filter was placed in front of the photodiode and a laser beam incident on the photodiode to ensure that it registers a voltage. The voltage change was measured using an oscilloscope. A knob on the photodiode varied the gain by steps, and there were two suitable positions with the

oscilloscope set to 0.2V/division.

The diode laser current was varied and a power meter measured the intensity of light. The meter was moved and the photodiode voltage change recorded (table 5.2). This is a linear relationship, as can be seen in figure 5.11.

LD current (mA)	**Power (μW)**	**PD voltage change (V)**
115	32.7	1.38
108	28.34	1.2
100	24.8	1.1
95	22.9	1.02
90	19.82	0.94
85	17.1	0.82
80	15.8	0.72
75	14.22	0.66

Table 5.2: *Measurement of laser current, light intensity and photodiode voltage change for calibrating the photodiode*

Measuring the number of atoms

The cloud of atoms must be imaged onto the photodiode (figure 5.12). The focal length needed is given by the equation $\frac{1}{f} = \frac{1}{a} + \frac{1}{b}$. Magnification (m)is given by $m = -\frac{a}{b}$. The cloud must be measured to ensure that its image fits on the photodiode (11mm diameter). Using a still image from the video and comparing it to part of the prism holder, whose dimensions can be measured fairly accurately, the cloud was seen to be elliptical with diameters 2.3mm and 3.8mm. Therefore, magnification must be less than 2.8, but using 1x magnification means that the image will definitely fit on the photodiode. Using a lens of focal length 50mm

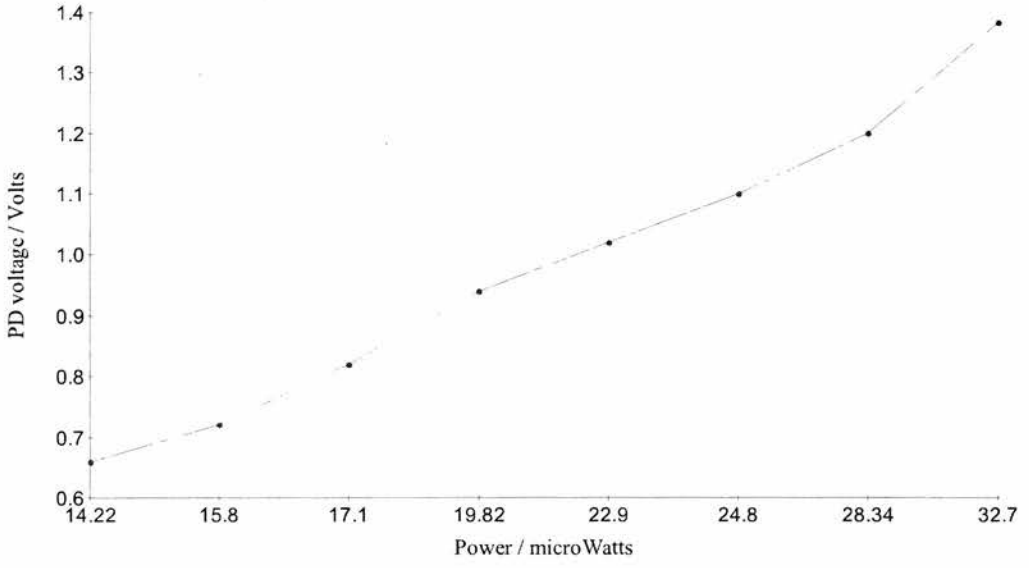

Figure 5.11: *Graph of power versus photodiode voltage change showing linear relationship*

meant that for 1x magnification the atoms and photodiode were both 100mm from it. The closest that anything outside the glass cell could get to the atoms was about 40mm. A paper tube was formed around the lens so that extraneous light would not affect the results too much. This tube extended 60mm to one side of the lens and 100mm to the other, to account for the glass cell.

Two CCD cameras were set up. One had a 'side' view of the atoms cloud, so that it could be seen that they were there before counting began. The other one was placed where the photodiode would eventually go, with its objective lens removed. The lens then imaged the cloud onto the CCD and it could be confirmed that the photodiode would be in the right place (figure 5.13. The photodiode was then put in place. To ensure less ambient light in the laboratory, readings were taken at night. This had the added benefit that fewer people were around to vibrate the floor and thus the laser diodes. With the whole system on but with no atoms trapped, the light level seen by the photodiode and visualised on the

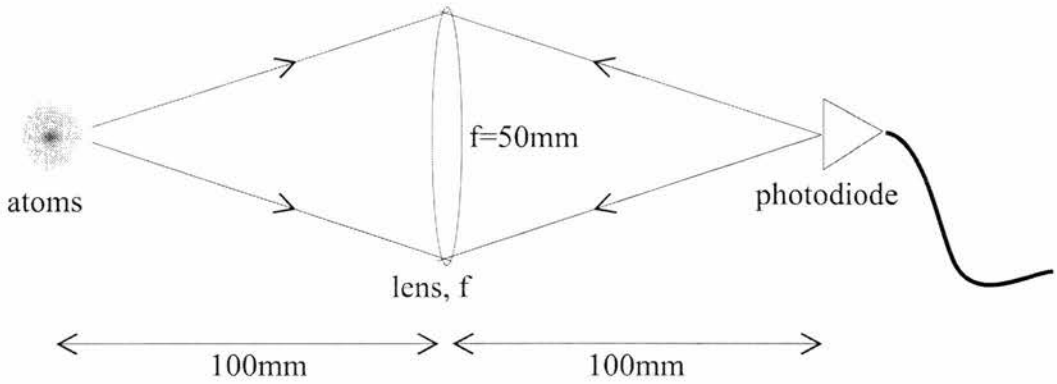

Figure 5.12: *Focusing atoms onto the photodiode using a lens*

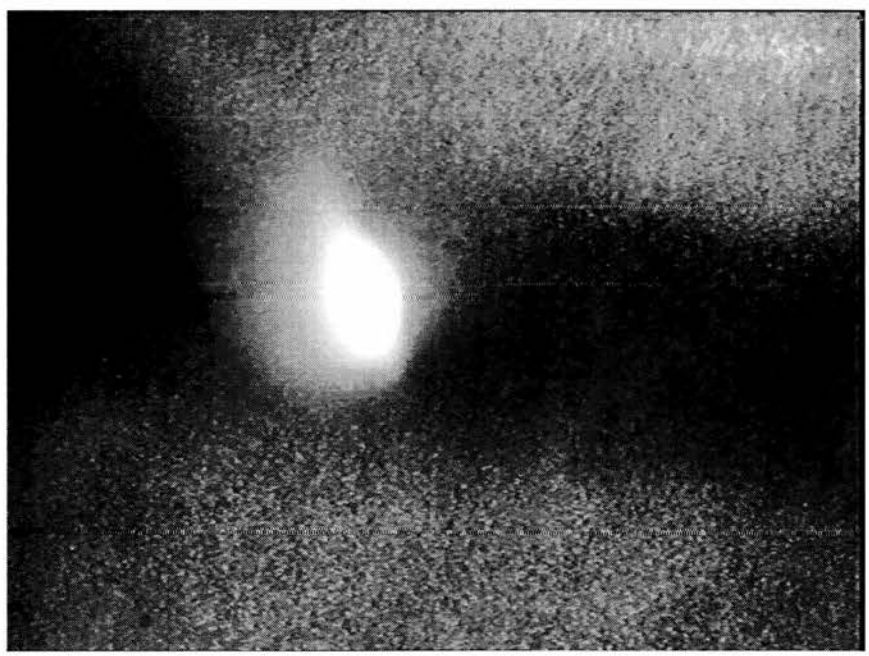

Figure 5.13: *The atom cloud imaged directly onto the CCD chip using the atom counting geometry*

oscilloscope was noted. The frequency of the trapping laser was then changed gradually (and minutely) until atoms were trapped and the oscilloscope showed a change in light level. This was noted down and repeated several times for accuracy. For this it was necessary that the CCD monitor was not on (to reduce extraneous light levels). The base level was 0mV on the oscilloscope, while it changed to 80mV (maximum 100mV) when the atoms were trapped. Since these photodiode levels were so much less than those measured when calibrating it, it was decided to recalibrate. Using a neutral density filter (ND3) to reduce laser light levels sufficiently, it was seen that 77.1mA applied to the ECDL produced an 80mV change (from zero), whilst 81.6mA produced a 100mV change on the oscilloscope. Using the power meter again, these were seen to correspond to powers of 430nW and 488.9nW (both $\pm 6nW$) respectively.

The rate at which an individual atom scatters photons is given by

$$R = \frac{(\frac{I}{I_s})\pi\Gamma}{1 + (\frac{I}{I_s}) + 4(\frac{\Delta}{\Gamma})^2} \tag{5.1}$$

where I=sum of intensities of all beams per unit area, Γ=6MHz natural linewidth of transition, Δ=detuning of laser from transition frequency, and $I_s = 1.6mW/cm^2$ saturation intensity. I_{sat} (or I_s), the saturation parameter, depends on the transition and the initial m level.

From the light levels measured above, the difference in light was calculated to be 58.9nW ($\pm 6nW$). The lens used to collect light from the atoms has a focal length of +50mm and a radius of 12.7mm, a distance 100mm from the atoms. Its collection area is thus $\pi r^2 = 506.71mm^2$. The solid angle from the atoms to the lens is given by the fraction of the surface area of a sphere of radius 100mm that is taken by the collection area:

$$= \frac{506.71}{4 \cdot \pi \cdot 100^2} \simeq 4.032 \times 10^{-3}$$

Therefore, the total power per second emitted from the atom cloud is

$$\frac{58.9}{4.032 \times 10^{-3}} \simeq 14.6\mu W$$

The energy of one photon at 780nm wavelength is given by

$$E = h\nu = \frac{hc}{\lambda} = 2.55 \times 10^{-19} J$$

Therefore, the number of photons emitted by the cloud per second is

$$\frac{14.6 \times 10^{-6}}{2.55 \times 10^{-19}} = 5.728 \times 10^{13}$$

The scattering rate is given by equation 5.1, where $\Delta \simeq 2.27 \times \Gamma$, the optimal detuning.

Trapping power $\simeq$ 3.2mW in beams of radius $\simeq$ 1cm. Therefore, for a beam of area $\pi.1^2 = 3.142cm^2$

$$\Rightarrow I = \frac{Power}{area} = \frac{3.2mW}{3.142} = 1.019mW/cm^2$$

$$\Rightarrow R = \frac{(\frac{1.019}{1.6}).\pi \times 6.1 \times 10^6}{1 + (\frac{1.019}{1.6}) + 4(\frac{2.27\Gamma}{\Gamma})^2} = 5.486 \times 10^5 photons/(s.atom)$$

$\Rightarrow$ the number of atoms in the cloud

$$= \frac{5.728 \times 10^{13}}{5.486 \times 10^5} \approx 1.044 \times 10^8 atoms$$

From this, the density of atoms can be calculated, with the cloud measured to of approximately 2.5mm radius.

$$Density = \frac{1.044 \times 10^8}{4 \cdot \pi \cdot 2.5^3} = 5.317 \times 10^{14} atoms/m^3$$

Measurement of trap lifetime

The lifetime of atoms in the trap is dictated by the following. A low vapour pressure means that there will be fewer atoms to be trapped, but also means that

there will be fewer high energy atoms that could knock cold, trapped atoms out of the trap.

The trap filling time (which is the inverse of the lifetime), which is found using the equation:

$$N(t) = N_0(1 - e^{-t/\tau}) \tag{5.2}$$

where τ=the time constant for trap to fill to steady state value N_0

The output of the photodiode was recorded on a digital oscilloscope (Tektronix) using the same geometry for counting atoms. The vertical and horizontal axes of the 'scope were chosen to be 20mV/div and 250ms/div respectively, to be close to the minute voltage change and guessed trap filling time. With the lasers aligned and 'held' in position for trapping, the magnetic field was turned off and then back on. Although the magnetic field may alter the background fluorescence, this change is generally much smaller (1/100) than the signal of a typical cloud of trapped atoms [13]. Light intensity (measured as photodiode voltage) change as the trap refilled was recorded against time. This was repeated for different rubidium pressures[6]. These traces can be seen in figure 5.14. As before, the voltage difference for the trap with and without atoms was about 80mV, corresponding to 58.9nW of power.

On the traces of intensity (or voltage) versus time, fitting an exponential curve (with the formula being equation 5.2) will give the trap filling time, and thus the trap lifetime. The different traces/graphs give the following results:

Graph 1: slope is 0.2 seconds

Graph 2: slope is 0.16 seconds

Graph 3: slope is 0.2 seconds

Graph 4: slope is 0.2 seconds.

[6]Pressures were not recorded, because the reading from the ion pump was too inaccurate.

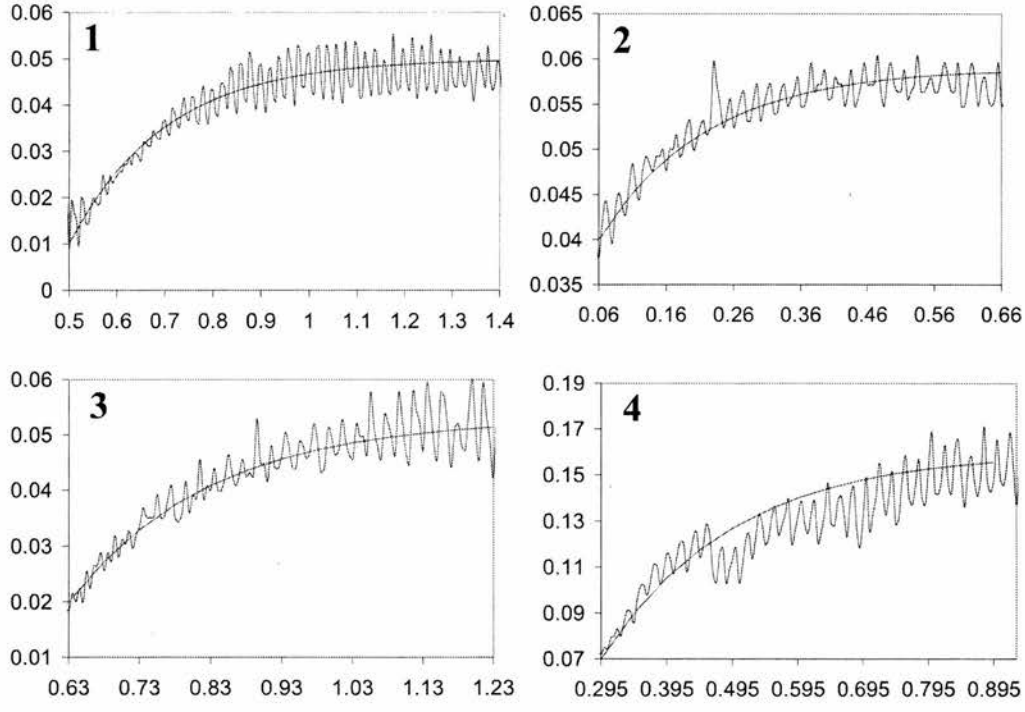

Figure 5.14: *Traces recorded on a digital oscilloscope of intensity versus time (trap refilling time) for different vapour pressures. Exponential curves calculated from equation 5.2 are fitted to the signals.*

Therefore, it should be assumed that the trap lifetime is about 0.2 seconds or less, depending on, for example, alignment and magnetic field uniformity.

5.5 Future work

One way that atoms can be extracted from the mirror-MOT is using a version of the LVIS scheme [2]. A glass slide with a dot on it is introduced into one of the trapping beams, producing a diffraction limited 'hollow beam'. A Laguerre-Gaussian beam was used in a similar way. However, the atoms were not removed through the hole in the glass prism, so this should be tried in future. Either a LG or Bessel beam could be used for this purpose, as discussed above. Using additional 'shim' coils would make it easier to manipulate a cloud of atoms over the hole, and thus into the guiding beam.

5.6 Conclusions and Summary

We have realised a magneto-optical trap (MOT) which is able to trap neutral atoms near to a surface, by making that surface into a mirror. This has been useful for loading cold atoms into a magnetic trap within the surface. The mirror reflects two beams at right angles, which means that fewer beams are needed than in a conventional MOT (four beams rather than six). By drilling a hole through the mirrored surface (which is on a 45° prism), it should be possible to guide atoms out into a hollow beam (or fibre) quite easily. The use of the prism also means that the atomic vapour source (getter/oven) can be placed nearer to the trapping region, resulting in less loss by wall pumping and a more controllable vapour pressure. The getter should also last longer! The mirror-MOT trapped about 10^8

atoms and the trap filling time (equivalent to trap lifetime) was measured to be about 0.2 seconds.

Bibliography

[1] M.A.Clifford, G.P.T.Lancaster, R.H.Mitchell, F.Akerboom and K.Dholakia, J.Mod.Opt. **48**, 1123 (2001)

[2] J.Reichel, W.Hänsel, T.W.Hänsch, Phys.Rev.Lett. **83**, 3398 (1999)

[3] E.A.Hinds, I.G.Hughes, J.Phys.D **32**, R119 (1999)

[4] E.A.Hinds, M.G.Boshier, I.G.Hughes, Phys.Rev.Lett. **80**, 645 (1998)

[5] R.Folman, D.Cassettari, B.Hessmo, T.Maier, J.Schmiedmayer, Phys.Rev.Lett. **84**, 4749 (2000)

[6] G.P.T.Lancaster, W.Sibbett, K.Dholakia, Rev.Sci.Instrum. **71**, 1 (2000)

[7] I.D.Lindsay, G.A.Turnbull, M.H.Dunn, M.Ebrahimzadeh, Opt.Lett. **23**, 1889 (1998)

[8] G.P.T.Lancaster, R.S.Conroy, M.A.Clifford, J.Arlt, K.Dholakia, Opt.Comm. **170**, 79 (1999)

[9] J.Yin, Y.Zhu, W.Wang, Y.Wang, W.Jhe, J.Opt.Soc.Am.B **15**, 25 (1998)

[10] K.Dholakia, Contemp.Phys. **39**, 351 (1998)

[11] Z.T.Lu, K.L.Corwin, M.J.Renn, M.H.Anderson, E.A.Cornell, C.E.Wieman, Phys.Rev.Lett. **77**, 3331 (1996)

[12] G.P.T.Lancaster, private communication.

[13] C.Wieman, G.Flowers, S.Gilbert, Am.J.Phys. **63**, 317 (1995)

Conclusions

In the field of atom cooling, trapping and guiding, diode lasers are a very small and inexpensive source. Although they do not produce as much power as a Ti:Sapphire laser, this is not a problem, since very little power is required for trapping atoms. The use of the Littrow configuration makes diode lasers easily tuneable and more stable. Various simple techniques can be employed to lock the laser frequency, which is necessary for cooling, trapping and guiding atoms. Inherent problems can be easily overcome, so that diode lasers in an extended cavity (ECDL) geometry are a good compact source for use in various cold atom situations.

One method of stabilising an ECDL is to use the Zeeman effect produced by using annular permanent magnets with an atomic vapour cell. I studied the effect in caesium vapour, using an 852nm ECDL. In the process I found that the locked ECDL could be tuned by using an optical offset. The Zeeman (DAVLL) method is versatile and simple, with the resulting stabilised ECDL being suited for many applications, including laser cooling. The same system can be used for locking to other atomic transition frequencies, such as rubidium at 780nm.

Laser beams with a hollow or annular cross-section are useful in both trapping and guiding cold atoms. Laguerre-Gaussian modes have an annular form when the radial term of their equation is zero. They can easily be produced by using

computer-generated holograms. In a trapping environment, a dark-spot MOT with a Laguerre-Gaussian beam used for repumping leads to higher densities of trapped atoms. Cold atoms have been guided along the centre of Laguerre-Gaussian beams. This would be useful for taking cold atoms away from their source trap to another region, for example produce a Bose-Einstein condensate by magnetic cooling. On other occasions it might be more expedient to use the more robust hollow-core fibre. This can be used to transport atoms between different vessels, whilst maintaining the vacuum. Also, the flexible fibre allows atoms to be guided (within limits) around corners.

I have realised a MOT which is able to trap neutral atoms near to a surface, by making that surface into a mirror. This allows cold atoms to be loaded into a magnetic trap within the surface. Fewer beams are needed for this trap, four rather than the usual six, since two of the beams are reflected by the mirror. A drilled hole in the mirror allows atoms to be guided into a hollow beam or fibre. Since the mirror is a surface on a prism, the atomic vapour source (e.g. rubidium getter) can be placed much closer to the trapping region, resulting in less loss by wall pumping and a more controllable vapour pressure. In experiment, I trapped about 10^8 atoms with a trap lifetime of about 0.2 seconds.

In a field as fast-moving as atom trapping, cooling and guiding, these methods and schemes will improve and assist in various ways. Since there are different directions that this research area is heading, having alternate schemes available which have strengths in different areas can only help in this diversification.

Appendix A

Modelling of DAVLL and Guiding Potential

DAVLL signal modelling for Rubidium

$\lambda := 780.2 \cdot 10^{-9}$ m — Transition Wavelength of Rb

$\theta := \frac{\pi}{4}$ radians — Angle of QWP to plane of linear polarisation

$c := 299792458$ ms^{-1} — Speed of light

$\nu 00 := \frac{c}{\lambda}$ Hz — Central frequency of transition

$\nu z := 600 \cdot 10^{6}$ Hz — Peak separation (for 100G field)

$\nu 0 := \nu 00 - \frac{\nu z}{2}$

$\nu 1 := \nu 00 + \frac{\nu z}{2}$ Hz — Zeeman shifted peaks

$k := 1.3806 \cdot 10^{-23}$ — Boltzman constant

$T := 293$ K — Temperature

$amu := 1.660531 \cdot 10^{-27}$ — Atomic Mass Unit

$ma := 85.4678 \cdot amu$ — mass of Rb

$\alpha := \sqrt{\frac{2 \cdot k \cdot T}{ma}}$ ms^{-1} — Most probable velocity

$Io := \cos(\theta)^4 + \sin(\theta)^4$ Wm^{-2} — Central intensity of one peak

$I1 := 2 \cdot \sin(\theta)^2 \cdot \cos(\theta)^2$ — Relative intensity of second peak

$\nu := \left(\nu 0 - 1 \cdot 10^{9}\right), \left(\nu 0 - .99 \cdot 10^{9}\right) .. \nu 1 + 1 \cdot 10^{9}$ Hz — Frequency scan over both peaks

$I(\nu) := Io \cdot e^{-c^2 \cdot \frac{(\nu 0 - \nu)^2}{\nu 0^2 \cdot \alpha^2}} - I1 \cdot e^{-c^2 \cdot \frac{(\nu 1 - \nu)^2}{\nu 1^2 \cdot \alpha^2}}$ — DAVLL signal

DAVLL signals for different proportion peaks

$$Ia(\nu) := .6\cdot e^{-c^2\cdot\frac{(\nu 0-\nu)^2}{\nu 0^2\cdot\alpha^2}} - .4\cdot e^{-c^2\cdot\frac{(\nu 1-\nu)^2}{\nu 1^2\cdot\alpha^2}}$$

$$Ib(\nu) := .7\cdot e^{-c^2\cdot\frac{(\nu 0-\nu)^2}{\nu 0^2\cdot\alpha^2}} - .3\cdot e^{-c^2\cdot\frac{(\nu 1-\nu)^2}{\nu 1^2\cdot\alpha^2}}$$

$$Ic(\nu) := .8\cdot e^{-c^2\cdot\frac{(\nu 0-\nu)^2}{\nu 0^2\cdot\alpha^2}} - .2\cdot e^{-c^2\cdot\frac{(\nu 1-\nu)^2}{\nu 1^2\cdot\alpha^2}}$$

The Zeeman split absorptions

$$I0(\nu) := e^{-c^2\cdot\frac{(\nu 0-\nu)^2}{\nu 0^2\cdot\alpha^2}} \qquad I2(\nu) := e^{-c^2\cdot\frac{(\nu 1-\nu)^2}{\nu 1^2\cdot\alpha^2}}$$

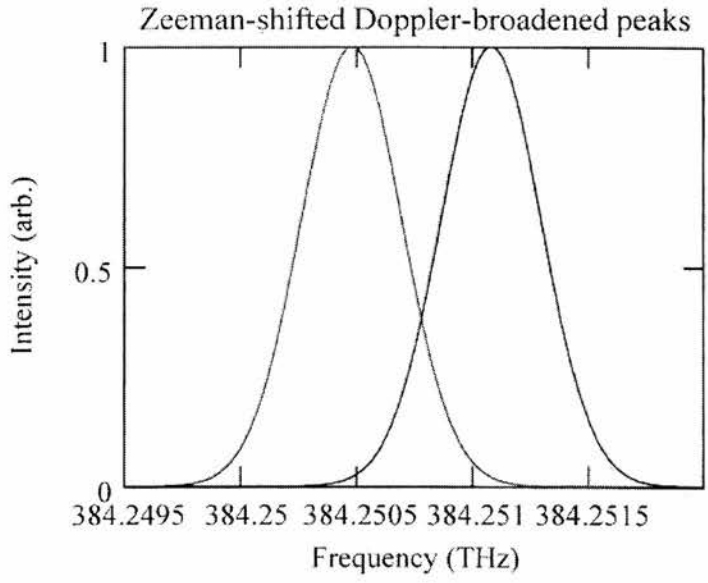

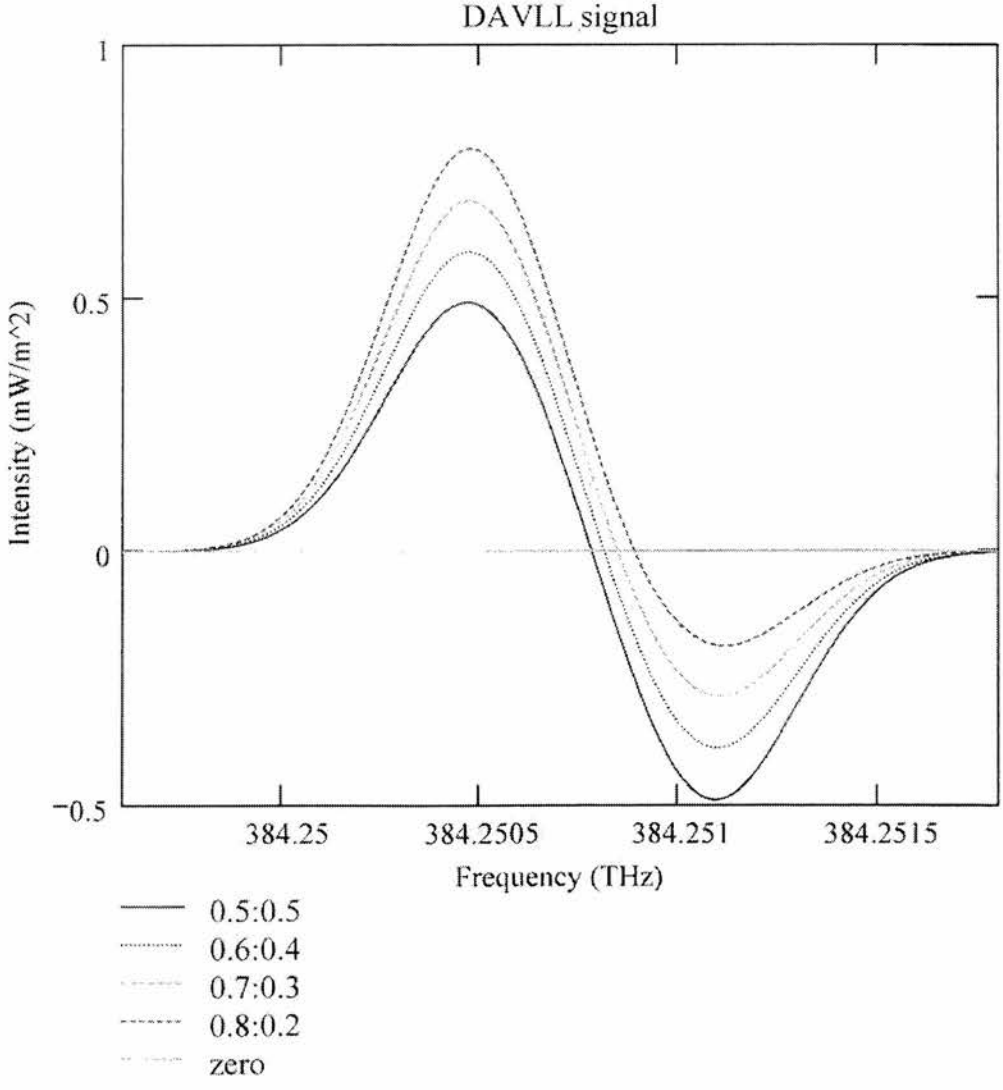

Frequency ν when I(ν)=0 (zeropoint) given when:

$$Io \cdot e^{-c^2 \cdot \frac{(\nu 0-\nu)^2}{\nu 0^2 \cdot \alpha^2}} - I1 \cdot e^{-c^2 \cdot \frac{(\nu 1-\nu)^2}{\nu 1^2 \cdot \alpha^2}} = 0$$

Thus:

$$\ln\left(\frac{I1}{I0}\right) \cdot \left(\frac{\alpha \cdot \nu 0 \cdot \nu 1}{c}\right)^2 = -\nu \cdot \left[\nu \cdot (2 \cdot \nu 0 + \nu z) \cdot \nu z - 2 \cdot \nu z \cdot \left(\nu 0^2 + \nu z \cdot \nu 0\right)\right]$$

solve where $a\nu^2 + b\nu + c = 0$

$Io := I1$

$ratio := \frac{I1}{Io}$

$a := \nu z \cdot (2 \cdot \nu 0 + \nu z)$

$b := -2 \cdot \nu 0 \cdot \nu z \cdot (\nu 0 + \nu z)$

$cc := \ln(ratio) \cdot \left[\frac{\alpha \cdot \nu 0 \cdot (\nu 0 + \nu z)}{c}\right]^2$

$$zerominus := \frac{-b - \sqrt{b^2 - 4 \cdot a \cdot cc}}{2 \cdot a} \qquad zeroplus := \frac{-b + \sqrt{b^2 - 4 \cdot a \cdot cc}}{2 \cdot a}$$

$zerominus = 0$

Don't use this value!

$zeroplus = 3.84250779287128 \times 10^{14}$

This is the zero crossing point for equal peaks

$\theta := 45, 46 .. 65$ degrees

converted to radians in equation

$\Delta\nu(\theta)$ is the difference between the zeropoint and that for equal peaks

$$\Delta\nu(\theta) := \frac{-b + \sqrt{b^2 - 4 \cdot a \cdot \ln\left(\frac{2 \cdot \sin\left(\theta \cdot \frac{\pi}{180}\right)^2 \cdot \cos\left(\theta \cdot \frac{\pi}{180}\right)^2}{\cos\left(\theta \cdot \frac{\pi}{180}\right)^4 + \sin\left(\theta \cdot \frac{\pi}{180}\right)^4}\right) \cdot \left[\frac{\alpha \cdot \nu 0 \cdot (\nu 0 + \nu z)}{c}\right]^2}}{2 \cdot a} - \left(\frac{\nu 0 + \nu 1}{2}\right)$$

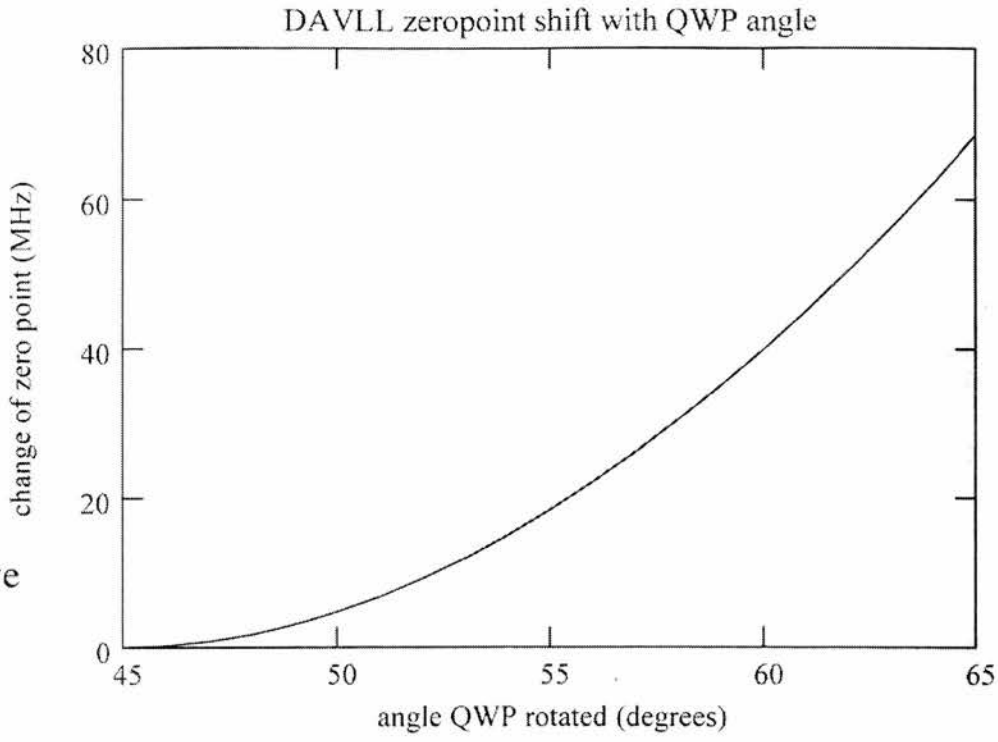

Turning the quarter-wave plate, from its position 45 degrees to linear polarization, causes the peak amplitudes to vary relative to one another, & thus the zeropoint.

$\theta := 0,1..45 \quad Io := 1$

$$I1(\theta) := Io \cdot \cos\left(\theta \cdot \frac{\pi}{180}\right)^2$$

Malus' law

Turning a linear polarizer in front of one photodiode varies t amplitude of that peak relative to the other, & thus zeropoint

$$ratio(\theta) := \frac{I1(\theta)}{Io} \qquad cc(\theta) := \ln(ratio(\theta)) \cdot \left(\frac{\alpha \cdot \nu 0 \cdot \nu 1}{c}\right)^2$$

$$\Delta\nu(\theta) := \frac{-b + \sqrt{b^2 - 4 \cdot a \cdot cc(\theta)}}{2 \cdot a} - \left(\frac{\nu 0 + \nu 1}{2}\right)$$

90

DAVLL freq shift with polarizer angle

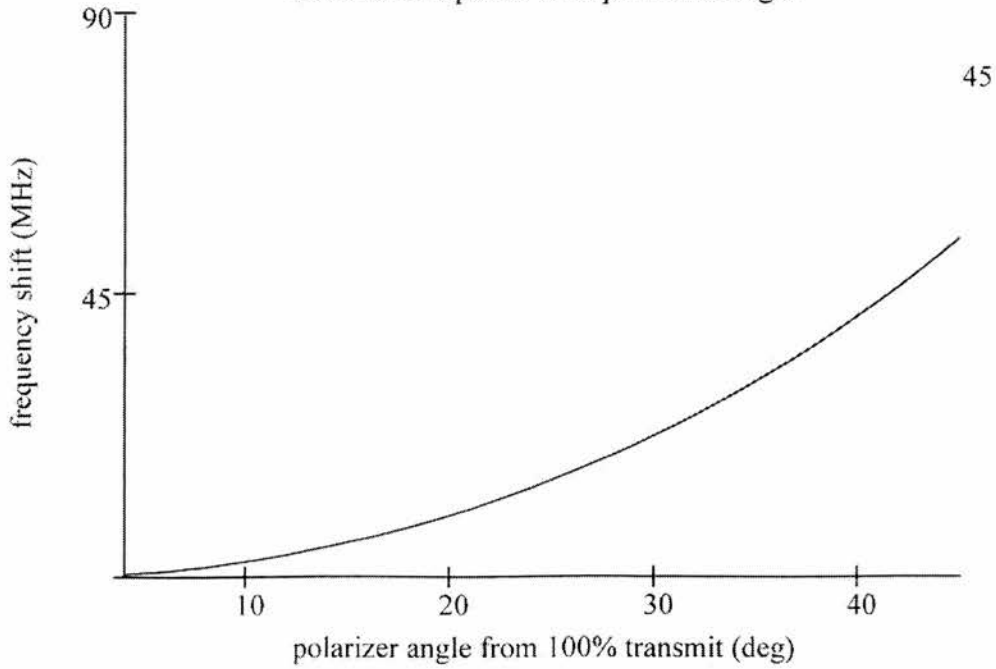

DAVLL signal modelling for Caesium

$\lambda := 852.3 \cdot 10^{-9}\ m$ Transition Wavelength of Cs

$\theta := 45\ deg$ Angle of QWP to plane of linear polarisation

$c := 299792458\ ms^{-1}$ Speed of light

$\nu 0 := \frac{c}{\lambda}\ Hz$ Central frequency of transition (arbitrary)

$\nu z := 500 \cdot 10^{6}\ Hz$ Peak separation

$\nu 1 := \nu 0 + \nu z\ Hz$ Central frequency of Zeeman shifted peak

$k := 1.3806 \cdot 10^{-23}$ $T := 298$ $amu := 1.660531 \cdot 10^{-27}$ $ma := 132.9054 \cdot amu$

$\alpha := \sqrt{\frac{2 \cdot k \cdot T}{ma}}$ Most probable velocity

$Io := 1\ Wm^{-2}$ Central intensity (arbitrary value)

$\nu := (\nu 0 - 1 \cdot 10^{9}), (\nu 0 - .99 \cdot 10^{9}) .. (\nu 1 + 1 \cdot 10^{9})\ Hz$ Frequency scan

$I1 := 1 \cdot Io$ Relative intensity of second peak

$$I(\nu) := Io \cdot e^{-c^2 \cdot \frac{(\nu 0 - \nu)^2}{\nu 0^2 \cdot \alpha^2}} - I1 \cdot e^{-c^2 \cdot \frac{(\nu 1 - \nu)^2}{\nu 1^2 \cdot \alpha^2}}$$

$$I1(\nu) := Io \cdot e^{-c^2 \cdot \frac{(\nu 0 - \nu)^2}{\nu 0^2 \cdot \alpha^2}}$$

$$I2(\nu) := Io \cdot e^{-c^2 \cdot \frac{(\nu 1 - \nu)^2}{\nu 1^2 \cdot \alpha^2}}$$

$$Ia(\nu) := Io \cdot \left[e^{-c^2 \cdot \frac{(\nu 0 - \nu)^2}{\nu 0^2 \cdot \alpha^2}} - e^{-c^2 \cdot \frac{(\nu 1 - \nu)^2}{\nu 1^2 \cdot \alpha^2}} \cdot .75 \right]$$

$$Ib(\nu) := Io \cdot \left[e^{-c^2 \cdot \frac{(\nu 0 - \nu)^2}{\nu 0^2 \cdot \alpha^2}} - e^{-c^2 \cdot \frac{(\nu 1 - \nu)^2}{\nu 1^2 \cdot \alpha^2}} \cdot .5 \right]$$

$$Ic(\nu) := Io \cdot \left[e^{-c^2 \cdot \frac{(\nu 0 - \nu)^2}{\nu 0^2 \cdot \alpha^2}} - e^{-c^2 \cdot \frac{(\nu 1 - \nu)^2}{\nu 1^2 \cdot \alpha^2}} \cdot .25 \right]$$

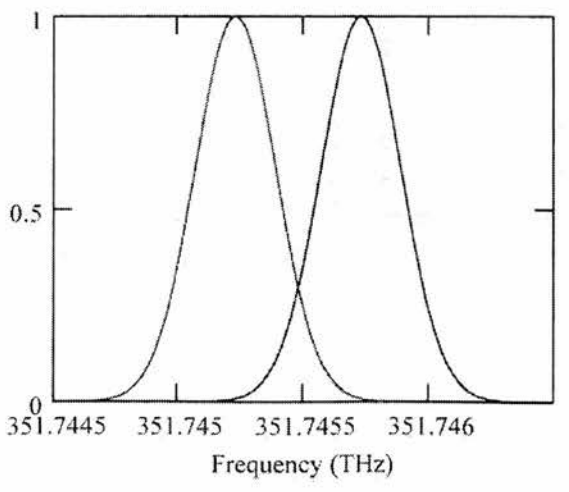

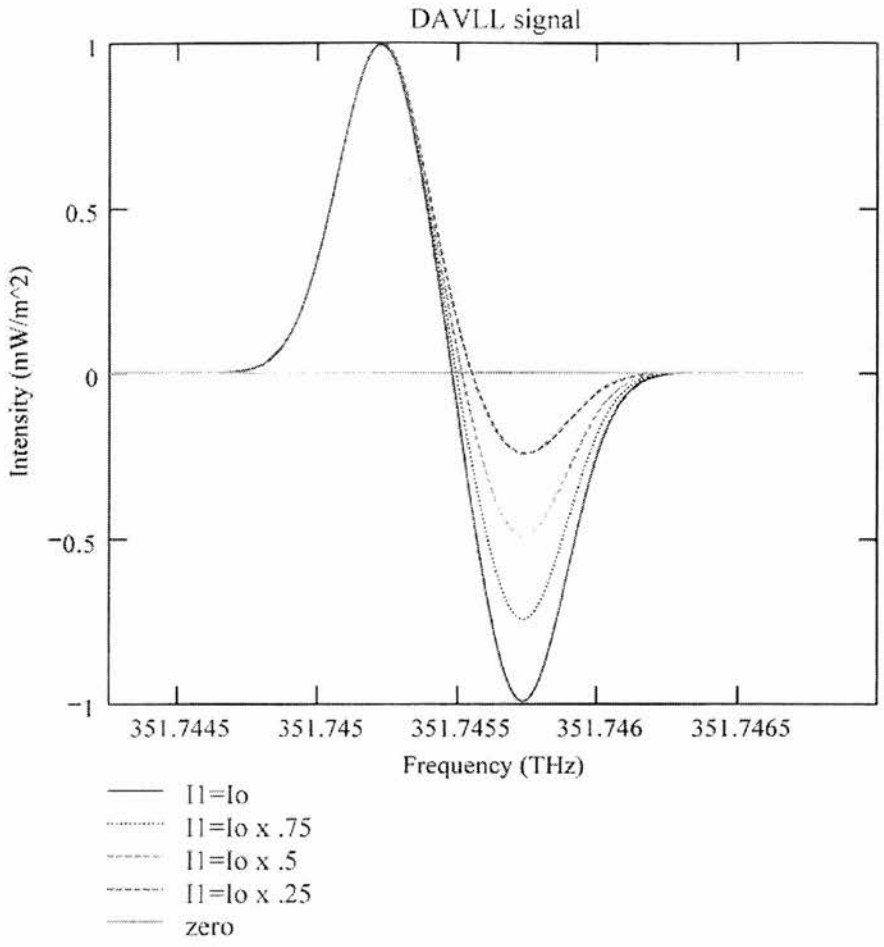

$I1 := Io$

Frequency ν when I(ν)=0 given when:

$$Io \cdot e^{-c^2 \cdot \frac{(\nu 0 - \nu)^2}{\nu 0^2 \cdot \alpha^2}} - I1 \cdot e^{-c^2 \cdot \frac{(\nu 1 - \nu)^2}{\nu 1^2 \cdot \alpha^2}} = 0$$

Thus:

$$\ln\left(\frac{I1}{Io}\right) \cdot \left(\frac{\alpha \cdot \nu 0 \cdot \nu 1}{c}\right)^2 = -\nu \cdot \left[\nu \cdot (2 \cdot \nu 0 + \nu z) \cdot \nu z - 2 \cdot \nu z \cdot \left(\nu 0^2 + \nu z \cdot \nu 0\right)\right]$$

solve $ax^2 + bx + c = 0$

where

$$a := 1600 \cdot 10^6 \cdot \nu 0 + 64 \cdot 10^{16}$$

$$b := -\left(1600 \cdot 10^6 \cdot \nu 0^2 + 128 \cdot 10^{16}\right)$$

$$cc := \ln\left(\frac{I1}{Io}\right) \cdot \left(\frac{\alpha \cdot \nu 0 \cdot \nu 1}{c}\right)^2$$

$$zeroplus := \frac{-b + \sqrt{b^2 - 4 \cdot a \cdot cc}}{2 \cdot a}$$

$$zerominus := \frac{-b - \sqrt{b^2 - 4 \cdot a \cdot cc}}{2 \cdot a}$$

$zeroplus = 3.517 \times 10^{14}$

$zerominus = 0$

$$p := 1, .9999 .. 0 \qquad cc(p) := \ln(p) \cdot \left(\frac{\alpha \cdot \nu 0 \cdot \nu 1}{c} \right)^2$$

$$\Delta\nu(p) := \frac{-b + \sqrt{b^2 - 4 \cdot a \cdot cc(p)}}{2 \cdot a}$$

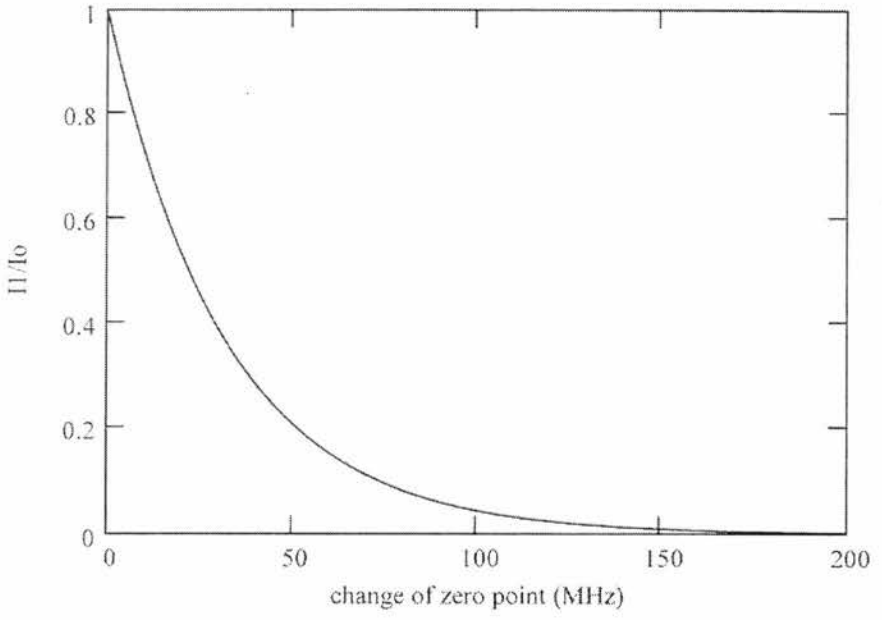

Rubidium guiding potential in a hollow fibre

$k := 1.4 \cdot 10^{-23}$

Planck's Constant $h := \frac{6.6 \cdot 10^{-34}}{2 \cdot \pi}$

Saturation Intensity of Rb $Isat := 1.63 \cdot 10^{-3}$

Natural Linewidth $\Gamma := 5.9 \cdot 10^{6}$

$r0 := 10 \cdot 10^{-4}$

$r := 100 \cdot 10^{-4}$

$Power := 10 \cdot 10^{-3}$

$n := 1.5$

$\theta := 0.26$

$\lambda := 780.2 \cdot 10^{-7}$

$$Io := \frac{Power}{\pi \cdot \left(r^2 - r0^2\right)}$$

$$\alpha := 2 \cdot \sqrt{\frac{n^2}{\left(n^2 - 1\right)}} \cdot \cos(\theta) \qquad \kappa := 2 \cdot \frac{\pi}{\lambda} \cdot \sqrt{n^2 \cdot \sin(\theta)^2 - 1}$$

$$I(x) := Re\left(Io \cdot \alpha^2 \cdot \exp(-2 \cdot \kappa \cdot x)\right) \qquad x := 1 \cdot 10^{-7}, 2 \cdot 10^{-7} .. 1.05 \cdot 10^{-5}$$

$I(0) = 216.198$

$\Delta := -5000 \cdot 10^{6}, -4990 \cdot 10^{6} .. 5000 \cdot 10^{6}$

$$U(x, \Delta) := \frac{h}{2} \cdot \Delta \cdot \left(\ln\left(1 + \frac{\frac{I(x)}{Isat}}{1 + \frac{4 \cdot \Delta^2}{\Gamma^2}} \right) \right)$$

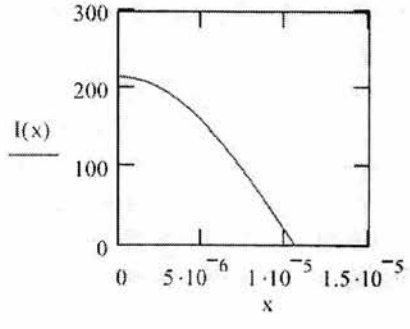

$\ln(1.3) = 0.262$

$$T(x, \Delta) := \frac{2}{3} \cdot \frac{U(x, \Delta)}{k}$$

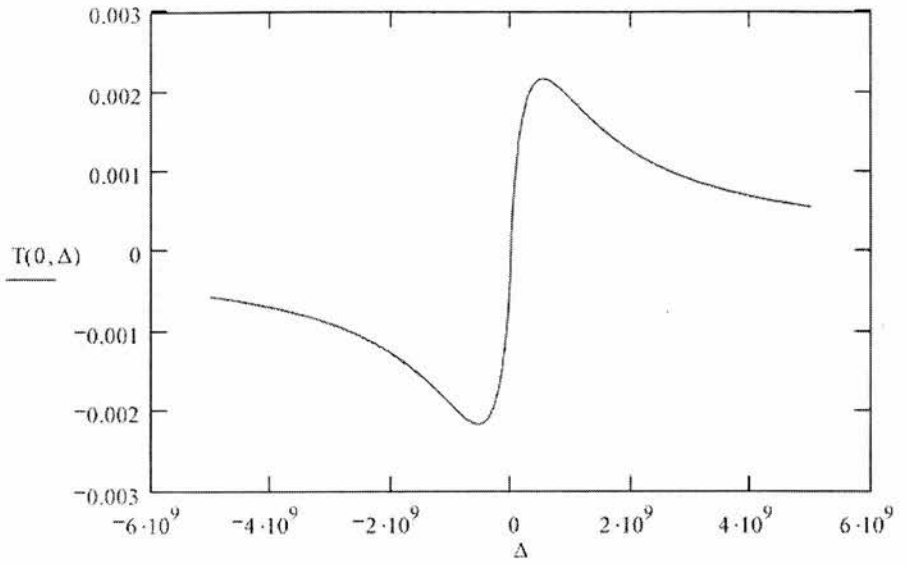

$A := 0.11$

$$Uvdw(x) := A \cdot h \cdot 2 \cdot \pi \cdot \Gamma \cdot \left(\frac{\lambda}{2 \cdot \pi \cdot x} \right)^3 \qquad \frac{\lambda}{2 \cdot \pi} = 1.242 \times 10^{-5}$$

$$Tvdw(x) := \frac{2}{3} \cdot \frac{Uvdw(x)}{k}$$

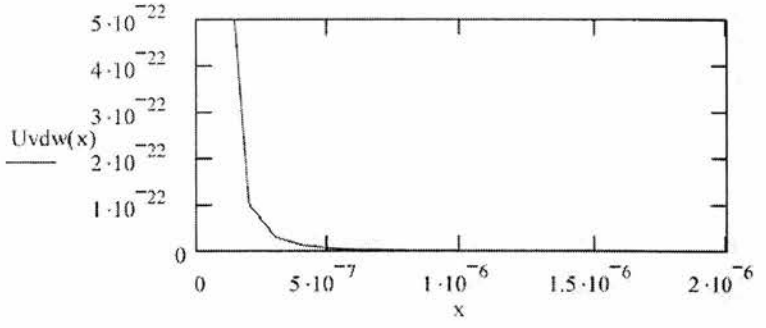

$$Unew(x, \Delta) := U(x, \Delta) - Uvdw(x)$$

$$Tnew(x, \Delta) := \frac{2}{3} \cdot \frac{Unew(x, \Delta)}{k}$$

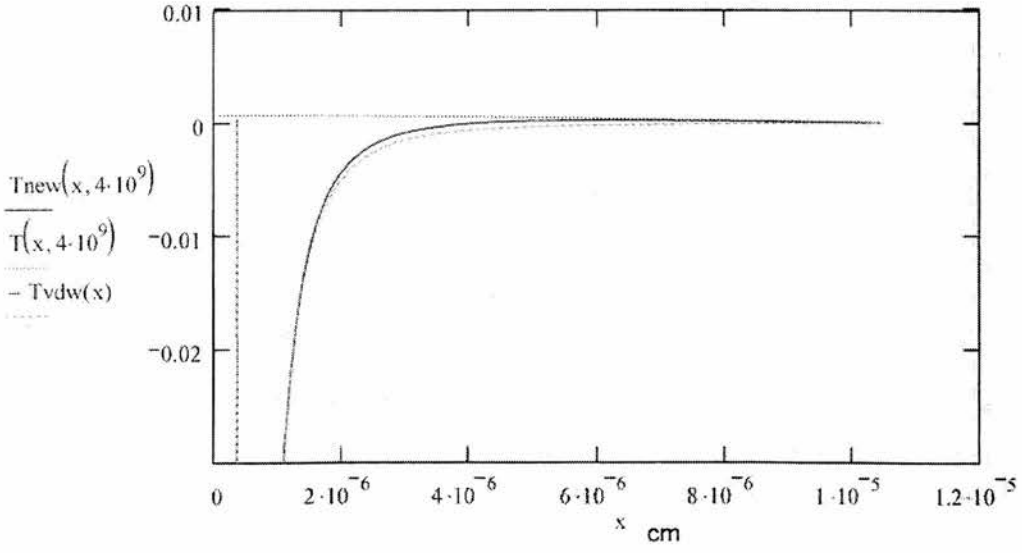

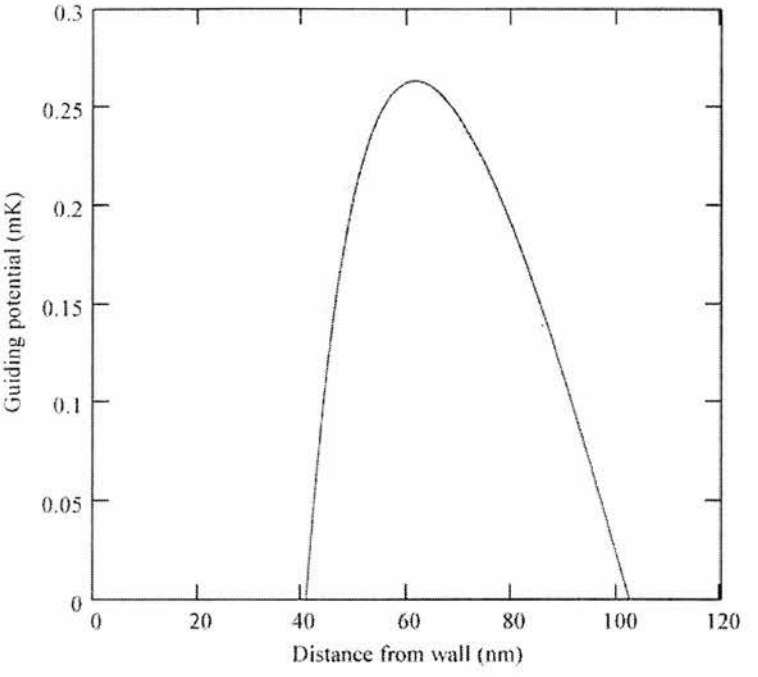
0.3
0.25
0.2
0.15
0.1
0.05
0
Guiding potential (mK)
0
20
40
60
80
100
120
Distance from wall (nm)

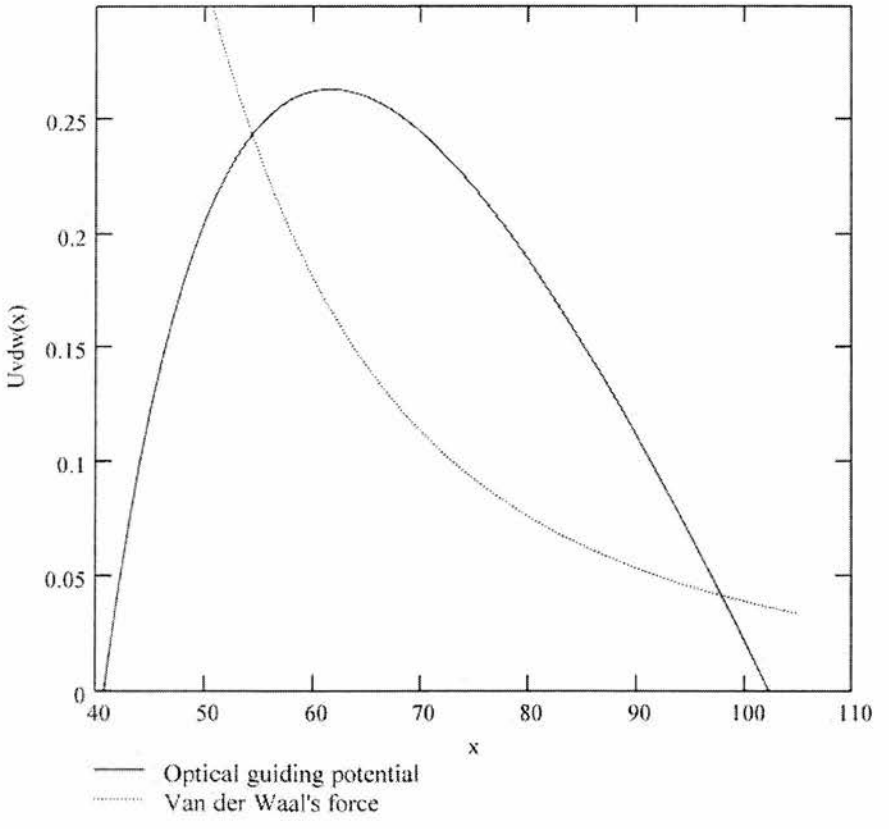
0.25
0.2
0.15
0.1
0.05
0
Uvdw(x)
40
50
60
70
80
90
100
110
x
Optical guiding potential
Van der Waal's force

Caesium guiding potential in a hollow fibre

$k := 1.4 \cdot 10^{-23}$

Planck's Constant $h := \frac{6.6 \cdot 10^{-34}}{2 \cdot \pi}$

Saturation Intensity of Rb $Isat := 1.06 \cdot 10^{-3}$

Natural Linewidth $\Gamma := 5.0 \cdot 10^{6}$

$r0 := 10 \cdot 10^{-4}$

$r := 100 \cdot 10^{-4}$

$Power := 100 \cdot 10^{-3}$

$n := 1.5$

$\theta := 0.26$

$\lambda := 852.3 \cdot 10^{-7}$

$$Io := \frac{Power}{\pi \cdot \left(r^2 - r0^2\right)}$$

$$\alpha := 2 \cdot \sqrt{\frac{n^2}{\left(n^2 - 1\right)}} \cdot \cos(\theta) \qquad \kappa := 2 \cdot \frac{\pi}{\lambda} \cdot \sqrt{n^2 \cdot \sin(\theta)^2 - 1}$$

$$I(x) := Re\left(Io \cdot \alpha^2 \cdot \exp(-2 \cdot \kappa \cdot x)\right) \qquad x := 1 \cdot 10^{-7}, 2 \cdot 10^{-7} .. 1.05 \cdot 10^{-5}$$

$$I(0) = 2.162 \times 10^{3}$$

$$\Delta := -5000 \cdot 10^{6}, -4990 \cdot 10^{6} .. 5000 \cdot 10^{6}$$

$$U(x, \Delta) := \frac{h}{2} \cdot \Delta \cdot \left(\ln\left(1 + \frac{\frac{I(x)}{Isat}}{1 + \frac{4 \cdot \Delta^2}{\Gamma^2}} \right) \right)$$

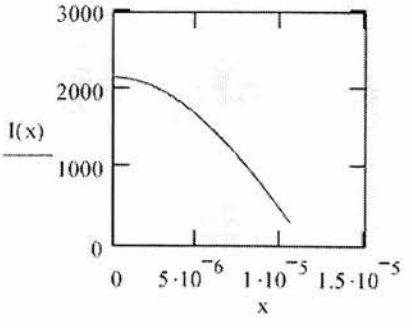

$\ln(1.3) = 0.262$

$$T(x,\Delta) := \frac{2}{3}\cdot\frac{U(x,\Delta)}{k}$$

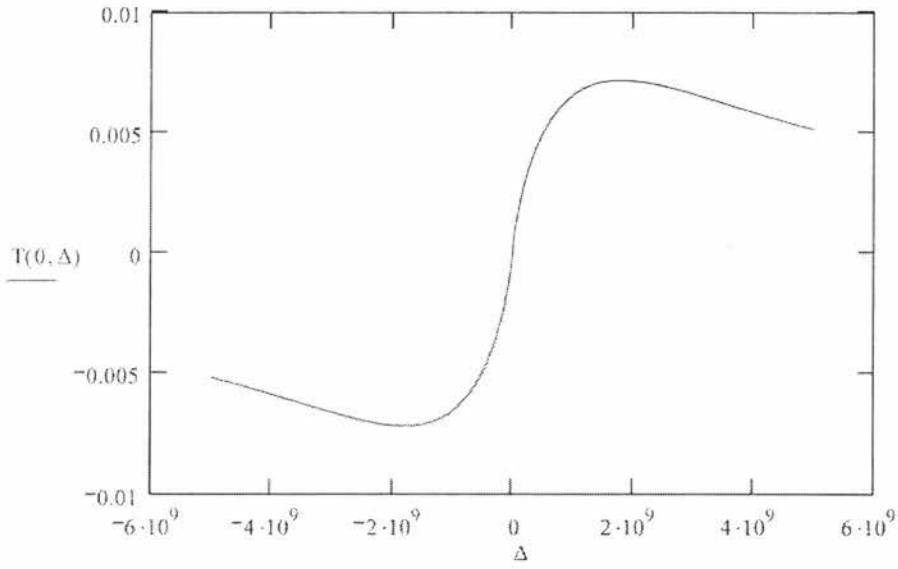

$$A := 0.11$$

$$Uvdw(x) := A\cdot h\cdot 2\cdot\pi\cdot\Gamma\cdot\left(\frac{\lambda}{2\cdot\pi\cdot x}\right)^3$$

$$Tvdw(x) := \frac{2}{3}\cdot\frac{Uvdw(x)}{k}$$

$$\frac{\lambda}{2\cdot\pi} = 1.356\times 10^{-5}$$

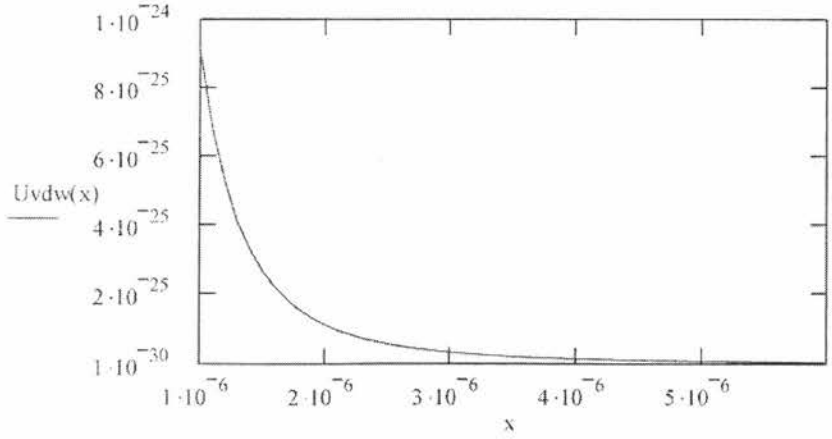

$$Unew(x,\Delta) := U(x,\Delta) - Uvdw(x)$$

$$Tnew(x,\Delta) := \frac{2}{3}\cdot\frac{Unew(x,\Delta)}{k}$$

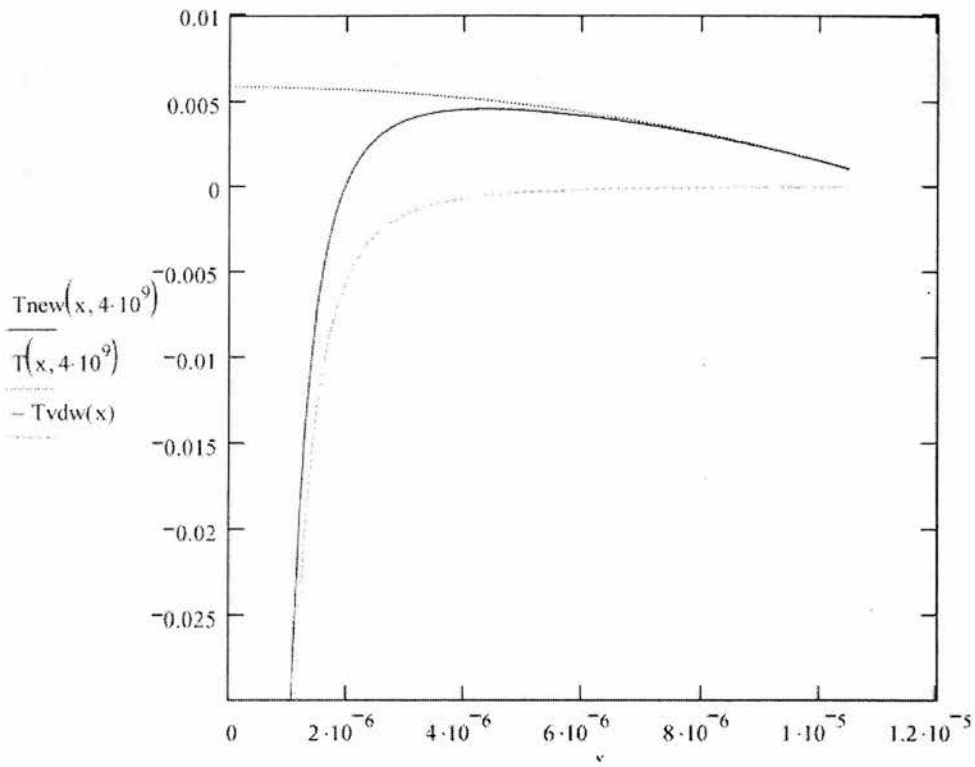

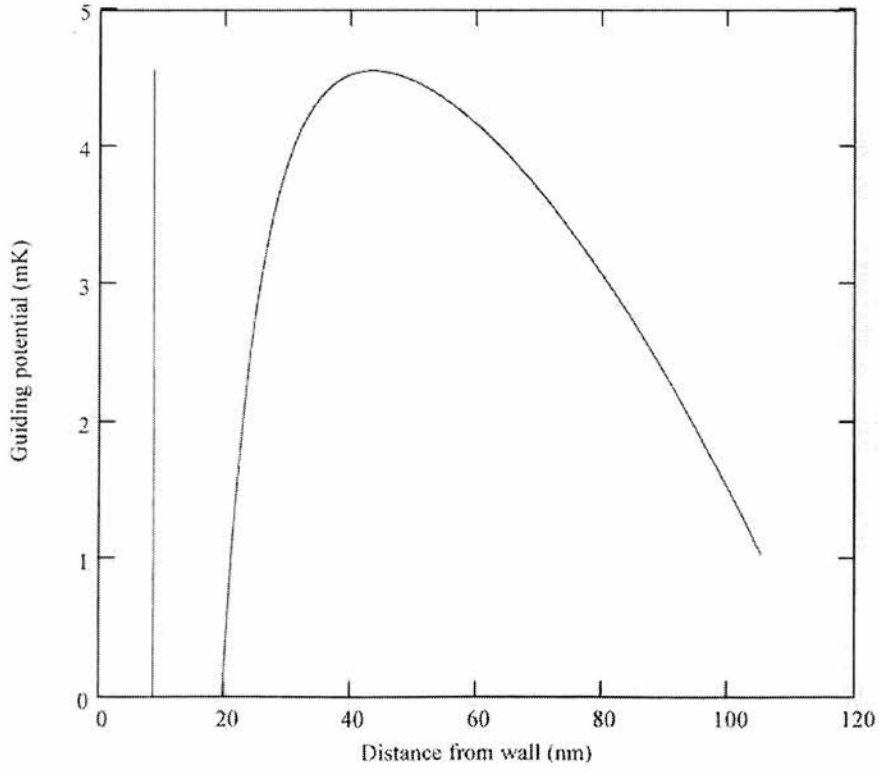

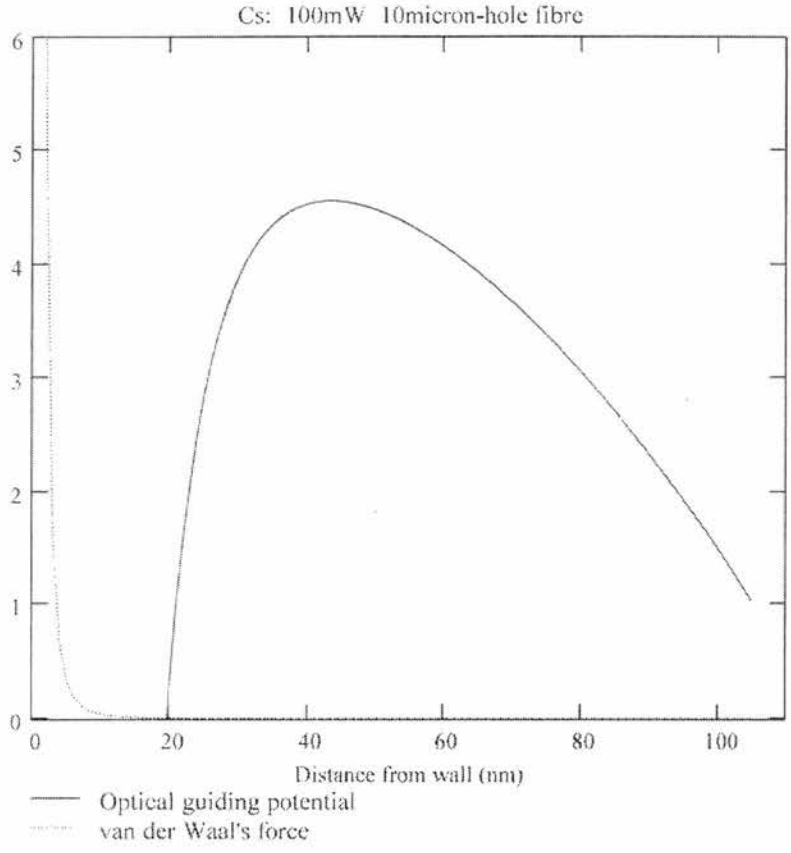
Cs: 100mW 10micron-hole fibre
6
5
4
3
2
1
0
0
20
40
60
80
100
Distance from wall (nm)
Optical guiding potential
van der Waal's force

Appendix B

Publications

ELSEVIER

15 November 1998

Optics Communications 156 (1998) 300–306

OPTICS COMMUNICATIONS

High-order Laguerre–Gaussian laser modes for studies of cold atoms

M.A. Clifford, J. Arlt, J. Courtial, K. Dholakia *

J.F. Allen Physics Research Laboratories, School of Physics and Astronomy, University of St. Andrews, North Haugh, St. Andrews, Fife KY16 9SS, Scotland, UK

Received 21 May 1998; revised 17 August 1998; accepted 18 August 1998

Abstract

The generation of high-order Laguerre–Gaussian (LG) laser modes at 780 nm from a simple external-cavity diode laser is demonstrated. The beams are derived from computer-generated holograms and a high conversion efficiency of 40% is achieved for LG beams with mode indices from $l = 1$ to $l = 6$. The line width of the external cavity diode laser is below 1 MHz. This system is suitable for studies of trapped and cooled atoms using LG beams.

PACS: 32.80.P; 42.60.H
Keywords: Laser cooling; Atom traps; Atom guiding; Angular momentum of light

1. Introduction

The circularly symmetric Laguerre–Gaussian (LG) laser modes form a complete basis set for paraxial light beams. A given mode is usually denoted LG_p^l where l and p are the two integer indices that describe the mode. l refers to the number of 2π phase cycles around the circumference of the mode and $(p+1)$ indicates the number of radial nodes in the mode profile. These modes have generated much recent interest as, for LG modes with $l \neq 0$, there is an azimuthal phase term $\exp(-il\phi)$ in the mode description that gives rise to a well defined orbital angular momentum, of $l\hbar$ per photon. This is in addition to any angular momentum the light may possess due to its polarisation state [1]. The field amplitude of a LG laser mode $E(\mathrm{LG}_p^l)$ of indices l and p is given by:

$$E\left(\mathrm{LG}_p^l\right) \propto \exp\left[\frac{-ikr^2 z}{2\left(z_r^2+z^2\right)}\right]\exp\left[\frac{-r^2}{\omega^2}\right] \times \exp\left[-i(2p+l+1)\arctan\left(\frac{z}{z_r}\right)\right] \times \exp[-il\phi](-1)^p\left(\frac{r\sqrt{2}}{\omega}\right)^l L_p^l\left(\frac{2r^2}{\omega^2}\right) \quad (1)$$

where z is the distance from the beam waist, z_r is the Rayleigh range, k is the wave number, ω is the radius at which the Gaussian term falls to $1/\mathrm{e}$ of its on-axis value, r is the radius, ϕ is the azimuthal angle and L_p^l is the generalised Laguerre polynomial. The term $\arctan(z/z_r)$ is the Guoy phase of the mode.

Several experiments have investigated the nature of the orbital angular momentum of these modes. This angular momentum has been transferred to particles trapped in an

* Corresponding author. E-mail: kd1@st-and.ac.uk

0030-4018/98/$ - see front matter
PII: S0030-4018(98)00464-7

optical tweezer causing them to rotate [2]. Further, these beams have been used to demonstrate controlled rotation of particles trapped in optical tweezers by using both the spin and orbital angular momentum of light [3,4]. More recently [5,6] there has been work performed studying the role of these beams in non-linear media. In the case of second harmonic generation a mode transformation was observed between the fundamental and frequency doubled beam that was due to the conservation of orbital angular momentum between the light fields. Lately, there has been considerable interest in using these beams for the study of trapped cold atoms and some theoretical work has been performed [7,8]. Only very limited experimental work has been done with LG modes and atomic systems: Snadden and coworkers used such beams for high-resolution spectroscopy in a magneto-optical trap [9]. They use a combination of standard TEM_{00} light beams and LG_0^1 beams for trapping. The use of LG beams is beneficial as they reduce the ac stark shift and broadening of transitions at trap centre. Recently, a novel trapping scheme was shown by Kuga and coworkers using LG beams [10]. They trapped atoms along the centre of an LG light beam. This experimental work exploited the spatial profile of LG modes with $p = 0$, which have the form of a ring of light. Both experiments however generated their modes in a very different, and rather more complicated fashion than the work presented here. Hollow beams (such as LG beams) are increasingly important in laser cooling and trapping experiments. The repulsive optical dipole force for blue-detuned laser light allows the atomic motion to be restricted to the inner (dark) region of the laser beam where photon scattering and the associated heating is minimised.

There are a number of techniques by which Laguerre–Gaussian laser modes may be generated. It is possible to generate them directly from a laser though this is rather rare. Insertion of an intra-cavity cross-wire into a laser cavity may be used to generate a high-order Hermite–Gaussian (HG) laser mode which may then be converted to a Laguerre–Gaussian laser mode using a mode converter [11]. A mode converter consists of two cylindrical lenses canonically disposed with respect to one another. This system of lenses introduces a Guoy phase shift on an incident laser beam that converts a HG mode of indices m and n to a Laguerre–Gaussian mode of indices $l = (m - n)$ and $p = \min(m, n)$. Central to using this technique, however, is the ability to generate high-order Hermite–Gaussian modes which is impractical for a number of laser cavities, in particular for external cavity diode lasers as discussed in this paper. From a fundamental Gaussian (TEM_{00}) mode one may use two techniques to generate Laguerre–Gaussian modes: a spiral phase plate may be employed [12] or a computer-generated hologram may be used [13]. It is with computer-generated holograms that this paper is concerned.

External-cavity diode lasers are now established as workhorse tools for high-resolution spectroscopy. A straightforward technique is to use standard diode lasers in a Littrow external cavity arrangement where the output of the diode is sent onto a diffraction grating. The first order diffracted beam is sent back into the diode and the ensuing optical feedback leads to an external resonator being formed consisting of the back facet of the diode and the grating. This leads to a dramatic reduction in the linewidth of the laser and allows for precise control of the laser frequency by tuning the grating position using a piezo-electric (PZT) element. Several designs for such systems have been shown and some commercial systems are now available. The external cavity diode laser system we have constructed is dramatically simpler than all but one other reported to date. It uses standard commercial opto-mechanical components and a few machined components to achieve a performance comparable to more elaborate systems. It is noted that Arnold et al. have very recently shown a similar system to the one presented here [14] though there are some key differences in design.

In this paper, we discuss the experimental holographic generation of Laguerre–Gaussian laser modes. This system is operated at 780 nm and is suitable for studies of trapped and cooled rubidium atoms. We have used an external cavity diode laser in conjunction with very simple holographic elements to generate Laguerre–Gaussian laser modes with an azimuthal mode index l ranging from 1 to 6 ($p = 0$). The external-cavity diode laser system readily gives up to 40 mW of tunable narrow-linewidth laser light at 780 nm. The holograms have an efficiency approaching 40% and thus we are able to obtain around 15 mW of laser light in a LG mode which is more than sufficient for many experiments in trapping and cooling. Similar holograms have already been produced by ourselves, but they were for generating multi-ringed ($p > 0$) LG modes with azimuthal index $l = 1$, using a standard He–Ne laser [15]. To date, experimental generation of Laguerre–Gaussian laser modes using holographic techniques has only been, we believe, experimentally demonstrated for $l = 3$ modes by He and coworkers [16]. They generated 3 mW from a 7 mW He–Ne laser in an LG_0^3 mode. Here we present experimental data for a range of holograms and generate LG modes with $l = 1$ to 6 with efficiencies for all approaching 40%. As the azimuthal index l increases the inner dark region of the light gets larger and the outer ring of light gets narrower. These are the highest order LG modes efficiently produced to date with this technique.

2. Holographic elements for LG modes

A hologram is simply a recording of a diffraction pattern between an electromagnetic field of interest and a reference field. For holographic generation of a Laguerre–Gaussian mode, the diffraction pattern takes the form of a forked diffraction grating with l dislocations. This results in a screw phase dislocation on the beam axis that gives us

the characteristic $\exp(-il\phi)$ phase structure of these beams. In addition, we obtain an annular intensity pattern (for $p = 0$ modes) in the far field.

A straightforward formula is used to determine the form of the forked hologram. For a binary grating we have (in polar co-ordinates):

$$l\frac{\phi}{\pi} = n + \frac{2r}{\Lambda}\cos\phi. \tag{2}$$

This formula relates the boundaries between the transparent and opaque areas of the hologram. $n = 0, \pm 1, \pm 2, \ldots$ and Λ denotes the grating period. High efficiency holographic elements may be obtained by converting such an amplitude hologram into a phase hologram and blazing it to maximise the light in the first diffracted order. In this instance, the transmittance function of the hologram may be written as [16]:

$$T(r,\phi) = \exp(i\delta H(r,\phi)) \tag{3}$$

δ denotes the amplitude of the phase modulation. The holographic pattern H is given by:

$$H(r,\phi) = \frac{1}{2\pi}\mathrm{mod}\left(l\phi - \frac{2\pi}{\Lambda}r\cos\phi, 2\pi\right) \tag{4}$$

where $\mathrm{mod}(a, b) = a - \mathrm{int}(a/b)$.

Generally when such a hologram is irradiated with a fundamental Gaussian mode (TEM_{00}), the output is a superposition of an infinite number of LG modes, each having the same l index but with a range of values for the p index. An analytical decomposition of the output beam shows that the $p = 0$ mode contributes 78.5% of the intensity in the first diffracted order. Higher order LG modes have contributions of $p \neq 0$ which may be simply determined [13]:

$$E_{lp} = \sqrt{\frac{p!}{(p+1)!}}\, l\Gamma\left(p + \frac{l}{2}\right)\Big/ 2p! \tag{5}$$

For a given azimuthal index the above formula allows us to determine the contribution E_{lp} of each radial index p to the field amplitude. This formula assumes identical input and output beam waists.

The manufacturing of the holograms is as follows: a computer-generated pattern was written directly onto colour film (Kodak Ektachrome Professional 100) using a slide writer film recorder. Contact prints were then made onto standard holographic film (Edmund Scientific Ltd.). The film was developed and bleached using a rehalogenation bleach as detailed by Kim [17]. This allowed diffraction efficiencies of approximately 40% into the first order. Higher efficiencies have been achieved but only with the use of specialist holographic glass plates. Further improvement may be achieved by using more expensive plates and compensating for the non-linearity of the film. However, our simple technique has the advantage of using only standard holographic film and a slide writer.

3. Tunable external cavity diode lasers

The laser system used here is of a very straightforward design and is in a standard Littrow external cavity geometry (see Fig. 1). A Hitachi 7851G single longitudinal mode laser diode operating at 780 nm with a maximum power output of 50 mW was used. The laser was placed in an external cavity geometry with a 1200 lines/mm or 1800 lines/mm diffraction grating used to achieve grating feed-

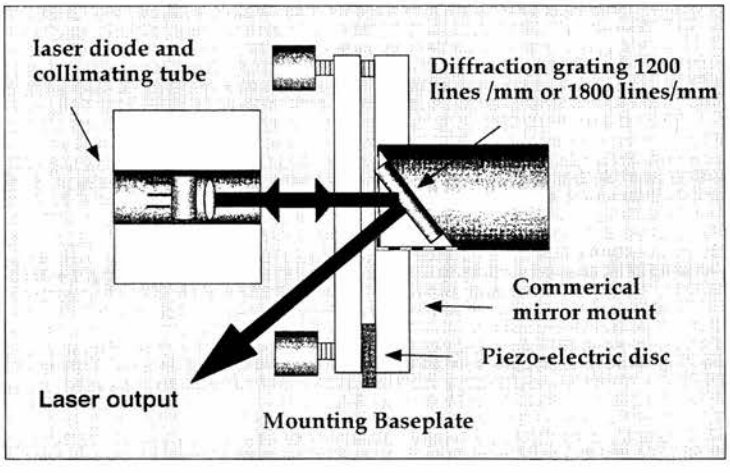

Fig. 1. Layout of the external cavity diode laser. A commercial mirror mount houses a machined holder for the diffraction grating. The laser diode is mounted in a collimating tube (Thorlabs, LT110P-B). The resonator length is around 3 cm. The whole assembly is mounted inside a sealed box.

back. The first-order beam was reflected back into the laser. This allowed an external resonator to be formed, consisting the back facet of the laser diode and the diffraction grating. About 20% of the light was reflected back into the laser. The zeroth order output of the grating gave the output used for the experiment. In typical operating conditions, this meant that around 40 mW of laser light could be usefully employed for experimental purposes. The laser was tuned manually to the rubidium lines by adjusting the horizontal control on the mirror mount.

The diffraction grating is mounted on a machined holder inserted into a clear quadrant design commercial mirror mount (Newport P100-AC). The mirror mount design allowed easy access to the laser and also the freedom to use the laser with diffraction gratings of both 1200 lines/mm and 1800 lines/mm (Optometrics UK). The laser diode is mounted in a commercial collimating tube (Thorlabs LT110P-B) which is mounted on a baseplate. This assembly is placed on a large cylindrical base that is temperature stabilised to a few mK. Tuning is achieved by using a piezo-electric element (PZT) placed between the horizontal adjustment screw of the mirror mount and the main plate of the mirror mount, thus altering the position of the grating. This allowed continuous mode-hop free tuning of 8 GHz. Using a 300 MHz optical spectrum analyzer the laser was found to run stably in a single longitudinal mode and an upper limit of 4 MHz was placed on the linewidth from the output of this device. By per-

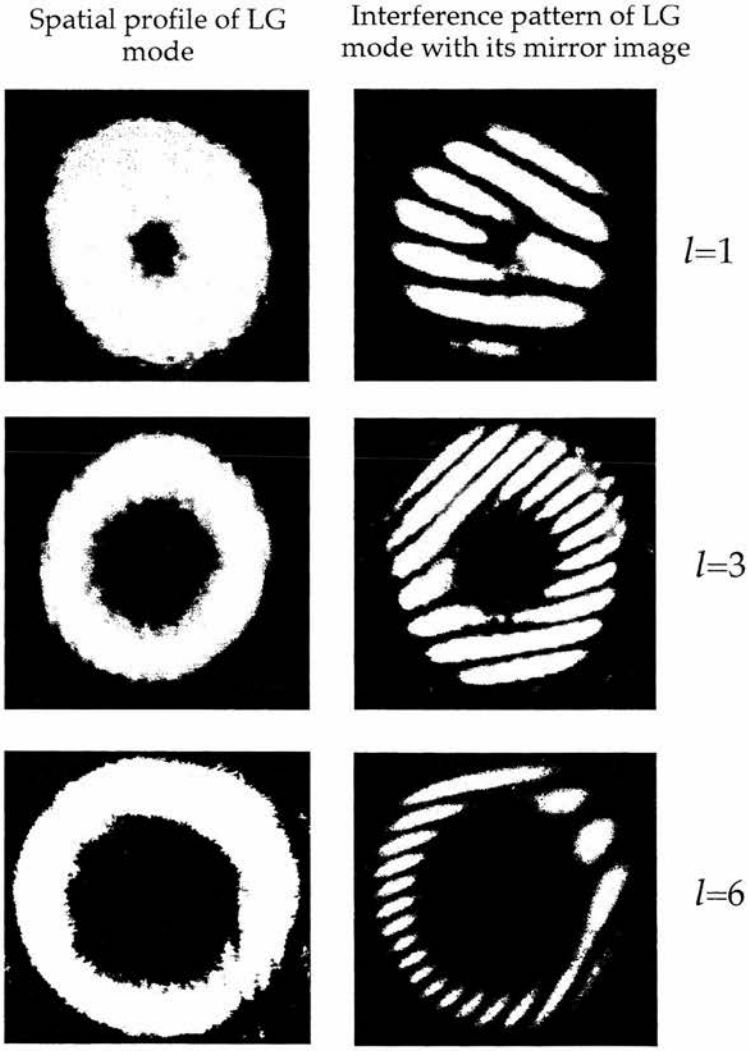

Fig. 2. The mode profiles and interference patterns for LG modes with mode indices $l = 1$, 3 and 6. In the interference patterns one can see the appearance of additional fringes on one side of the pattern with respect to the other.

Table 1
The intensity contribution of each radial mode p towards the respective holographically generated output beam of azimuthal index l

	$l=1$	$l=3$	$l=6$
$p=0$	93%	77%	62.8%
$p=1$	~0	0	0
$p=2$	3.4%	11.1%	15.5%

This data is calculated by optimising the overlap of beam waists for the input and output beams in comparison to the analysis of Eq. (5).

forming a heterodyne measurement using two similar lasers and a rf spectrum analyser, we were able to find that the linewidth of each external cavity diode laser was well under 1 MHz. This is similar to the linewidths achieved by Arnold and coworkers [14]. The laser was locked to a saturated absorption feature in rubidium for long-term reproducibility in experiments with trapped atoms.

This laser was then used to generate LG modes from our computer-generated holograms. The diode laser output beam was shaped using anamorphic prisms to obtain a near-circular beam and was then passed through centre of the holographic elements described. The LG mode was diffracted into the first order. This LG beam was then sent into a mode analyser. This device was a Mach–Zender interferometer with a Dove prism in one arm and allowed the interference of the Laguerre–Gaussian mode with its own mirror image. This allowed the direct evaluation of the azimuthal mode index of the LG beam [5,6].

Fig. 2 shows the interference patterns obtained with this arrangement for LG modes with $l=1$, 3 and 6. The figures clearly show that additional fringes occur in the interference pattern due to differing angles of intersection of the modes on one side of the pattern with respect to the other. From the additional number of fringes, it is possible to determine the mode index l – an extra $2l$ fringes should appear in the pattern for each mode we observe. This occurs because the wavefronts of two LG modes of oppo-

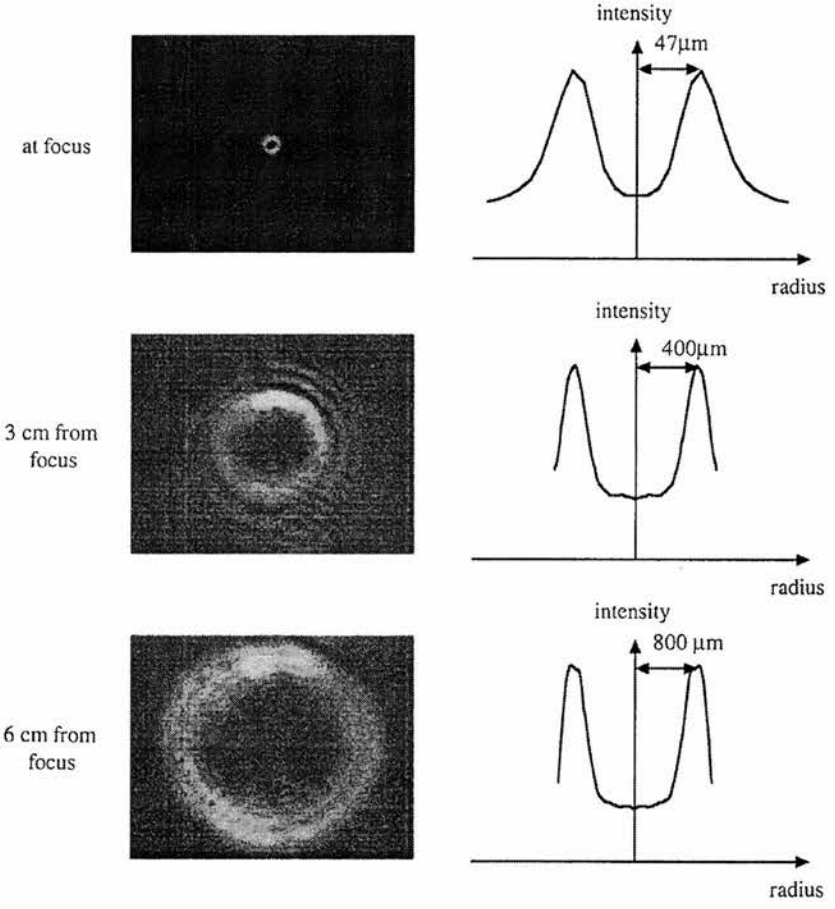

Fig. 3. The spatial profile of a $l=6$ mode as it is focused by a $f=150$ mm lens. The spatial profile changes slightly on propagation though the singularity stays intact.

site helicity (as in this case) intersect at different angles on either side of the interference pattern [18]. Importantly too, the figures show how the size of the central hole increases as we increase the azimuthal index l of the mode. The spatial profile of high-order LG modes is of direct importance for experiments with cold atoms utilising the optical dipole force [10].

We have also studied the composition and propagation of these holographically produced LG beams. We have numerically optimised the beam waist at the hologram output for maximum overlap with the input mode. This results in a different beam waist ω_o^{out} for the holographically produced LG beam when compared with the input beam ω_o^{in} dictated by the following [19]:

$$\frac{\omega_o^{out}}{\omega_o^{in}} \approx \frac{1}{\sqrt{l+1}}. \tag{6}$$

This is to be compared to the decomposition in Eq. (3) which is performed with *identical* input and output beam waists. Table 1 shows the relative intensity contributions of the $p = 0$ mode for various LG beams using a decomposition based on Eq. (6). We have experimentally measured the spatial profile for a $l = 6$ beam as it is focused by a $f = 150$ mm lens. Data are shown in Fig. 3. The radial profile for each position is obtained by averaging the profile over 80 azimuths. This mode has a dominant contribution of $p = 0$ (Table 1). We find that, as expected, the singularity remains intact during propagation and that the spatial form of the mode changes slightly as it propagates through a beam waist. The change in spatial profile is the result of a different Guoy phase shift (see Eq. (1)) for each different p mode contribution as the mode goes through a focus. We have verified this behaviour by using a simple computer model to look at the beam propagation [19].

4. Conclusions

We have shown the efficient experimental generation of Laguerre–Gaussian light beams with differing azimuthal mode indices up to $l = 6$ and studied their propagation. The profile of these modes is suitable for studies of cold atoms. Further, we have realised a particularly simple design for a tunable external cavity diode laser system that can generate suitable laser light for trapping and cooling rubidium atoms. This external cavity diode laser is simpler than virtually all others presented to date. In tandem, this system represents a simple but powerful basis for a number of experiments with cold atoms. We are currently studying the trapping conditions of cold atoms when using LG modes – the lack of light in the centre of these modes, when used as a repumping beam leads to a higher density of trapped atoms. Indeed these beams could be used to realise a 'dark spot' magneto-optical trap [20,21]. Other groups have generated LG modes for studying cold atoms [9,10]. Their schemes used the mode converter mentioned earlier and were more complicated than the method presented here and unsuitable for use with an external cavity diode laser. Notably, Kuga and coworkers [10] identify that the use of high order LG modes (such as those realised in this work) would greatly extend the lifetime of their novel dipole trap with cold atoms. Other applications for such laser modes include the prospect of atom guiding a cold atomic beam along the centre of a Laguerre–Gaussian light beam [22,23] and also the study of the interaction of the orbital angular momentum of light with trapped atomic particles – this has theoretically been shown to result in new effects [7,8].

Acknowledgements

We would like to thank Dr. Danny Segal for useful discussions about diode lasers. This work is supported by the UK Engineering and Physical Sciences Research Council under grant number GR/L54301. Kishan Dholakia is a Royal Society of Edinburgh Research Fellow.

References

[1] L. Allen, M.W. Beijersbergen, R.J.C. Spreeuw, J.P. Woerdman, Phys. Rev. A 45 (1992) 8185.
[2] H. He, M.E.J. Friese, N.R. Heckenberg, H. Rubensztein-Dunlop, Phys. Rev. Lett. 75 (1995) 826.
[3] M.J. Friese, J. Enger, H. Rubensztein-Dunlop, N.R. Heckenberg, Phys. Rev. A. 54 (1996) 1593.
[4] N.B. Simpson, K. Dholakia, L. Allen, M.J. Padgett, Optics Lett. 22 (1997) 52.
[5] K. Dholakia, N.B. Simpson, L. Allen, M.J. Padgett, Phys. Rev. A 54 (1996) R3742.
[6] J. Courtial, K. Dholakia, L. Allen, M.J. Padgett, Phys. Rev. A 56 (1997) 4193.
[7] L. Allen, M. Babiker, W.K. Lai, V.E. Lembessis, Phys. Rev. A 54 (1996) 4259.
[8] W.K. Lai, M. Babiker, L. Allen, Optics Comm. 133 (1997) 487.
[9] M.J. Snadden, A.S. Bell, R.B.M. Clarke, E. Riis, D.H. McIntyre, J. Opt. Soc. Am. 14 (1997) 544.
[10] T. Kuga, Y. Torii, N. Shiokawa, T. Hirano, Y. Shimizu, H. Sasada, Phys. Rev. Lett. 78 (1997) 4713.
[11] M.W. Beijersbergen, L. Allen, H.E.L.O. van der Veen, J.P. Woerdman, Optics Comm. 96 (1993) 123.
[12] G.A. Turnbull, D.A. Robertson, G.M. Smith, L. Allen, M.J. Padgett, Optics Comm. 127 (1996) 183.
[13] N.R. Heckenberg, R. McDuff, C.P. Smith, H. Rubenstein-Dunlop, M.J. Wegener, Optics Quantum Electron. 24 (1992) S951.
[14] A.S. Arnold, J.S. Wilson, M.G. Boshier, Rev. Sci. Instrum. 69 (1998) 1236.

[15] J. Arlt, K. Dholakia, L. Allen, M.J. Padgett, J. Mod. Optics 45 (1998) 1231.
[16] H. He, N.R. Heckenberg, H. Rubenstein-Dunlop, J. Mod. Optics 42 (1995) 217.
[17] N. Kim, Optics Comm. 105 (1994) 1.
[18] M. Harris, Contemp. Phys. 36 (1995) 215.
[19] J. Arlt, J. Courtial, private communication.
[20] W. Ketterle, K.B. Davis, M.A. Joffe, A. Martin, D.E. Pritchrd, Phys. Rev. Lett. 70 (1993) 2256.
[21] M.H. Anderson, W. Petrich, J.R. Ensher, E.A. Cornell, Phys. Rev. A 50 (1994) R3547.
[22] J. Yin, Y. Zhu, W. Wang, Y. Wang, W. Jhe, J. Opt. Soc. Am. B 15 (1998) 25.
[23] K. Dholakia, Contemp. Phys. 39 (1998) 351.

ELSEVIER

15 October 1999

Optics Communications 170 (1999) 79–84

OPTICS COMMUNICATIONS

www.elsevier.com/locate/optcom

A polarisation spectrometer locked diode laser for trapping cold atoms

G.P.T. Lancaster, R.S. Conroy *, M.A. Clifford, J. Arlt, K. Dholakia

J F Allen Physics Research Laboratories, School of Physics and Astronomy, University of St. Andrews, North Haugh, St. Andrews, Fife, KY16 9SS, UK

Received 13 May 1999; received in revised form 14 July 1999; accepted 3 August 1999

Abstract

We have modelled and used polarisation spectroscopy to lock a very compact, high-performance extended cavity diode laser system to the ^{85}Rb ($F = 3$ to $F' = 4$) transition. The laser has a linewidth of 135 kHz. Using this system we have trapped and cooled 1.5×10^8 Rb atoms in a magneto-optical trap. Atoms remained continuously trapped in the MOT for several minutes. © 1999 Elsevier Science B.V. All rights reserved.

PACS: 32.80.P; 42.60.H
Keywords: Laser cooling; Atom traps; External cavity diode lasers

1. Introduction

Since the first demonstration of the magneto-optical trap (MOT), rapid worldwide advances have seen a dramatic simplification of the apparatus and associated laser systems required to trap and cool atoms. Notable achievements include the ability to use a simple atomic vapour cell rather than an atomic beam to generate the atomic sample [1], and the use of inexpensive diode lasers for laser cooling [2]. These advances have enabled experimentalists to realise temperatures close to or below the recoil limit and have led to a number of diverse experiments with cold atoms including Bose–Einstein condensation [3], high precision spectroscopy [4] and atom guiding [5,6].

The characteristics of free running, commercially available diode lasers are not usually suitable for high-precision spectroscopic studies. In practice, it can be difficult for a user to locate the atomic or molecular transition of interest and tune smoothly around this region. Also, whilst diode lasers can be made to run in a single longitudinal mode, they usually have a linewidth of the order of ~ 50 MHz for near infrared (IR) wavelengths, much broader than the linewidths of the transitions being examined.

Optical feedback can be used to convert free-running diode lasers into true narrow linewidth tunable laser sources. The major technique developed to utilise this sensitivity to feedback is the use of a diffraction grating external to the diode laser. One popular configuration used is termed the 'Littrow geometry', where light from the diode is sent onto a blazed diffraction grating and the first diffracted

* Corresponding author. Fax: +44-1334-463-104; e-mail: r.conroy@st-andrews.ac.uk

0030-4018/99/$ - see front matter
PII: S0030-4018(99)00433-2

order is fed back into the diode. The zeroth order provides the output for the laser. The diode lases on a pseudo-external cavity that consists of the back facet of the diode laser and the diffraction grating. This is known as an extended-cavity diode laser (ECDL). Extended-cavity diode lasers now offer an inexpensive, high-performance route for performing atomic and molecular spectroscopy.

For the trapping and cooling of atoms, the laser has to be to an atomic resonance for long term reproducibility. In this paper we present details of a hitherto unexplored locking scheme for diode lasers to trap atoms — namely using polarisation spectroscopy to provide a locking signal. This is used in conjunction with a very compact ECDL that we have developed and was briefly mentioned in earlier work [7]. Here we have modelled the expected signal profiles from polarisation spectroscopy and demonstrate its use in stabilising this laser system to the appropriate transition in rubidium for laser cooling. We are able to cool and trap ^{85}Rb using these laser systems and have continuously trapped more than 10^8 atoms of ^{85}Rb in our MOT for several minutes. To the best of our knowledge, this is the first time this laser diode stabilisation technique has been modelled and applied to diode lasers for trapping and laser cooling rubidium atoms.

2. Tunable external cavity diode laser

A Hitachi 7851G single longitudinal mode laser diode operating at 780 nm with a maximum power output of 50 mW was used for these experiments. The laser was placed in an external-cavity Littrow geometry with a 1200 lines/mm diffraction grating. The first-order beam was reflected back into the laser. This allowed an external resonator to be formed, consisting of the back facet of the laser diode to the diffraction grating. About 20% of the light was reflected back into the laser. In typical operating conditions, this meant that up to 40 mW of laser light could be usefully employed for experimental purposes. The laser was coarsely tuned to the rubidium lines by adjusting the horizontal control on the mirror mount, with continuous fine-tuning provided by PZT control of the mount angle.

Using a 300 MHz optical spectrum analyzer (finesse > 300) the laser was found to run stably in a

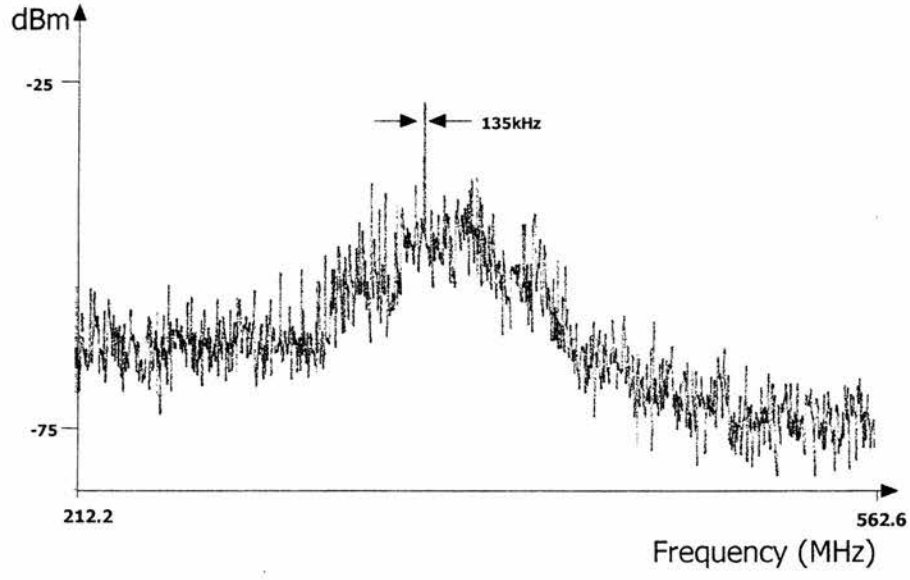

Fig. 1. A heterodyne experiment between two of the external cavity diode lasers. The width of the peak allows us to determine that the linewidth of the diode is 135 kHz.

single longitudinal mode and an upper limit of 2 MHz was placed on the linewidth from the output of this device. By performing a heterodyne measurement using two similar lasers and a RF spectrum analyser, we were able to find that the linewidth of each external cavity diode laser was approximately 135 kHz in a 100 ms sampling time (Fig. 1). (This is significantly below the natural linewidth of the ^{85}Rb transition (6.1 MHz) used for trapping and cooling.)

3. Polarisation spectroscopy

Locking the extended cavity diode laser to an atomic resonance is essential for stabilising the laser frequency when trapping and cooling atoms. Widely used locking techniques employ feedback from Doppler-free signals to control the current and/or the PZT voltage to maintain the laser frequency at the desired value. Doppler-free signals can be generated using saturated absorption spectroscopy [8] and frequency modulation to generate a dispersive signal [9]. However, these techniques have disadvantages in terms of sensitivity for weak transitions and complexity respectively. Here, we demonstrate the use of polarisation spectroscopy as a simple, highly sensitive, alternative Doppler-free technique that readily generates an appropriate dispersive signal that we have used for stabilising a laser.

Polarisation spectroscopy [10,11] is a widely known technique in atomic spectroscopy. It is based on a light induced birefringence of an absorbing gas and is closely related to the widely used saturated absorption techniques. However, instead of monitoring the change in absorption of the probe beam due to a strong counter-propagating pump beam, the polarisation rotation of the probe is monitored. This technique is particularly attractive for providing a frequency reference, because it is typically 1–2 orders of magnitude more sensitive than saturated absorption and the dispersion profile of the polarisation allows stabilisation without frequency modulation. Additionally with a side-of-fringe locking technique the laser can be stabilised over a 100 MHz range around the cooling transition $(F = 3) \rightarrow (F' = 4)$. It is worth noting that for optimum trapping the diode laser needs to be red-detuned by 2–3 linewidths from the line centre [12], easily achieved by this system without the need for acousto-optic modulators.

Previous studies of polarisation spectroscopy have included its use for optical feedback to stabilise a free-running laser diode [13]. However, the systems used were more elaborate than the one presented here. In comparison, our system stabilises an ultra-compact extended cavity diode laser using a very simple geometry of polarisation spectrometer. Importantly, extended cavity diode lasers in the Littrow configuration form the basis of many atom trapping and cooling experiments worldwide.

Fig. 2 shows our polarisation spectrometer used to generate our dispersive locking signal. A linearly polarised probe beam passes through a 10 cm long rubidium cell. This beam passes through crossed polarisers as shown. Any induced anisotropy will alter the transmission of light through this set of crossed polarisers. This will result in an easily detectable signal. The anisotropy is introduced by means of a circularly polarised pump beam that counter-propagates through the rubidium cell. The linearly polarised probe beam may be decomposed into two counter-rotating circularly polarised beams, one rotating with the polarising beam and one rotating in the opposite sense. The polarising beam intro-

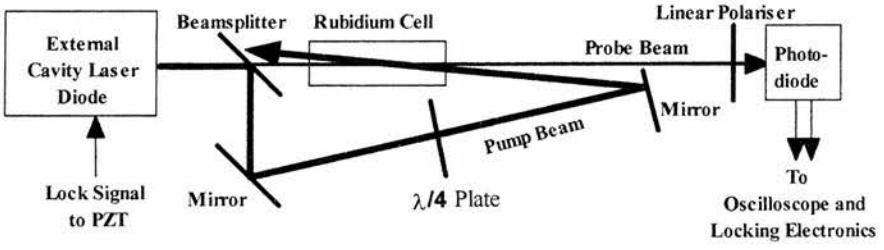

Fig. 2. The polarisation spectrometer set-up used for this work.

duces a difference in absorption and refractive index for each of these two beams because of the non-uniform pumping of the sub-levels. On recombination after passing through the cell, the plane of linear polarisation of the probe is rotated and may be detected as an increase in signal on the photodiode.

The intensity of the probe light at the photodiode of a polarisation spectrometer, ignoring cell window birefringence, can be modelled as [14]:

$$I_T = I_{BACK} \times \left[\varepsilon + \theta^2 + \frac{(\Delta\alpha_0 L)^2 - 2\theta\left(\frac{\nu_0 - \nu}{\gamma}\right)\Delta\alpha_0 L}{4\left(1 + \left(\frac{\nu_0 - \nu}{\gamma}\right)^2\right)} \right] \quad (1)$$

where $I_{BACK}(\varepsilon + \theta^2)$ is the constant background term caused by imperfect polarisers, with leakage ε, at a small misalignment, θ, transmitting a fraction of the background saturated absorption, $\Delta\alpha_0 L$ is the change in absorption from saturated absorption at line centre, γ is the natural linewidth of the transition, and $\nu_0 - \nu$ is the frequency detuning from line centre. In this work we have assumed no birefringence in the cell windows ($b = 0$), because of the cell window specifications. With no constant background, the choice of angle θ between the crossed polarisers can lead to either a dispersion shape (θ large) or Lorentzian shape ($\theta \sim 0$). The dispersion shape is desirable both in terms of allowing easy location of the correct hyperfine transition using the background absorption profile and giving a zero-crossing slope on which to lock and is easily achieved experimentally through slight misalignment of the polariser with respect to the polarisation of the laser.

The saturated absorption background can be expressed as [14]:

$$I_{BACK} = I_0 \times \left[\exp\left(- \frac{M(\nu_0 - \nu)^2}{1.845 \times 10^{-13} \nu_0^2 T} \right) \right] \times \left[\sum_{F \to F' = 0 \pm 1} 1 - \frac{S_{F'}}{2} \left[1 + \frac{\left(\frac{\gamma_{F'}}{2}\right)^2}{(\nu - \nu_{F'})^2 + \left(\frac{\gamma_{F'}}{2}\right)^2} \right] \right] \quad (2)$$

where the first part represents the Doppler broadened profile of the transition at a given temperature T and the second term is the sum of the saturated lines for the allowed hyperfine transitions $F \to F^1$ in question with a saturation parameter $S_{F'}$.

Fig. 3 shows the difference in expected locking signal between saturated absorption and polarisation

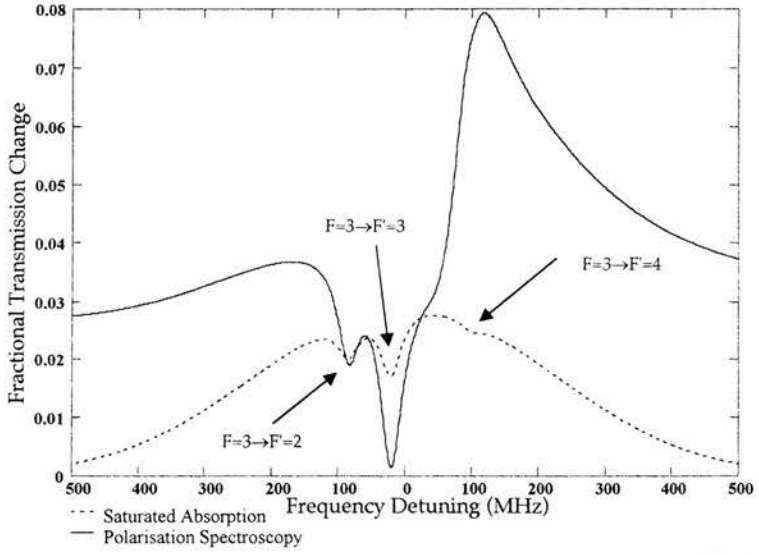

Fig. 3. Expected locking signals from polarisation spectroscopy and saturated absorption spectroscopy of the $^{85}Rb\ ^5S_{1/2} \to {}^5P_{3/2}$ transition.

spectroscopy for our experimental set-up. The signal has been modelled with a 5° angle between the polariser and the polarisation of the diode laser to show both the Lorentzian and dispersion line shapes. The polarisation signal is approximately seven times larger than the saturated absorption signal and has a broad range (~ 100 MHz) over which it can be locked and therefore can be used to access the optimum trapping frequency, some 15–20 MHz below the ^{85}Rb ($F = 3 \rightarrow F' = 4$) transition line centre, with ease.

4. Experimental apparatus

Our trap consists of simple six-way Pyrex glass cross, mounted on standard vacuum components. The trap was held at a base pressure of 10^{-10} mbar by a 40 L/s ion pump. We used Rb metal getter ovens in our system to controllably introduce rubidium into the vacuum system. Typically we operated with a background rubidium vapour pressure of 10^{-8} mbar. A set of anti-Helmholtz coils was placed around the trap to generate a field gradient of 10 G/cm. The trapping lasers were expanded to approximately 1.5 cm in diameter and overlapped at trap centre.

The hyperfine-repumping laser (tuned to the $F = 2 \rightarrow F' = 3$ transition) was overlapped with this beam in the centre of the trap. A CCD camera and photodiode were used to monitor the trapped atoms and record their fluorescence to infer the number trapped.

Fig. 4 shows the measured locking signals obtained from our set-up for the ^{85}Rb $^5S_{1/2} \rightarrow {}^5P_{3/2}$ transition in both saturated absorption mode and as a polarisation spectrometer. These results are in good agreement with the modelling from Fig. 3 and illustrate the higher sensitivity offered by polarisation spectroscopy.

This locking signal was fed into a side of fringe locking scheme, similar in design to that reported by Macadam et al. [15]. This locking scheme was then used to stabilise the trapping laser frequency. The locking scheme allowed for small changes, up to tens of MHz, in the position of the lock point using an offset, which was used to optimise the number of trapped atoms. We were able to maximize the number of trapped atoms in this way to achieve 1.5×10^8 atoms continuously for times in excess of 2 min. The frequency drift of the laser while locked was less than 10 MHz. The trapping time was limited only by the background vapour pressure and the unlocked repumping laser. Locking the repumping laser using

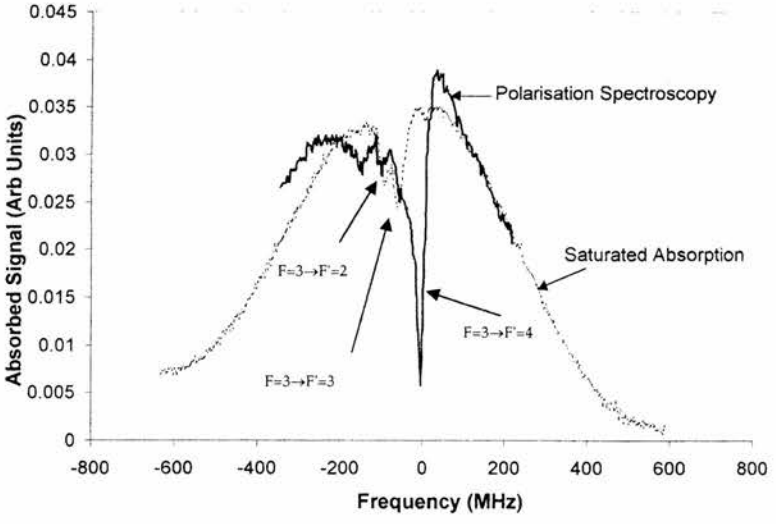

Fig. 4. Experimental measurement of the saturated absorption spectra and polarisation spectrometer signal from the experimental set-up in Fig. 2.

a polarisation spectrometer would increase the trapping time.

5. Conclusions

We have demonstrated the use of a polarisation spectrometer technique to stabilise a compact external cavity diode laser system to the ^{85}Rb ($F = 3 \rightarrow F' = 4$) cooling transition. We have for the first time, to the best of our knowledge, used this locking scheme to trap and laser cool Rb atoms in a simple vapour cell trap. We have also modelled the expected lineshapes for the polarisation spectroscopy of rubidium and found good agreement with experimental results. Using this simple scheme we have continuously held 10^8 atoms in our MOT for several minutes' duration.

This laser locking technique has several advantages over saturated absorption spectroscopy: it provides a broader and larger locking range (~ 100 MHz) with minimal optics and a better signal-to-noise ratio than saturated absorption techniques. This technique will prove very useful for stabilising diode lasers for our future experiments on atom guiding from a MOT.

Acknowledgements

We would like to thank F. Akerboom and R.H. Mitchell for their assistance in machining and assembling the vacuum apparatus. This work is supported by the UK Engineering and Physical Sciences Research Council under grant number GR/L54301 and the Royal Society. RC acknowledges the support of the Leverhulme Trust. Kishan Dholakia is a Royal Society of Edinburgh Research Fellow.

References

[1] C. Monroe, W. Swann, H. Robinson, C. Wieman, Phys. Rev. Lett. 65 (1990) 1571.
[2] R.N. Watts, C.E. Wieman, Opt. Lett. 11 (1986) 291.
[3] M.H. Anderson, J.R. Ensher, M.R. Matthews, C.E. Wieman, E.A. Cornell, Science 269 (1995) 198.
[4] C.S. Adams, E. Riis, Progr. Quantum Electron. 21 (1997) 1.
[5] M.J. Renn, D. Montgomery, O. Vdovin, D.Z. Anderson, C.E. Wieman, E.A. Cornell, Phys. Rev. Lett. 75 (1995) 3253.
[6] K. Dholakia, Contemp. Phys. 39 (1998) 351.
[7] M.A. Clifford, J. Arlt, J. Courtial, K. Dholakia, Opt. Commun. 156 (1998) 300.
[8] K.B. McAdam, A. Steinbach, C.E. Wieman, Am. J. Phys. 60 (1992) 12.
[9] G.D. Rovera, G. Santarelli, A. Clairon, Rev. Sci. Instrum. 65 (1994) 1502.
[10] C. Wieman, T.W. Hansch, Phys. Rev. Lett. 36 (1976) 1170.
[11] J.J. Maki, N.S. Campbell, C.M. Grande, R.P. Knorpp, D.H. McIntyre, Opt. Commun. 102 (1993) 251.
[12] K. Lindquist, M. Stephens, C. Wieman, Phys. Rev. A 46 (7) (1992) 4082.
[13] M. Kozuma, M. Kourogi, M. Ohtsu, H. Hori, Appl. Phys. Lett. 61 (16) (1992) 1895.
[14] W. Demtroder, Laser Spectroscopy, Springer-Verlag, 1981 (Chapter 10).
[15] K. MacAdam, A. Steinbach, C. Wiemann, Am. J. Phys. 60 (12) (1992) 1098.

JOURNAL OF MODERN OPTICS, 2000, VOL. 47, NO. 11, 1933–1940

Stabilization of an 852 nm extended cavity diode laser using the Zeeman effect

M. A. CLIFFORD, G. P. T. LANCASTER, R. S. CONROY and K. DHOLAKIA

J F Allen Physics Research Laboratories, School of Physics and Astronomy, University of St Andrews, Fife, Scotland, KY16 9SS, UK

(*Received 18 October 1999*)

Abstract. We demonstrate the use of the Zeeman effect in Cs vapour to stabilize an ultra-compact extended cavity diode laser (ECDL) operating at 852 nm. We investigate the expected laser stabilization error signal for a range of magnetic fields and are able to tune the locked ECDL by variation of the magnetic field. We also study in detail the tuning of the laser frequency using optical methods. The ECDL has a linewidth of 520 kHz and the drift, when locked, is of the order of 5 MHz h^{-1}.

1. Introduction

Diode lasers have rapidly become established as powerful tools for high-resolution spectroscopy. A narrow linewidth and smooth tunability in wavelength are desirable characteristics of an ideal spectroscopic source. Whilst diodes are compact and inexpensive devices they do not readily exhibit these required attributes for high-resolution spectroscopy. As a consequence of a number of factors, diode lasers are very susceptible to optical feedback [1]. This can be detrimental to the output characteristics of the laser but may also be used to one's advantage to convert the diode laser into a spectroscopic laser source. This optical feedback can increase the Q factor of the cavity and reduce the output linewidth of the laser by around two orders of magnitude.

One can use various techniques to feedback light in a controlled manner to the diode. The two most widely used geometries are the Littman–Metcalf [2] and the Littrow [3] configurations. The Littrow configuration is the simpler of the two and uses a diffraction grating as an external mirror. The first order diffracted light from this grating is returned directly to the laser. The zero order of the grating forms the output of the laser system. The lasing cavity is now composed of the back facet of the laser diode and the diffraction grating and is commonly known as the extended cavity diode laser (ECDL).

Extended cavity diode lasers are prone to acoustic and thermal noise. Thus such a laser system must be locked to an external stable reference to ensure long term frequency stability in the system. Typical stabilization methods include current modulation and saturated absorption spectroscopy.

In this paper we start by briefly discussing the development and performance of an ultra-compact external cavity diode laser at 852 nm built using standard

Journal of Modern Optics ISSN 0950-0340 print/ISSN 1362-3044 online © 2000 Taylor & Francis Ltd
http://www.tandf.co.uk/journals

opto-mechanical components. Then we discuss the use of a locking scheme using the Zeeman effect in a caesium vapour cell to stabilize the laser frequency. Additionally, we study the locking signal for this system for a range of magnetic fields and demonstrate a novel method for tuning the laser frequency using this technique. Furthermore, we study alternative methods for tuning the locked laser frequency using optical offsets introduced into the experimental arrangement. This work represents the first time that this locking system has been studied in this detail and employed for work in caesium.

2. Extended cavity diode laser at 852 nm

The ECDL we have developed is based on a previous geometry we realized for 780 nm laser diodes [3]. Here, we discuss its implementation for the first time at 852 nm. The design is based around a standard 1″ opto-mechanical mount. A machined holder is used to hold the diffraction grating (1200 lines mm^{-1} grating blazed at 300 nm) at the Littrow angle in this design. Approximately 20% of the diode output is redirected back into the diode laser. This is sufficient to ensure external cavity operation. A piezo-ceramic disc (PZT) is positioned between the horizontal control of the mirror mount and the main body of the mount to enable the cavity length of the diode to be changed. In this work we study the performance of this system with an 852 nm laser diode (SDL-5410-G1). We achieve an output power of 70 mW from this ECDL. We are able to tune the ECDL smoothly over 8 GHz using solely the PZT. We can achieve discontinuous tuning of up to 13 nm by rotation and translation of the grating. The linewidth of the system is measured to be 520 kHz using a high finesse (~600) etalon of free spectral range 300 MHz (see figure 1). Thus the performance of this system is comparable with that observed at 780 nm in similar geometries [3, 4]. To the best of our knowledge, this represents possibly the simplest high-performance ECDL operating at 852 nm.

3. Stabilization using the Zeeman effect

Our main motivation in this work is to study the application of a hitherto little used locking scheme. We use the Zeeman effect in caesium vapour to stabilize this

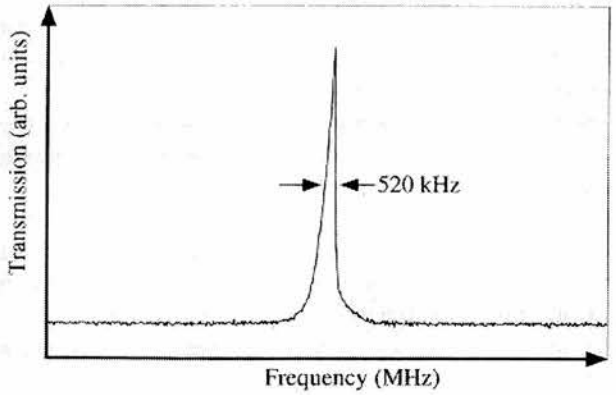

Figure 1. The linewidth of the 852 nm ECDL measured using the high finesse etalon.

ECDL. This technique was first demonstrated with a laser in helium [5] and then developed at 780 nm for rubidium [6]. In this work we show for the first time its application to caesium. We study the tuning characteristics of the ECDL using optical offsets and demonstrate a new method of tuning the laser whilst locked to the atomic transition using the magnetic field.

The stabilization method uses a weak magnetic field to separate the Zeeman components of an atomic absorption signal, that is Doppler-broadened, into two components. In the presence of a magnetic field, and when probed with circularly polarized light, the central absorption frequency of a Doppler broadened lineshape shifts. For σ^+ polarized light propagating in the z-direction and a **B**-field in the same direction, the central frequency of the absorption increases and for the opposite handedness of polarization (σ^-) this central frequency decreases (see figure 2 (*a*)). A dispersive error signal is required for locking. This is generated by subtracting the absorption profiles recorded for the two components of circularly polarized light. The act of subtraction in this instance reduces any fluctuations that may arise in the error signal from variations in lineshape or absorption. This is

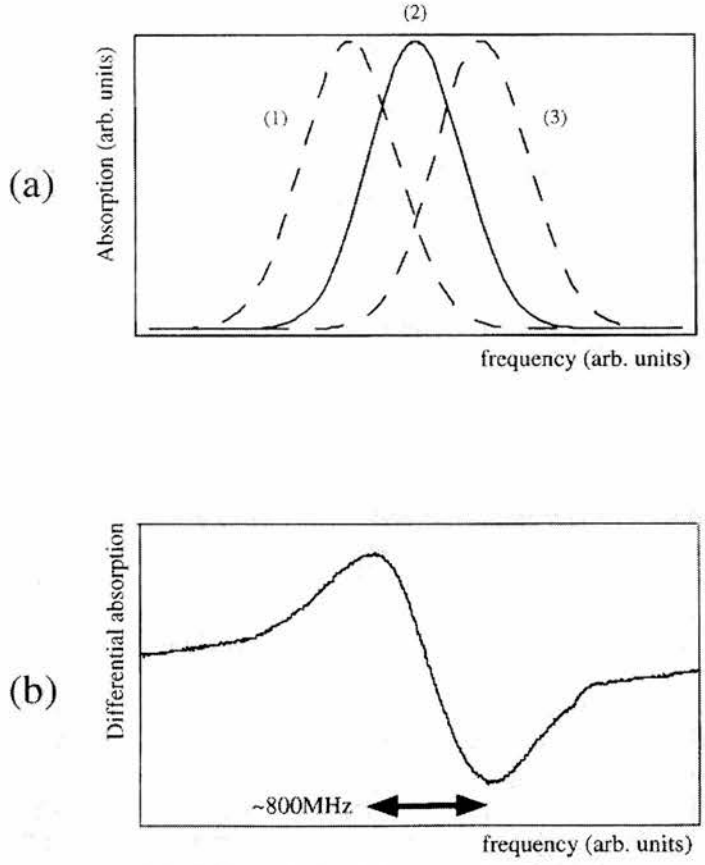

Figure 2. (*a*) The origin of the DAVLL error signal. Peaks (1) and (3) are Doppler broadened features for both senses of circularly polarized light incident on the vapour. (*b*) Subtraction of peaks (1) and (3) can give a DAVLL signal. This is a DAVLL signal we have recorded for caesium.

because the locking point is at zero as it occurs when the incident light on both photodetectors is equivalent. This locking scheme has been termed a dichroic-atomic vapour laser lock (DAVLL) [6].

Experimentally, the locking geometry is realized in the following manner: pure linearly polarized light (which may be considered to consist of equal amounts of left and right handed components of circularly polarized light) is sent through a vapour cell placed in a magnetic field. To generate this field we have used two methods: a series of annular discs cut from magnetic embedded material [6] and a standard electromagnet. The variation of magnetic field along the length of the cell in both instances was less than 9%. Immediately after passing through the vapour cell the light is incident on a quarter-wave plate oriented with both its fast and slow axes at 45° to the plane of incidence of the incoming linearly polarized light. Following this, the light is separated into two components by a polarizing beam splitting cube and each orthogonal polarization component is incident on a separate photodiode. Subtraction of these photodiode signals leads immediately to a dispersive signal that passes through zero. A typical dispersive DAVLL curve, which we have generated for caesium, is shown in figure 2 (*b*). The capture range of the locking signal is large (800 MHz) allowing the laser to recover from large perturbations in frequency. The drift of our laser system using the DAVLL locking system in caesium was observed to be of the order of 5 MHz h^{-1}, which was more than an order of magnitude improvement on the unlocked laser. This can readily be improved by stabilizing the temperature of the system [6].

We also set up the DAVLL system with a 780 nm ECDL in rubidium as we had very high quality optics at this wavelength. We recorded DAVLL signals for various magnetic fields by using a vapour cell placed in an electromagnet (see figure 3). The use of an electromagnet allowed us the flexibility to vary the magnetic field very easily. The data shown is for rubidium, although caesium showed similar data.

We can make several observations from this experimental data. Firstly, the DAVLL signal gradient does not vary at fields between ~60 G and ~130 G. The large slope will minimize the sensitivity of the system to laser intensity noise. The data also shows that the zero crossing of the DAVLL signal is **B**-field dependent. This has not been considered in the literature to date. This effect is believed to be due to the different splitting of the various lines within the Doppler broadened envelope and to optical pumping effects. This causes an imbalance (that is **B**-field dependent) to appear between the individual Doppler broadened peaks. This is an important feature which means the laser locks to a different point in frequency that is **B**-field dependent. Indeed we can make use of this by adjusting the **B**-field to tune the locked laser. This is discussed later in this paper.

4. Modelling of transition frequencies for the DAVLL signal

The equations governing the effect of an external magnetic field on the energy levels of caesium (or rubidium) can be simplified dependent on the strength of the magnetic field relative to the splitting of the hyperfine levels. If $g_F \mu_B \mathbf{B} \ll A$, where A is the hyperfine splitting constant for the level under consideration, g_F the lande g-factor, μ_B is the Bohr magnetron and **B** is the external magnetic field, then the field is considered weak and the normal Zeeman equations can be used. Conversely if $g_F \mu_B \mathbf{B} \gg A$ then the field is considered strong and can be modelled according to

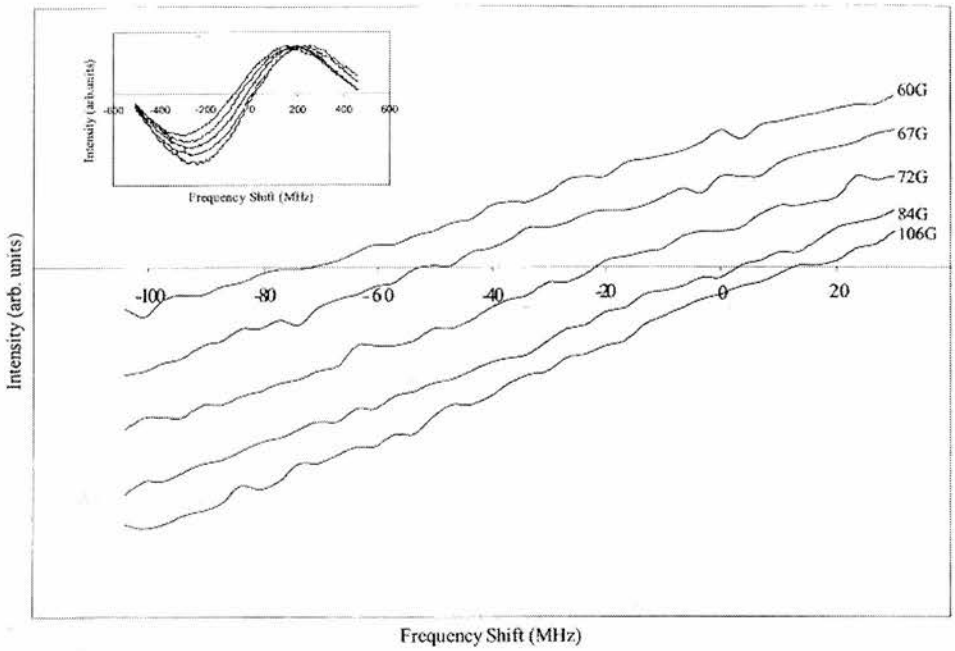

Figure 3. The DAVLL locking signal measured by us for various magnetic fields. Note that the point of zero crossing alters. The main part of figure is an enlargement of the central region of the insert.

Table 1. Hyperfine splitting constants and field strengths for ^{133}Cs, ^{85}Rb and ^{87}Rb.

Energy level	Hyperfine splitting constant A	Intermediate field strength (T)
^{133}Cs $^{6}P_{3/2}$	50.5 MHz	0.0036
^{133}Cs $^{6}S_{1/2}$	2.298 GHz	0.164
^{85}Rb $^{5}P_{3/2}$	25.03 MHz	0.0018
^{85}Rb $^{5}S_{3/2}$	3.035 GHz	0.217
^{87}Rb $^{5}P_{3/2}$	85.8 MHz	0.0061
^{87}Rb $^{5}S_{1/2}$	6.834 GHz	0.489

Paschen–Back equations. For intermediate cases, the Breit–Rabi equations can be used for levels with $J = 1/2$ and for other levels the equations can be calculated from the diagonalized hyperfine Hamiltonian [7].

The small splitting of the P-levels of the isotopes shown in table 1 illustrate how only a relatively weak external field is required to change from the normal weak Zeeman splitting into the Paschen–Back effect, for a magnetic field of the order of a hundred Gauss. Thus the normally degenerate magnetic sublevels of the hyperfine levels can be split significantly by applying an external field, giving different transition frequencies dependent on the polarization of the incident radiation. In particular, π (plane polarized) radiation will excite $\Delta m_F = 0$ transitions and σ^+ and σ^- circularly polarized light will excite $\Delta m_F = \pm 1$ transitions.

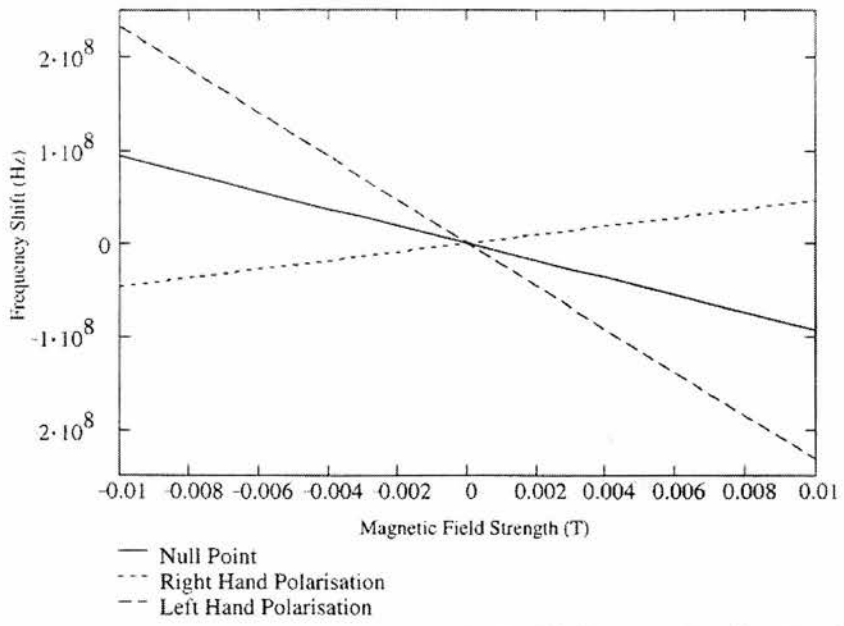

Figure 4. The calculated frequency shift for the Cs D2 line transition $F = 4$ to $F' = 5$. Note that the zero crossing point alters.

We have modelled the ^{133}Cs transition $^6S_{1/2}$ ($F = 4$) to $^6P_{3/2}$ ($F' = 5$) as an example to show how the asymmetric splitting of the levels can be used to achieve frequency tuning with variation of the magnetic field strength. Figure 4 shows how the above transition excited by the orthogonal circularly polarized light tunes with respect to the zero field case, and also shown is the expected null point between the transitions. These results are in good agreement with the work of Ikegami *et al.* [8] and show that the frequency can be tuned over several hundred megahertz using an external magnetic field: the zero point in the DAVLL locking signal is seen to shift in frequency. To model these experimentally measured Doppler profiles accurately, it is necessary to account for the population distribution in the magnetic sublevels and to calculate the strengths of each of the possible hyperfine and sublevel transitions. The calculation is a non-trivial task although we are developing a model to predict the expected Doppler profiles for DAVLL [9]. Nevertheless, to date we have seen that the frequency of each of the lines within the Doppler broadened profile shifts to varying degrees—this accounts for a broadening of the transition with increasing magnetic field.

5. Tuning of the locked laser

An advantage of the DAVLL locking method is its simplicity. An important attribute is the ability to tune the locking point of the ECDL whilst locked. Reference [6] makes very brief mention of the fact that rotating the waveplate imbalances the signals at both photodiodes and allows one to tune the locked laser, although no details for tuning were given.

We have developed a simpler and more flexible method to tune the locked laser frequency. By placing either a rotating polarizer or variable neutral density (ND)

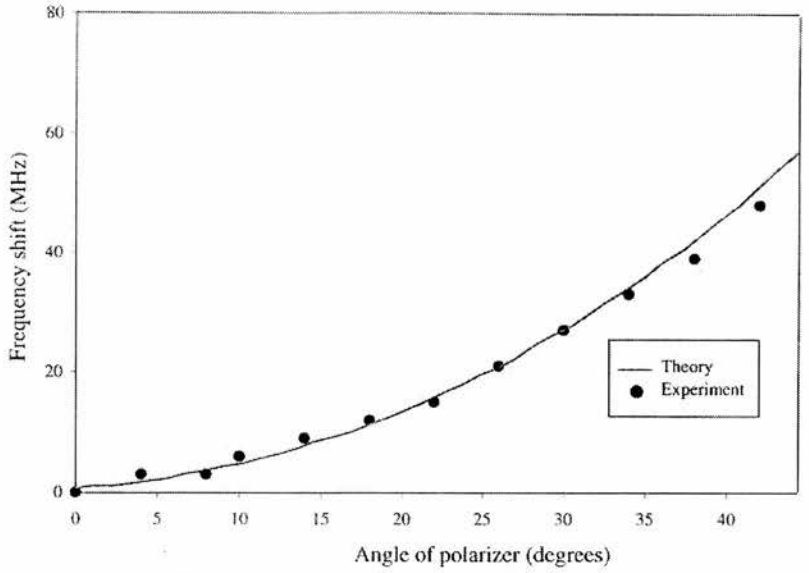

Figure 5. Tuning the frequency by rotating a linear polarizer in front of a photodiode. A good fit to the numerical model is shown.

filter in front of one or other of the photodiodes full flexibility of the locking point is achieved. Adjusting the polarizer or altering the value of ND filter varies the amount of light reaching the photodiode, thus imbalancing the signal of the two Doppler broadened peaks. We have numerically modelled this and we show experimental data for frequency tuning in figure 5. A very good fit is seen between theory and experiment. The lock point is a zero in net photocurrent. We find experimentally that this technique offers greater flexibility over the rotation of the waveplate and the ability to tune both up and down in frequency from the original lock-point.

As previously stated we have used both an electromagnet, as well as permanent magnetic material, to generate the dispersive locking signal. The use of an electromagnet offers the possibility of varying the magnetic field *in situ* in a controlled fashion. As seen in figure 3 the DAVLL signal varies as we vary the **B**-field though the gradient of the lock signal stays approximately constant. We have varied the magnetic field and recorded data for the tuning of the lock point position with field in rubidium (see figure 6). These data clearly show that purely adjusting the magnetic field gives a powerful and novel method for tuning a DAVLL stabilized laser.

6. Conclusions

We have studied a method of stabilizing an extended cavity diode laser at 852 nm which is based upon the Zeeman effect in caesium vapour. To the best of our knowledge, this is the first time this locking method has been applied to a simple ECDL at 852 nm. Within this work we have identified a completely new method of tuning the laser whilst locked that relies on small variations of the applied **B**-field. We have studied the tuning of the locked ECDL using an optical

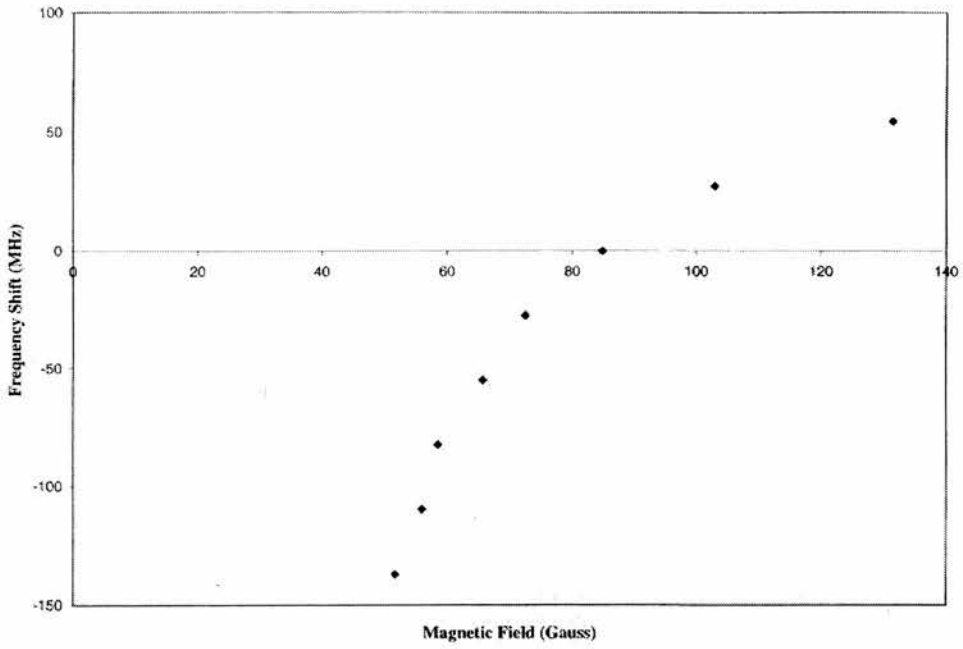

Figure 6. Tuning the laser frequency by adjusting the dc magnetic field applied to the vapour cell.

offset and modelled and experimentally recorded the expected shifts in frequency. The Zeeman (DAVLL) method is versatile and simple. The stabilized ECDL is suited for many applications including laser cooling of caesium.

Acknowledgments

We thank the Royal Society, the Leverhulme Trust and the UK Engineering and Physical Sciences Research Council for supporting this work. KD is a Royal Society of Edinburgh Research Fellow.

References

[1] Wieman, C. E., and Hollberg, L., 1991, *Rev. Sci. Instrum.*, **62,** 1.
[2] Harvey, K. C., and Myatt, C. J., 1991, *Optics Lett.*, **16,** 910.
[3] Clifford, M. A., Arlt, J., Courtial, J., and Dholakia, K., 1998, *Optics Commun.*, **156,** 300.
[4] Arnold, A., Wilson J. S., and Boshier, M., 1998, *Rev. Sci. Instrum.*, **69,** 1236.
[5] Cheron, B., Gilles, H., Havel, J., Moreau, O., and Sorel, H., 1994, *J. Phys. III*, **4,** 401.
[6] Corwin, K. L., Lu., Z. T., Hand, F., Epstein, R. J., and Wieman, C. E., 1998, *Appl. Optics*, **37,** 3295.
[7] Arimondo, E., Inguscio, M., and Violino, P., 1977, *Rev. mod. Phys.*, **49,** 31.
[8] Ikegami, T., Ohshima, S., and Ohtsu, M., 1989, *Jpn. J. appl. Phys.*, **28,** L1839.
[9] Conroy, R., Lancaster, G. P. T., Clifford, M. A., and Dholakia, K., 1999, unpublished.

Channelling of cold atoms along a Laguerre-Gaussian light beam

G.P.T. Lancaster, J. Arlt, M.A. Clifford and K. Dholakia

School of Physics and Astronomy, University of St Andrews,

St. Andrews, Fife, KY16 9SS, Scotland, UK

Tel: +44 1334 463165 *fax: +44 1334 463104* *e-mail:* gpl1@st-and.ac.uk

Abstract: we channel cold atoms directly out of a magneto-optical trap along a Laguerre-Gaussian (LG) light beam. The LG beams are holographically generated and have an annular form. We study this process as a function of trapping laser parameters.

Extracting cold atoms from a magneto-optical trap (MOT) has been the subject of central interest in recent years. This has seen the emergence of the area of atom guiding along hollow core optical fibres and also along light beams [1]. The guiding and the extraction of cold atoms is of central importance in generating bright, high flux atomic sources for various experiments in atom optics. In this paper we describe and experimentally realise a scheme for extracting cold atoms directly from a magneto-optical trap along a Laguerre-Gaussian light beam.

The circularly symmetric Laguerre-Gaussian (LG) laser modes form a complete basis set for paraxial light beams. The azimuthal index l of the mode refers to the number of 2π phase cycles around the circumference of the mode. Importantly for this work, we note that LG beams with $l \neq 0$ have an annular form and that the size of the central minimum is dependent on the azimuthal index l of the mode

[2]. Further, they are true free-space propagating light modes and diffraction does not fill the central dark region.

In this work we have substituted one or more of the conventional light beams in a MOT with a holographically generated Laguerre Gaussian light beam. This allows us a mechanism for extracting the atoms along the dark centre of the LG beam [2,3]. Furthermore, we have observed novel cloud formations in our trap using this light beam geometry (figure 1). Our scheme has some similarities with the recently developed low-velocity intense atomic source (LVIS) beam [4] though for the LVIS beam a simple dark spot was used and diffraction fills the central dark region. The use of LG beams obviates this problem and could allow atom transport directly from a MOT over extended distances. Figure 2 shows some data that we have recorded for a cold atom beam emanating along an l −1 mode. We will present data relating to the obtained output atomic flux using LG beams of various orders and also as a function of trap operating parameters.

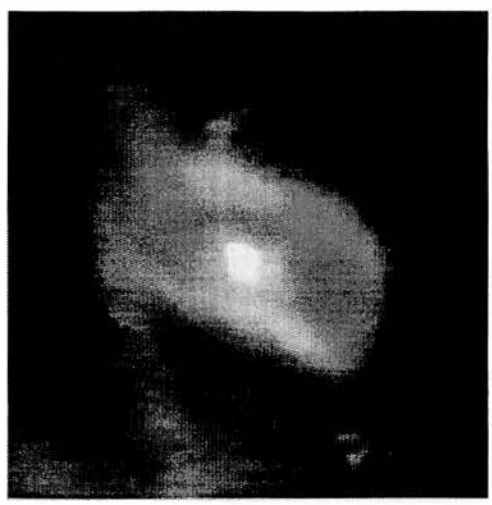

Fig. 1: The cloud formed using an l=3 light beam. A halo of cold atoms is seen with a bright central cloud of atoms

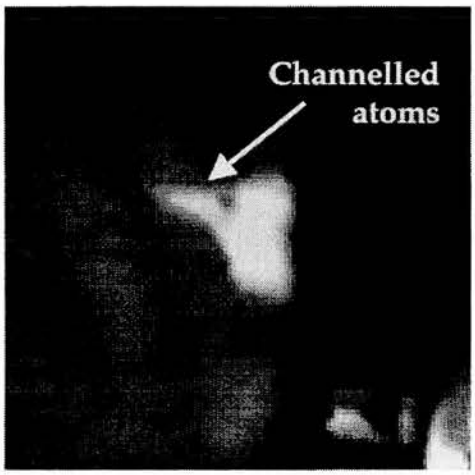

Fig. 2: Channelled cold atoms along an l=1 LG beam. The cold atoms can be seen leavinbg trap entre along the minimum of the LG beam.

References

[1] M.J. Renn *et al.*, Phys. Rev. A **53**, R618 (1996); H. Ito et al., Phys. Rev. Lett. **76**, 4500 (1996); K. Dholakia, Contemp. Phys., **39**, 351 (1998)

[2] M.A. Clifford, J. Arlt, J. Courtial and K. Dholakia, Opt. Comm. **156**, 300 (1998).

[3] M. Schiffer *et al.*, Appl. Phys. B **67**, 705 (1998)

[4] Z.T. Lu *et al.* Phys. Rev. Lett., **77**, 3331 (1996)

JOURNAL OF MODERN OPTICS, 2001, VOL. 48, NO. 6, 1123-1128

Realization of a mirror magneto-optical trap

M. A. CLIFFORD, G. P. T. LANCASTER, R. H. MITCHELL, F. AKERBOOM and K. DHOLAKIA

J. F. Allen Research Laboratories, School of Physics & Astronomy, The University of St Andrews, North Haugh, St Andrews, Fife, KY16 9SS, UK

(*Received 17 July 2000; revision received 26 September 2000*)

Abstract. We present details for construction and the operation of a mirror magneto-optical trap for cooling and trapping rubidium atoms. For trap operation, only four input laser beams are needed in contrast to the normal six for a standard trap. In excess of 10^8 atoms have been trapped with this arrangement, with the atomic ensemble only ~1mm from the surface of a reflective mirror. This trap is highly suited to studies of magnetic guiding and magnetic manipulation of cold atomic ensembles.

1. Introduction

The magneto-optical trap (MOT) is now firmly established as the workhorse for numerous cold-atom experiments worldwide [1]. Notably it forms the basis for experiments in atom optics and is also the first step to realizing Bose-Einstein condensation in an atomic ensemble [2]. Various advances have been achieved with the MOT including the ability to use diode lasers to cool atoms [3] and the use of a glass vapour cell [4], allowing atoms to be trapped and confined directly from a thermal background vapour. A standard MOT is formed by intersecting six mutually perpendicular beams (three orthogonal light beams, usually retroreflected) in a cell containing a thermal vapour of neutral atoms.

Controlled manipulation of a cold atomic ensemble is a necessary prerequisite for developing matter-wave devices and guides. Optical dipole forces [5, 6] and the interaction with magnetic fields [7] are two methods to achieve such manipulation. Microscopic control of atomic ensembles could open up possibilities in quantum logic gates and atom optics components. Magnetic traps can deliver very tight confinement and microfabricated conductors embedded on a surface can be used for trapping and manipulation [8]. This could realize atom 'chips' [9] for coherent matter-wave manipulation. A major experimental obstacle to realizing microfabricated atom traps is the loading of such chips and structures with a cold atomic ensemble. The experimentalist requires the ability to place a microfabricated substrate very close to a cold atomic ensemble. In recent work, brief mention was made of a mirror MOT [8, 9] to realize such a goal. However, very few details were given as to its operation or indeed its construction. In this paper, we describe in detail the construction and operation of such a trap and contrast this with a standard MOT. The ability to simply realize and operate such a trap is of direct interest in the field of cold atom manipulation using microfabricated structures.

Journal of Modern Optics ISSN 0950-0340 print/ISSN 1362-3044 online © 2001 Taylor & Francis Ltd
http://www.tandf.co.uk/journals
DOI: 10.1080/09500340010023409

The work we present allows the replication of this potentially significant new type of atom trap. We are able to trap in excess of 10^8 rubidium atoms in the trap, more than an order of magnitude greater than reported in previous work with rubidium [8]. Further, we employ a novel form of extended cavity diode laser system to trap and cool the atoms that makes use of a circularized diode [10]. This system directly delivers a *circular* output beam and removes the need for any beam shaping optics in the trap experimental arrangement.

2. Construction of the mirror MOT

The trap is mounted on one flange of a standard six-way UHV cross-piece. The whole apparatus is held at a base pressure of 10^{-9} mbar by a $25\,l\,s^{-1}$ ion pump. A blank vacuum flange is bored with a 25 mm hole. A metallic cylindrical holder is placed on this hole (2 cm in length) upon which a right-angled metal-coated prism is attached. Two small holes on one side of the flange are drilled to allow placement of a rubidium getter oven (SAES Getters, UK). This is an alkali metal dispenser that releases rubidium vapour when sufficient current flows through it. Placing the rubidium source in close proximity (~2 cm) to the trapping region allows accurate control of the rubidium pressure in the trap region. Further, the walls of the vacuum vessel act as pumps for any excess rubidium vapour present and thus the remainder of the vacuum system (notably the ion pump) is not contaminated by rubidium. We find experimentally it is advantageous to have an unobstructed path between the Rb oven and the trapping region, although this need not be a direct line of sight. The Rb oven is connected, using kapton wire, to an electrical feedthrough placed on one arm of the six-way arm of the cross. Typically we run a current of a few amperes through the oven to generate sufficient rubidium at the trap region. Placed over this right-angled prism, the Rb getter is a quartz cuboid that is affixed to the flange using a low vapour pressure torr seal (Caburn, UK). We use an inexpensive commerically available cuboid (Hellma, England) that has outer dimensions 40 mm × 40 mm × 70 mm and a wall thickness of 4 mm. The cuboid has one open end and is fused on all other sides. The glass is of high optical quality, the typical use for this cuboid being a cell for spectrometry. We have used several of these cells and find that they serve as excellent and very inexpensive cells for atom traps. Figure 1 shows a picture of the assembled mirror MOT. The position of the Rb getter oven is indicated. We note that we have drilled a hole through the centre of the mirror in our system. This is to allow the possible *extraction* of cold atoms directly from the mirror MOT and details will be given in future work [11].

Only two mutually orthogonal laser beams are required to operate the mirror MOT. One beam is reflected at 45° by the mirror and is retroreflected. In the half-space defined by the mirror, this creates immediately four orthogonal overlapping beams. The term half-space here refers to the region of overlap above the mirror surface created by this first beam and its retroreflected counterpart. A second beam (also retroreflected) is sent in at grazing incidence to the mirror surface. Figure 2 shows the optical beam geometry in detail for this trap and also shows the relative polarizations of the beams used. Two coils are placed around the trap in an anti-Helmholtz configuration. Each has around 100 turns and carries a current of approximately 1.5 A in typical experimental conditions yielding a field gradient of $\sim 10\,G\,cm^{-1}$. We note that for successful MOT operation, one of the reflected

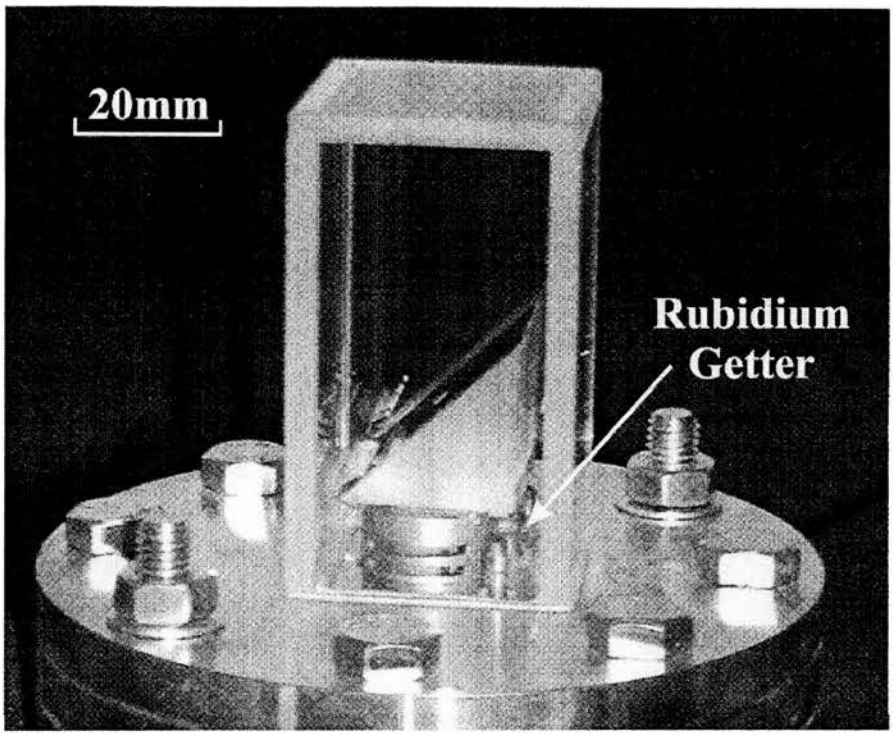

Figure 1. A photograph of the assembled mirror magneto-optical trap. The Rb getter is located behind the right-angled mirror. Although Rb is pumped by the walls of the trap we find the gap of a few millmetres between the mirror and the wall is enough to allow sufficient Rb vapour to reach the trapping region.

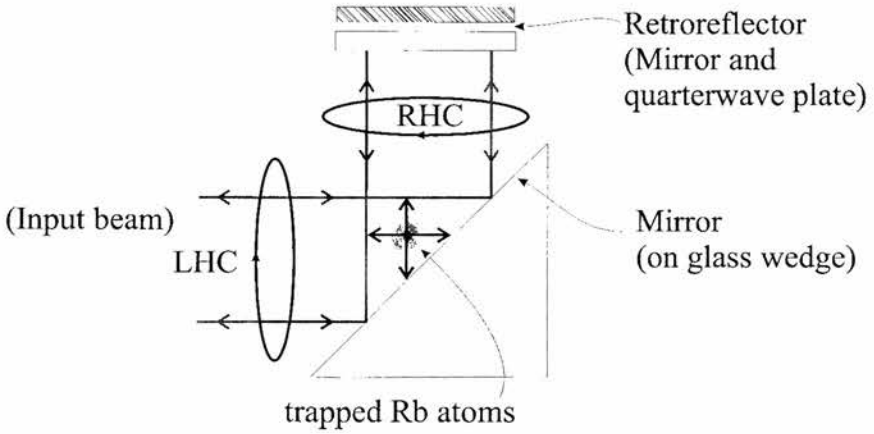

Figure 2. A layout showing the polarizations and laser requirements for trapping. The arrows in the overlap region show how a single incident beam can generate two orthogonal trapping beams by reflection above the mirror surface. The overlap region here also denotes what is termed the 'half-space' above the mirror surface. Note that there is a further beam in and out of the plane of the page that is not shown.

trapping beams should be directed along the axis of the trap coils. Further, experimentally we find that careful positioning of these trap coils is quite critical due to the relatively small trapping region above the mirror MOT.

3. Operation of the mirror MOT

Two diode laser systems were used to provide cooling light on the $F = 3 \rightarrow F' = 4$ transition and repumping light on the $F = 2 \rightarrow F' = 3$ respectively for ^{85}Rb. We use two novel extended cavity diode laser (ECDL) systems for this purpose. We present brief details here, a full account of its performance is given elsewhere [12].

The ECDL systems we use are based on a previous design [13]. In this instance however, we use a 50 mW diode laser at 780 nm with a virtual point microlens attached [10]. This immediately produces a circular divergent output beam. This circularized diode is collimated by a lens in a collimating tube and is used in a Littrow geometry with a diffraction grating of 1200 lines mm^{-1}. The system provides a highly stable, narrow linewidth (<500 kHz) laser source with a circular output beam. This removes the need for use of any further beam shaping components in the trap optics and substantially simplifies the trapping experiment. As a consequence of the microlens attached to the diode facet, we find that the system is particularly stable to long-term drift and indeed we have seen clouds of trapped atoms for several minutes with the ECDL systems *unstabilized* to any external reference. However for reproducibility in our experiments we stabilize the lasers using polarization spectroscopy [14]. The output of two such ECDL laser systems is expanded to a beam size of around 1.5 cm in diameter and directed at the trap.

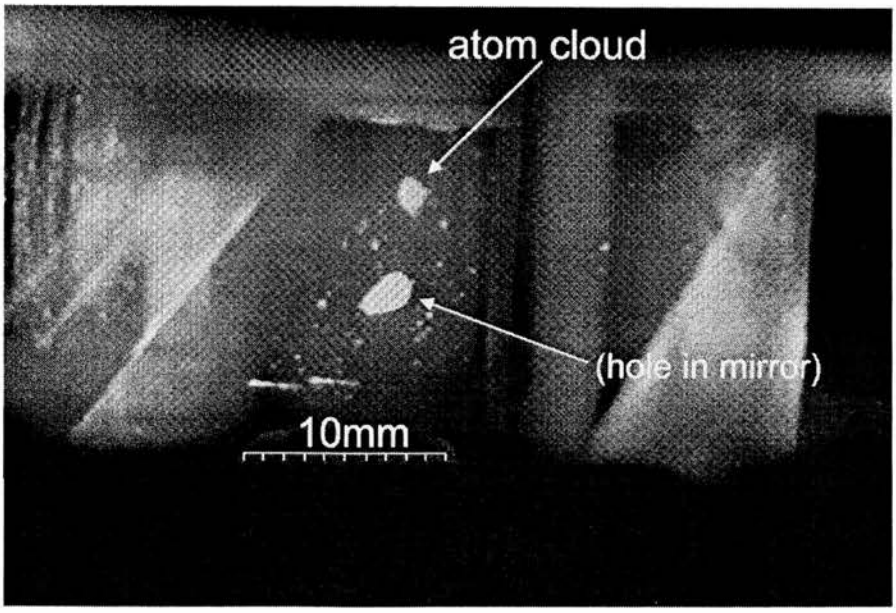

Figure 3. Trapped atoms (indicated by the arrow) only 1 mm above the surface of the mirror MOT.

Figure 3 shows a cloud of trapped atoms in the mirror magneto-optical trap. Clouds of atoms can only be observed when the trap centre is located a few millmetres away from the trap surface. Varying the relative currents in the coils, the cloud can be moved up and down in a controlled fashion. As it nears the mirror surface, however, the cloud size reduces dramatically until it vanishes altogether. Beginning from a pair of magnetic coils with equal current flowing in each, the measured movement of the atom cloud was approximately 1mm for each 10^{-4} Tesla difference induced between the coils (by varying the current). This is to be expected considering that the field gradient in the vicinity of the trap centre is $10\,\mathrm{G\,cm^{-1}}$. We carefully maximized the overlap of the trapping beams by alignment. We recorded approximately 10^8 atoms from atomic fluorescence measurements on a photodiode with well-aligned beams of 1.5 cm diameter and power of $7\,\mathrm{mW\,cm^{-2}}$ in each beam. Trap lifetime was determined by monitoring the trap fluorescence versus time and fitting the resultant curves to extract the characteristic time constant ('trap lifetime') [1, 15]. In this manner, we measured the lifetime to be approximately 0.2 s for typical operating parameters for our Rb oven. We note that in comparison to operation of a standard MOT in our laboratory we observed the trapping of an equivalent number of atoms.

4. Conclusion

We have presented details for construction and operation of a mirror magneto-optical trap. This trap requires only four beams in contrast to the six required for a standard MOT. Up to 10^8 trapped atoms are observed only 1 mm from the surface. Our experience shows this trap, once assembled, is simple to operate and can trap as many atoms as a standard vapour cell trap. We have also used a novel circularized diode laser source in an extended cavity geometry. This compact extended cavity diode laser directly delivers a circular output beam suitable for trapping atoms. The trap presented here is of central importance for loading atom optics components fabricated on a structure [8, 9]. The work presented here should allow the reader to simply replicate this type of novel atom trap for subsequent magnetic manipulation and atom optics on a surface.

Acknowledgments

We would like to thank the UK Engineering and Physical Sciences Research Council for supporting this work.

References

[1] Raab, E. L., Prentiss, M., Cable, A., Chu, S., and Pritchard, D. E., 1987, *Phys. Rev. Lett.*, **59,** 2631.
[2] Anderson, M. H., Ensher, J. R., Matthews, J. R. , Wieman, C. E., and Cornell, E. A., 1995, *Science*, **269,** 198.
[3] Watts, R. N., and Wieman, C. E., 1986, *Optics Lett.*, **11,** 291.
[4] Monroe, C., Swann, W., Robinson, H., and Wieman, C., 1990, *Phys. Rev. Lett.*, **65,** 1571.
[5] Dholakia, K., 1998, *Contemp. Phys.*, **39,** 351.
[6] Dowling, J. P., and GeaBanacloche, J., 1996, *Adv. at. mol. Phys.*, **37,** 1.
[7] Hinds, E. A., and Hughes, I. G., 1999, *J. Phys. D Appl. Phys.*, **32,** R119.

[8] REICHEL, J., HÄNSEL, W., and HÄNSCH, T. W., 1999, *Phys. Rev. Lett.*, **83,** 3398.
[9] FOLMAN, R., KRUGER, P., CASSETTARI, D., HESSMO, B., MAIER, T., and SCHMIEDMAYER, J., 2000, *Phys. Rev. Lett.*, **84,** 4749.
[10] BlueSky Research, San Jose, USA, Circulaser^{TM} Diode, part no. PS026-00.
[11] LANCASTER G. P. T., and DHOLAKIA, K., private communication.
[12] LANCASTER, G. P. T., SIBBETT, W., and DHOLAKIA, K., 2000, *Rev. Sci. Instrum.*, **71,** 3646.
[13] CLIFFORD, M. A., ARLT, J., COURTIAL, J., and DHOLAKIA, K., 1998, *Optics Commun.*, **156,** 300.
[14] LANCASTER, G. P. T., CONROY, R. S., CLIFFORD, M. A., ARLT, J., and DHOLAKIA, K., 1999, *Optics Commun.*, **170,** 79.
[15] WIEMAN, C., FLOWERS, G., and GILBERT, S., 1995, *Am. J. Phys.*, **63,** 317.